NAVAL POSTGRADUATE SCHOOL
Monterey, California

THESIS

ANGULAR RATE ESTIMATION FOR MULTI-BODY SPACECRAFT ATTITUDE CONTROL

by

William J. Palermo

June 2001

Thesis Advisor:	Brij N. Agrawal
Second Reader:	Harold A Titus

Approved for public release; distribution is unlimited

Form SF298 Citation Data

Report Date *("DD MON YYYY")* 15 Jun 2001	**Report Type** N/A	**Dates Covered (from... to)** *("DD MON YYYY")*

Title and Subtitle ANGULAR RATE ESTIMATION FOR MULTI-BODY SPACECRAFT ATTITUDE CONTROL	**Contract or Grant Number**
	Program Element Number
Authors	**Project Number**
	Task Number
	Work Unit Number
Performing Organization Name(s) and Address(es) Naval Postgraduate School Monterey, CA 93943-5138	**Performing Organization Number(s)**
Sponsoring/Monitoring Agency Name(s) and Address(es)	**Monitoring Agency Acronym**
	Monitoring Agency Report Number(s)
Distribution/Availability Statement Approved for public release, distribution unlimited	
Supplementary Notes	
Abstract	
Subject Terms	
Document Classification unclassified	**Classification of SF298** unclassified
Classification of Abstract unclassified	**Limitation of Abstract** unlimited
Number of Pages 131	

REPORT DOCUMENTATION PAGE			Form Approved OMB No. 0704-0188
Public reporting burden for this collection of information is estimated to average 1 hour per response, including the time for reviewing instruction, searching existing data sources, gathering and maintaining the data needed, and completing and reviewing the collection of information. Send comments regarding this burden estimate or any other aspect of this collection of information, including suggestions for reducing this burden, to Washington headquarters Services, Directorate for Information Operations and Reports, 1215 Jefferson Davis Highway, Suite 1204, Arlington, VA 22202-4302, and to the Office of Management and Budget, Paperwork Reduction Project (0704-0188) Washington DC 20503.			
1. AGENCY USE ONLY *(Leave blank)*	**2. REPORT DATE** June 2001	**3. REPORT TYPE AND DATES COVERED** Engineer's Thesis	
4. TITLE AND SUBTITLE: Angular Rate Estimation for Multi-Body Spacecraft Attitude Control			**5. FUNDING NUMBERS**
6. AUTHOR(S) William J. Palermo			
7. PERFORMING ORGANIZATION NAME(S) AND ADDRESS(ES) Naval Postgraduate School Monterey, CA 93943-5000			**8. PERFORMING ORGANIZATION REPORT NUMBER**
9. SPONSORING / MONITORING AGENCY NAME(S) AND ADDRESS(ES) N/A			**10. SPONSORING / MONITORING AGENCY REPORT NUMBER**
11. SUPPLEMENTARY NOTES The views expressed in this thesis are those of the author and do not reflect the official policy or position of the Department of Defense or the U.S. Government.			
12a. DISTRIBUTION / AVAILABILITY STATEMENT Approved for public release; distribution is unlimited			**12b. DISTRIBUTION CODE**

13. ABSTRACT ***(maximum 200 words)***

Spacecraft with high performance attitude control systems requirements have traditionally relied on imperfect mechanical gyroscopes for primary attitude determination. Gyro bias errors are corrected with a Kalman filter algorithm that uses updates from precise attitude sensors like star trackers. Gyroscopes, however, have a tendency to degrade or fail on orbit, becoming a life limiting factor for many satellites. When errors become erratic, pointing accuracy may be lost during short star gaps. Unpredictable gyro degradations have impacted NASA spacecraft missions such as Skylab and Hubble Space Telescope as well as several DoD and ESA satellites. An alternative source of angular rate information is a software implemented real time dynamic model. Inputs to the model from internal sensors and known spacecraft parameters enable the tracking of total system angular momentum from which body rates can be determined. With this technique, the Kalman filter algorithm provides error corrections to the dynamic model. The accuracy of internal sensors and input parameters determine the effectiveness of this angular rate estimation technique. This thesis presents the background for understanding and implementation of this technique into a representative attitude determination system. The system is incorporated into an attitude simulation model developed in SIMULINK to evaluate the effects of dynamic modeling errors and sensor inaccuracies. Results are presented that indicate that real time dynamic modeling is an effective method of angular rate determination for maneuvering multi-body spacecraft attitude control systems.

14. SUBJECT TERMS dynamic gyro, Kalman filter, attitude determination, rate estimation, star trackers, attitude simulation, multi-body dynamics, quaternions, MATLAB, SIMULINK			**15. NUMBER OF PAGES**
			16. PRICE CODE
17. SECURITY CLASSIFICATION OF REPORT Unclassified	**18. SECURITY CLASSIFICATION OF THIS PAGE** Unclassified	**19. SECURITY CLASSIFICATION OF ABSTRACT** Unclassified	**20. LIMITATION OF ABSTRACT** UL

NSN 7540-01-280-5500 Standard Form 298 (Rev. 2-89)
Prescribed by ANSI Std. 239-18

THIS PAGE INTENTIONALLY LEFT BLANK

Approved for public release; distribution is unlimited

ANGULAR RATE ESTIMATION FOR MULTI-BODY SPACECRAFT ATTITUDE CONTROL

William J. Palermo
Lieutenant, United States Navy
B.S., United States Naval Academy, 1992

Submitted in partial fulfillment of the
requirements for the degree of

MASTER OF SCIENCE IN ASTRONAUTICAL ENGINEERING
and
AERONAUTICAL AND ASTRONAUTICAL ENGINEER

from the

NAVAL POSTGRADUATE SCHOOL
June 2001

Author: _____
William J. Palermo

Approved by: _____
Brij N. Agrawal, Thesis Advisor

_____
Harold A. Titus, Second Reader

_____
Max F. Platzer, Chairman
Department of Aeronautics and Astronautics

THIS PAGE INTENTIONALLY LEFT BLANK

ABSTRACT

Spacecraft with high performance attitude control systems requirements have traditionally relied on imperfect mechanical gyroscopes for primary attitude determination. Gyro bias errors are corrected with a Kalman filter algorithm that uses updates from precise attitude sensors like star trackers. Gyroscopes, however, have a tendency to degrade or fail on orbit, becoming a life limiting factor for many satellites. When errors become erratic, pointing accuracy may be lost during short star gaps. Unpredictable gyro degradations have impacted NASA spacecraft missions such as Skylab and Hubble Space Telescope as well as several DoD and ESA satellites. An alternative source of angular rate information is a software implemented real time dynamic model. Inputs to the model from internal sensors and known spacecraft parameters enable the tracking of total system angular momentum from which body rates can be determined. With this technique, the Kalman filter algorithm provides error corrections to the dynamic model. The accuracy of internal sensors and input parameters determine the effectiveness of this angular rate estimation technique. This thesis presents the background for understanding and implementation of this technique into a representative attitude determination system. The system is incorporated into an attitude simulation model developed in SIMULINK to evaluate the effects of dynamic modeling errors and sensor inaccuracies. Results are presented that indicate that real time dynamic modeling is an effective method of angular rate determination for maneuvering multi-body spacecraft attitude control systems.

THIS PAGE INTENTIONALLY LEFT BLANK

TABLE OF CONTENTS

THIS PAGE INTENTIONALLY LEFT BLANK

LIST OF FIGURES

LIST OF TABLES

THIS PAGE INTENTIONALLY LEFT BLANK

LIST OF SYMBOLS

Symbol	MATLAB/ SIMULINK Variable	Description	Units
Ät	dt	Computer Step Size	s
m_T	m1	Mass of Primary Body (Transmit Telescope)	kg
m_R	m2	Mass of Secondary Body (Receive Telescope)	kg
I_T	I1	Primary Body Inertia Matrix	kgm^2
I_R	I2	Secondary Body Inertia Matrix	kgm^2
I	I	Spacecraft Inertia Matrix	kgm^2
r_T	d1	Primary Body Center of Mass Offset	m
r_R	d2	Secondary Body Center of Mass Offset	m
ì	mu	Earth Gravitational Constant	km^3/s^2
R_e	Re	Earth Radius	km
h	h	Orbit Altitude	km
r	r	Orbit Radius	km
$ù_e$	we	Earth Rotation Rate	rad/s
$ù_o$	w0	Orbital Rate	rad/s
ν	nu	True Anomaly	rad
i	inc	Orbital Inclination	rad
ε	e1	Earth Magnetic Diploe Tilt Angle	rad
u	u	Angle of Magnetic Dipole Normal to Line of Ascending Nodes	rad
$\vec{B}$	B	Earths Magnetic Field Vector	N/Am
	Km	Magnetic Field Constant	Nm^2/A
$\vec{M}_{cmd}$	Mcmd	Magnetic Dumping Control Torque	Nm
$\vec{M}_G$	Mdg	Gravity Gradient Disturbance Torque	Nm
	Mdp	Periodic Disturbance Torque	Nm
	Mds	Secular Disturbance Torque	Nm
$\vec{H}$	H	Total System Angular Momentum	kgm/s
$\vec{H}_{S-}$	H’	System Angular Momentum Neglecting Relative Internal Momentum	kgm/s
$\vec{H}_w$	hw	Reaction Wheel Relative Angular Momentum	kgm/s
$\vec{H}_{rel}$	I2bd	Secondary Body Relative Angular Momentum	kgm/s
$Ä\vec{H}_{corr}$	dHc	Kalman Filter Momentum Correction	kgm/s
á	b	Appendage Relative Position Angle	rad
$\vec{ù}_{rel}$	bd	Appendage Relative Angular Rate Vector	rad/s
$\dot{\vec{ù}}_{rel}$	bdd	Appendage Relative Angular Acceleration	rad/s

		Vector	
$\vec{q}$	q	Spacecraft Attitude Quaternion Vector	
$\vec{\omega}$	w	Spacecraft Angular Rate	rad/s
$\dot{\vec{\omega}}$	wd	Spacecraft Angular Acceleration Vector	rad/s^2
$\vec{M}_c$	Mff	Feed Forward Command Torque	Nm/s
$\vec{q}_c$	qc	Commanded Attitude Quaternion Vector	
$\vec{\omega}_c$	wc	Commanded Angular Rate	rad/s
$\dot{\vec{\omega}}_c$	wdc	Commanded Angular Acceleration Vector	rad/s^2
$\hat{\vec{q}}$	qkf	Estimated Attitude Quaternion Vector	
$\hat{\vec{\omega}}$	wkf	Estimated Angular Rate	rad/s
A	A	Spacecraft Attitude (Direction Cosine) Matrix	
$\hat{A}$		Estimated Attitude (Direction Cosine) Matrix	
$\vec{x}$		State Vector	
$\hat{\vec{x}}$	x	Estimated Kalman State vector	
P	P	State Covariance Matrix	
Q	Q	Plant Error Covariance Matrix	
R	R	Measurement Error Covariance Matrix	
ö	S	State Transition Matrix	
K	K	Kalman Gain Matrix	
E	E	Measurement Selection Matrix	
T	T	Star Tracker to Body Alignment Matrix	
	RW	Body to Reaction Wheel Alignment Matrix	
	G	Body to Gyroscope Alignment Matrix	

Table 1. List of Symbols

ACKNOWLEDGMENTS

The author would like to thank several people for their contributions to this effort. Dr. F. Landis Markley of NASA Goddard Space Flight Center's Guidance, Navigation and Control Systems Engineering branch provided me with the background for the initial research. His vast insight and experience in all aspects of spacecraft design and control were invaluable to my understanding of attitude determination concepts. Also critical to the research were Girard Manke and Craig Heatwole of The Aerospace Corporation. Their hospitality and enthusiasm in a shared interest provided the focus for this study. The cooperative efforts and support of Marc Becraft and Don Kolve from Boeing are also appreciated. Finally, I would like to thank Professor Brij Agrawal and Hal Titus of the Naval Postgraduate School for their inspiration and guidance.

THIS PAGE INTENTIONALLY LEFT BLANK

I. INTRODUCTION

A. ANGULAR RATE ESTIMATION

The attitude control systems of today's high tech satellites require accurate angular rate knowledge for attitude propagation and control loop damping in order to meet pointing and tracking requirements. Gyroscopes offer varying degrees of precision for direct measurement of angular rates and have been the primary attitude determination sensor used by spacecraft for many years. However, high cost and low reliability has lead users and designers to explore other options. Using dynamic calculations, uncertainty based estimation algorithms or a combination of these two methods, onboard processors can estimate spacecraft angular rates without measuring them directly. Angular rate estimation techniques can be a viable alternative for back-up or even primary attitude determination system in many control schemes.

B. OPTIMAL ESTIMATION

"An optimal estimator is a computational algorithm that processes measurements to deduce a minimum error estimate, in accordance with stated optimality criterion, of the state of a system by utilizing: knowledge of system measurement dynamics, assumed statistics of system noises and measurement errors, and initial condition information." [Ref. 1] Estimation techniques provide filtering, smoothing and prediction of state variables in an imperfect model based on imperfect measurement update data. The most common optimal estimator used in stochastic systems is the Kalman filter. The dynamic model error and measurement error are assumed as zero mean Guassian white noise processes with known covariance. Estimators are commonly used even in systems where all state variables required by controller can be measured.

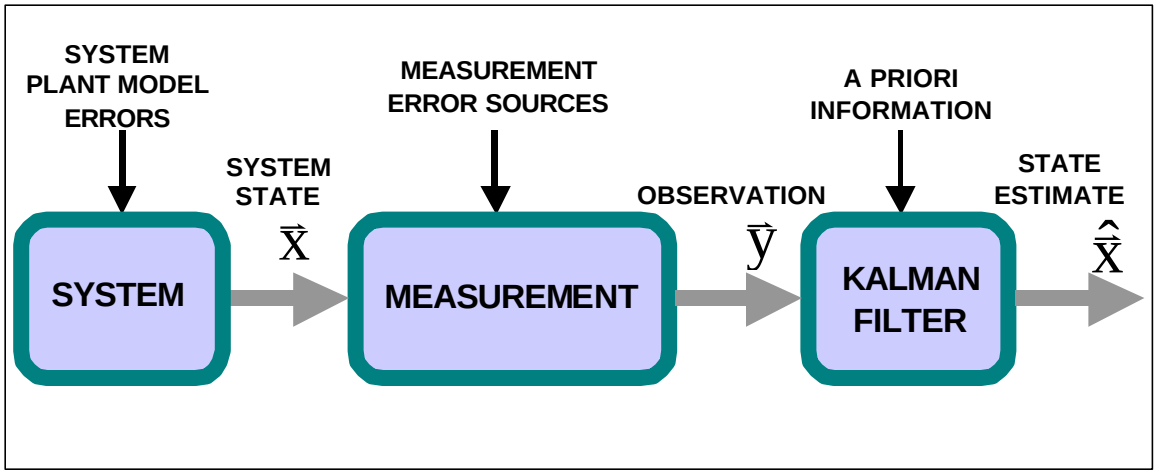

Figure 1. Basic Kalman Filter Block Diagram

Maybeck identifies three basic reasons why deterministic methods are insufficient for describing real systems. First, no mathematical model is perfect. There are always effects that are necessarily neglected to make the model practical and even modeled effects are only approximations to what is physically occurring. Second, dynamic systems are driven not only by control inputs but also by disturbances which we can neither control nor model deterministically. Lastly sensors do not provide perfect and complete data. [Ref. 2]

An important advantage of using an optimal estimator such as the Kalman filter is that the attitude determination output does not affect the controller design. Therefore the development of an optimal controller can be accomplished independently. An attitude control algorithm optimized for ideal state inputs will remain optimized with state estimates provided by an optimal estimator.

C. ANGULAR RATE ESTIMATION FROM VECTOR MEASUREMENTS

The concept of using attitude sensor data to produce an estimate of spacecraft angular rate without gyroscopes is not new. Gyroless attitude and angular rate estimation has been a prime concern for small inexpensive spacecraft that do not carry gyroscopes but still require rate information for attitude propagation and control. Estimation techniques also provide options for complex spacecraft that require back-up control modes in the event of gyro failures. The problem of angular rate estimation can be

treated separately from attitude determination. Several reliable algorithms have been developed that produce angular rate using on-board processors.

It is possible to extract angular rate directly from time derivatives of measured vectors resolved in the body coordinate frame and known in an inertial frame from a model or almanac data. This technique, however, requires at least two non-parallel vector measurements. It also exhibits time lag and produces very noisy data since the algorithms depend on derivatives of already noisy measurements. A better estimate of angular rate can be achieved by treating the problem as stochastic. For this method an estimating filter is applied that uses dynamic equations of motion to take advantage of past data in a recursive sense. This method has the additional advantage of being able to update rate estimates at time steps when only one vector measurement is available. The vector derivative is treated as a noisy measurement update to a Kalman rate estimator.

A Kalman filter requires a linear state-space dynamic model but the dynamics of a spacecraft in the rotating body coordinate frame are coupled and nonlinear. Attitude determination schemes deal with this problem in different ways. Several methods have been proposed for interlacing two or three linear Kalman filters together to capture the nonlinear dynamics [Ref. 3]. It is shown that the coupled equations of motion can be written as a linear combination of the spacecraft angular rate and two other newly defined vectors whose components are nonlinear combinations of the angular rate vector elements. The differential equations for each of these new vectors can be written as linear combinations of the other and the angular rate. Adding white noise vectors to these new equations of motion produces a set of three stochastic linear models that can be used in separate Kalman filters. The filters are interlaced with their estimated outputs treated as deterministic inputs to each other.

An effective method of dealing with non-linear dynamics is presented for use by the Pseudo-linear Kalman filter (PSELIKA) and the state-dependent algebraic Riccati equation filter (SDARE) [Ref. 4]. For these unique rate estimation techniques the equation of motion is transformed to express the nonlinear terms in angular rate as a product of a matrix whose elements depend on the components of the angular rate vector and the angular rate vector itself. The pseudolinear Kalman filter or PSELIKA is

implemented as an ordinary discrete Kalman filter with a time dependent state transition matrix whose angular rate dependent elements are formed from the current estimate of angular rate. The SDARE or state-dependent algebraic Riccati equation filter is also implemented as a discrete Kalman filter derived from the same representation of the dynamic equation. The Kalman gain used in this filter is computed from the solution of an algebraic Riccati equation involving the angular rate dependent matrix. This eliminates the need to propagate and update the filter state covariance which is normally used in the gain calculation.

The pseudolinear filter concept can be extended to use quaternion measurements. In the attitude determination system on board the Rossi X-Ray Timing Explorer (RXTE) satellite advanced star tracker software directly provides information in the form of quaternions [Ref. 5]. The same propagation algorithm is used with measurement updates in the form of quaternions. Since the device yielding the attitude measurement also conducts a star search and identification process a time delay is introduced. Two algorithms are presented for overcoming this delay problem.

D. FULL ORDER ESTIMATORS

It is not necessary to treat the problem of angular rate estimation separately from attitude determination. In fact, attitude sensor data also requires filtering to smooth out measurement noise and produce a clean attitude estimates. High precision control laws generally require both attitude and angular rate information. These components make up the full system state vector.

Full order estimators produce optimal state estimates in the case where imperfect measurement data related to all of the modeled states is continuously available. Spacecraft with a triad of rate gyroscopes and attitude sensors have the required state measurements but the bandwidth of the attitude sensors is normally too low for the control system. Additionally, there may be periodic gaps in sensor coverage and certain sensors do not provide reliable attitude information in all three orthogonal dimensions. Therefore standard full order state estimators are generally not used.

In most practical implementations of gyro-based attitude control systems rate information is used in the propagation stage of an attitude estimator based on kinematic equations. The estimator utilizes discrete vector observations, resolved in both body-fixed coordinates and a reference frame, to estimate spacecraft attitude and gyro drift rates.

In an ideal attitude determination system where perfect knowledge of the spacecraft angular rates is available, the accuracy of the kinematic model for determining attitude is limited only by the processor time step and the initial attitude state. Attitude sensors can be used to periodically reinitialize the kinematic model but the data they provide is discontinuous and corrupted by environmental effects and sensor design imperfections.

In real attitude determination systems, the source of angular rate information may be noisy as well as biased, as is the case with spacecraft gyroscopes. This results in additional errors in the spacecraft attitude determination system. For control systems where attitude and angular rate information is critical, optimal estimation techniques are employed to combat the effects of model and sensor inaccuracies. As gyros degrade the estimator can be made more robust to plant error at the expense of attitude determination accuracy. At some point the gyro outputs may become too erratic to meet control system requirements.

E. REDUCED ORDER ESTIMATORS

Obtaining satellite angular rate estimates without the use of rate gyroscopes or other deterministic rate data can be accomplished with a reduced order estimator. This class of filters produces estimates of all modeled state variables when only a subset is directly related to the measurement data. In this case, attitude sensor information is available but no direct rate measurement is performed. Since gyro data is not available no update to the spacecraft rate is available between attitude measurements.

The reduced estimator Kalman filter is formulated from the state space dynamic equations of motion linearized about the current estimate of state. Again, for spacecraft attitude control the state vector includes both the attitude and angular rate. The

deterministic inputs to the model are the known externally applied moments usually consisting only of control torques. Unmodeled disturbances and other dynamic effects must be accounted for by a robust plant noise model. The estimates of attitude and angular rate are propagated forward by the dynamic model with discrete corrections from the attitude sensors.

The performance of the reduced Kalman estimator can be improved by including higher order dynamic effects in the system plant model and including disturbance torques as deterministic inputs. However this costs extra processing power, requires additional sensors and cannot account for all of the unknowns. Additional dynamic complexities are introduced in multi-body satellites that have time varying moments of inertia, changing centers of mass and flexibility modes. Determining the magnitude and effects of disturbances and modeling simplifications for a particular spacecraft is an important design consideration that often requires rough calculations, simulation and engineering judgment. In general, since disturbances are of low amplitude and low frequency compared to control torques, their effects can be accounted for as plant error by the filter.

One approach that avoids the use of the typically uncertain dynamic model altogether is to treat the spacecraft as a noncooperative target whose rotation must be tracked by a stochastic estimator [Ref. 6]. This concept is borrowed from tracking theory where it has been widely used to estimate target motion. This algorithm adds angular acceleration to the state vector and substitutes attitude states with the integrated rate parameters to formulate a nine state linear Kalman filter. Since this set of variables serves as an approximate third-order attitude parameterization, the size must be controlled by sampling interval. Instead of using dynamics, time propagation of the estimated state variables is performed in the proposed filter by modeling the spacecraft angular acceleration as an exponentially autocorrelated stochastic process and using a polynomial kinematic model.

In reduced order estimators, time steps for state propagation must be kept small to minimize the effects of dynamic simplifications and linearization. The primary limitation of the reduced estimator becomes evident during prolonged intervals between attitude sensor measurement updates. Gaps in attitude sensor coverage must be kept short enough

to ensure that estimator errors do not grow beyond required precision of the attitude control system.

F. STAR SENSOR BASED ESTIMATORS

Bandwidth and accuracy limitations of attitude sensors have precluded the use of reduced order estimators for spacecraft missions with high performance pointing and tracking requirements. Aside from star trackers, most sensors do not provide accurate and stable enough attitude data for high performance tracking requirements. Additionally, these sensors provide discrete measurements unlike gyroscopes which produce nearly continuous data and can be sampled at extremely high frequency limited only by processing capabilities. However, recent advancements in sensor technology suggest that star trackers can provide updates accurately and frequently enough to be considered for use as primary attitude sensors for a wide range of spacecraft missions. Key technological improvements include a wide field of view, high sensitivity, low noise equivalent angles and high bandwidth iteration rate.

It has been proposed that advanced high-bandwidth star sensors can be used as the primary sensors for on-orbit attitude rate determination in place of angular rate gyroscopes [Ref. 7]. A Kalman filter algorithm, using updates from star tracker measurements, is presented that tracks errors in the attitude and angular rate for a kinematic based state space model. The spacecraft angular rate used for attitude propagation is separated into a nominal component and a component due to control and disturbance moments. The algorithm assumes that the bandwidths of the control system and disturbance effects are at least an order of magnitude smaller than the measurement bandwidth. This allows the rate of change in spacecraft angular rate due to unmodeled dynamic effects to be modeled as a first-order Gauss-Markov process. Nonlinear kinematics are used in the attitude propagation phase which is performed external to the estimator. The errors in the this model are then tracked using an ordinary linear discrete Kalman filter.

G. ANALYTICAL RATE DETERMINATION

Another method of obtaining estimates of spacecraft angular rates is through direct calculation from the dynamic equations of motion for the system. This rate calculation is performed in real time based on known, derived and sensed internal parameters of the spacecraft. The software implemented dynamic model can be adjusted to include varying levels of complexity for multi-body spacecraft that operate in different configurations. The Aerospace Corporation has patented one methodology for this process called the "Pseudo Gyro" [Ref. 8].

Information from internal sensors that detect relative orientations and angular rates of momentum exchange devices and appendages are used to continually update the parameters used in the dynamic calculations. These parameters determine component contributions to the system angular momentum and inertia dyadic. Control torques and modeled disturbances are integrated to capture external dynamic effects. Using the total system angular momentum and inertia dyadic and the relative momentum of internal components and appendages from the dynamic model the spacecraft angular rate can be calculated. If the appendage masses are small or their relative motions are slow the spacecraft inertia matrix is slow to change. The moment of inertia calculations can be performed at a lower frequency to save processing time. Cross product effects due to the rotating coordinate frame must also be accounted for in the dynamic model since all measurements are taken in the body frame.

The accuracy of the calculated rate is dependent on the quality of the dynamic model and the sensor information available. Error sources include imperfect knowledge of component or appendage inertia matricies and mass centers as well as relative angular position and rate data from the internal sensors. Often relative rates are not measured directly but derived from position encoders which adds extra noise to the momentum along the axis of rotation of the appendage. Errors are also introduced through external disturbance effects since they cannot be perfectly modeled. All of these dynamic influences effect the model precision in varying degrees. Additionally, due to the finite/discrete processing capabilities of the computer performing the calculations there will be a slight drift over time from the true state even in the case of perfect sensors and

input data. This drift is obviously minimized by increasing the frequency of the discrete model calculations.

H. ATTITUDE ESTIMATION FROM CALCULATED RATE

The rate estimate produced by the dynamic calculations can be fed into a Kalman filter in place measurement data from a gyroscope. The filter receives attitude update information from attitude sensors to produce smoothed attitude reference and angular rate error estimates to enhance satellite attitude determination accuracy. The plant error introduced into the filter is a combination of all the internal sensor and modeling errors that are used as inputs to the dynamic model. All known sensor biases must be incorporated into the plant model since the Kalman filter assumes errors to be zero mean Gaussian. Depending on different modes of operation, different plant noise models may be required for acceptable filter performance. Normally, filters that receive measurements from gyroscopes are designed to track gyro biases which remain relatively constant in the body frame. The rate error from the dynamic estimate, however, exhibits different characteristics. Since the dynamic model is external to the Kalman filter higher order effects can be more easily incorporated into the dynamics but onboard processing capability may still limit the complexity.

I. PURPOSE

The objective of this study is to develop and evaluate a practical attitude and rate estimation scheme for a multi-body spacecraft attitude control system that incorporates both real time angular rate calculation from the system dynamic model (dynamic gyro) and a Kalman filter estimator with attitude sensor updates provided by star trackers. It is hypothesized that acceptable attitude control performance can be realized by maneuvering multi-body spacecraft without hardware gyroscope data using this methodology.

The evaluation of this approach is performed through simulation using a model developed in SIMULINK. A MATLAB script file is used to set up the necessary initialization parameters and system specifications. Simulation results are presented graphically in MATLAB plots. The performance of the developed gyroless attitude

determination system is compared to a conventional gyro-based system that uses the same Kalman filter estimation algorithm and attitude updates. Results are also presented that analyze the affects of several major error sources on the performance of this dynamic gyro based attitude determination system.

II. SIMULATION OVERVIEW

The evaluation and analysis of attitude determination scheme proposed in this thesis is done through modeling and simulation. The context for the development of the attitude determination system is a multi-body attitude control system for a maneuvering spacecraft. An attitude simulation model for the spacecraft that includes vehicle dynamics, determination and control subsystems as well as modeled error sources is developed using MATLAB/SIMULINK. An overview of the simulation and top level subsystems is presented in this chapter. Subsequent chapters provide the descriptions of the subsystems and derivation of the equations on which the model is based. In the following chapters, actual SIMULINK diagrams are presented that show the implementation of associated subsystems.

A. CONCEPTUAL ATTITUDE SIMULATION MODEL

A conceptual representation of the simulation developed for this study is illustrated in Figure 2.

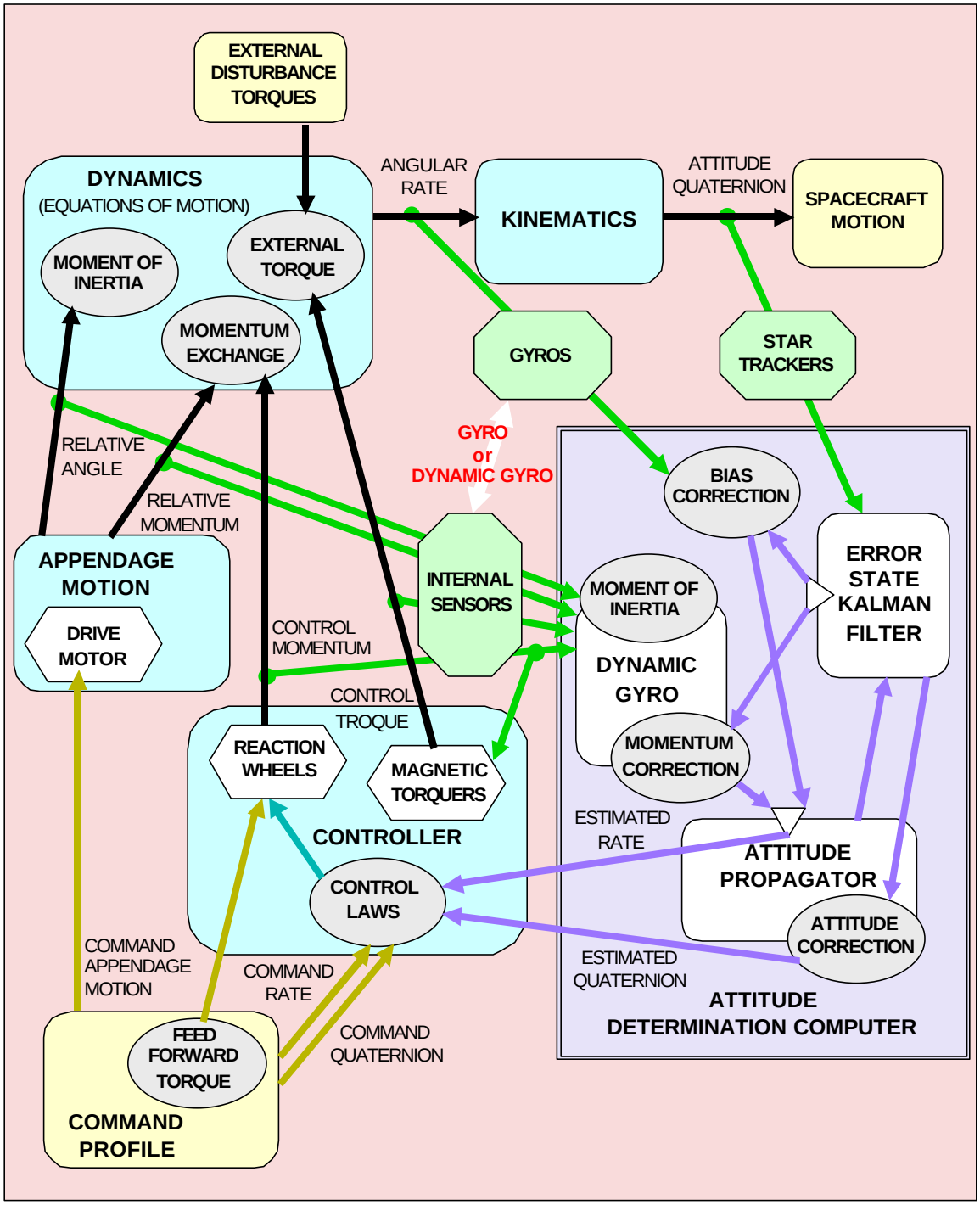

Figure 2. Conceptual Attitude Simulation Block Diagram

The model is divided into subsystems represented in color shaded blocks. This breakdown reduces the complexity of the overall model into manageable segments to aid in design and analysis. Arrows indicate the dynamic coupling and flow of data between subsystem blocks. The top level SIMULINK diagram that implements the concept is shown in Figure 3.

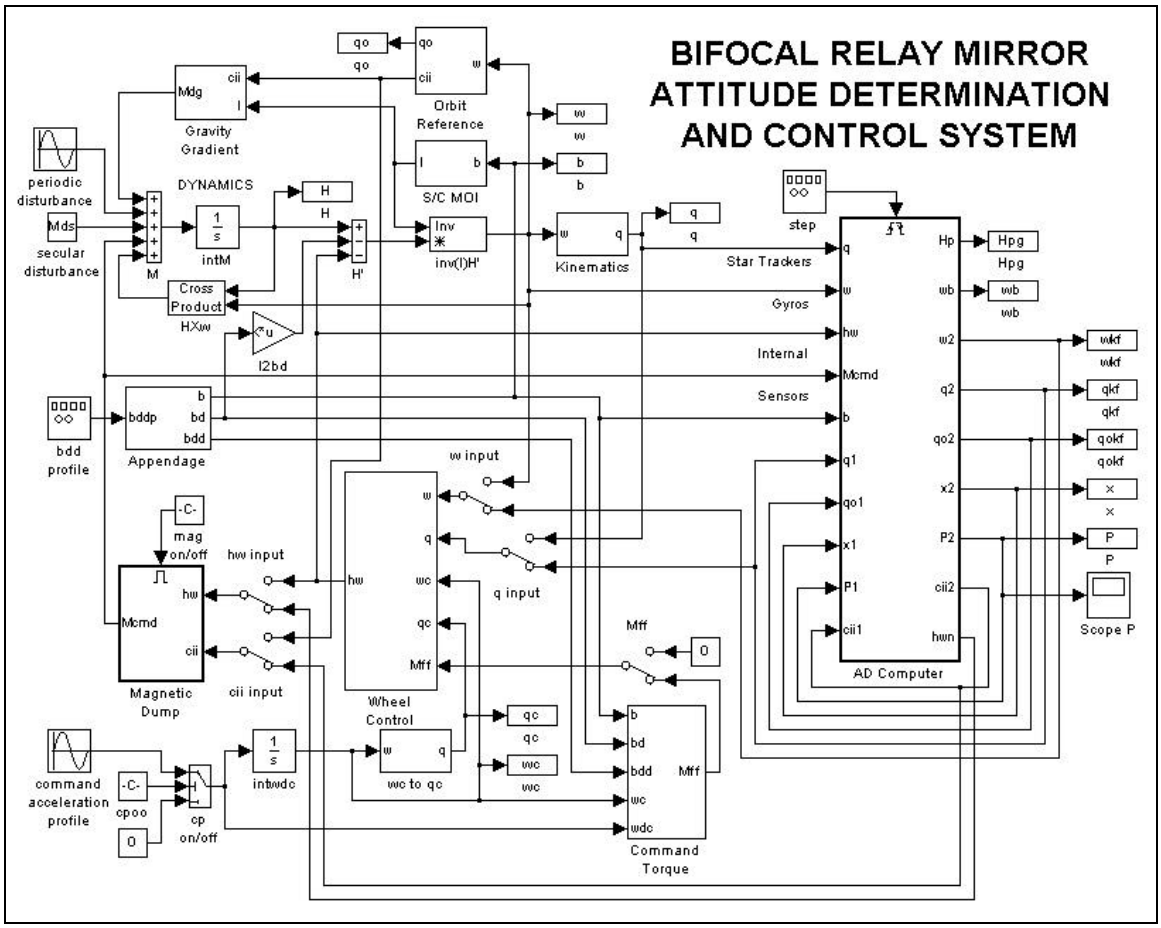

Figure 3. Top Level SIMULINK Attitude Simulation Model

B. SPACECRAFT MOTION

The actual spacecraft attitude motion is simulated in the rotational dynamics and kinematics subsystems with inputs and outputs represented by solid black lines. Relative motion of the secondary body or appendage is treated in a separate subsystem with dynamic effects coupled into the overall spacecraft motion through momentum exchange directly related to the drive motor rate. Dynamic effects of reaction wheel control are also realized through momentum exchange. Magnetic control effects are input to the

spacecraft dynamics as external torques along with modeled and approximated disturbance torques. The relative appendage motion also causes changes in the spacecraft's moments of inertia used in the dynamic model. The kinematics subsystem propagates the actual spacecraft attitude quaternions referenced to an inertially fixed coordinate frame.

C. CONTROL SYSTEM

Primary spacecraft attitude control is conducted through momentum exchange with reaction wheels. The reaction wheel commands are based on control laws and up-linked feed forward torque command profile. The control laws use errors between the measured and commanded (desired) spacecraft angular rates and attitude quaternions. The relative momentum generated in the wheels is subtracted from the spacecraft momentum in the dynamics subsystem. Magnetic torques are generated based on reaction wheel momentum build up when the system is set for momentum dumping. These torques are directly applied in the spacecraft dynamics block.

D. ATTITUDE DETERMINATION SYSTEM

The attitude determination subsystem is of primary concern in this thesis. It incorporates the dynamic modeling concept and an error state Kalman filter in order to correct for attitude propagation errors. The option of using modeled mechanical gyros to determine spacecraft angular rate is also maintained in order to allow comparison simulations to be conducted. The concept of using a dynamic model for analytical rate determination will be referred to in the sequel as the dynamic gyro.

The attitude determination computer simulation uses a trigger to control the bandwidth of discrete calculations. The basic data flow within the attitude determination computer is shown in the large rectangular subsystem block in Figure 2. The equivalent SIMULINK diagram that implements this subsystem is shown in Figure 4.

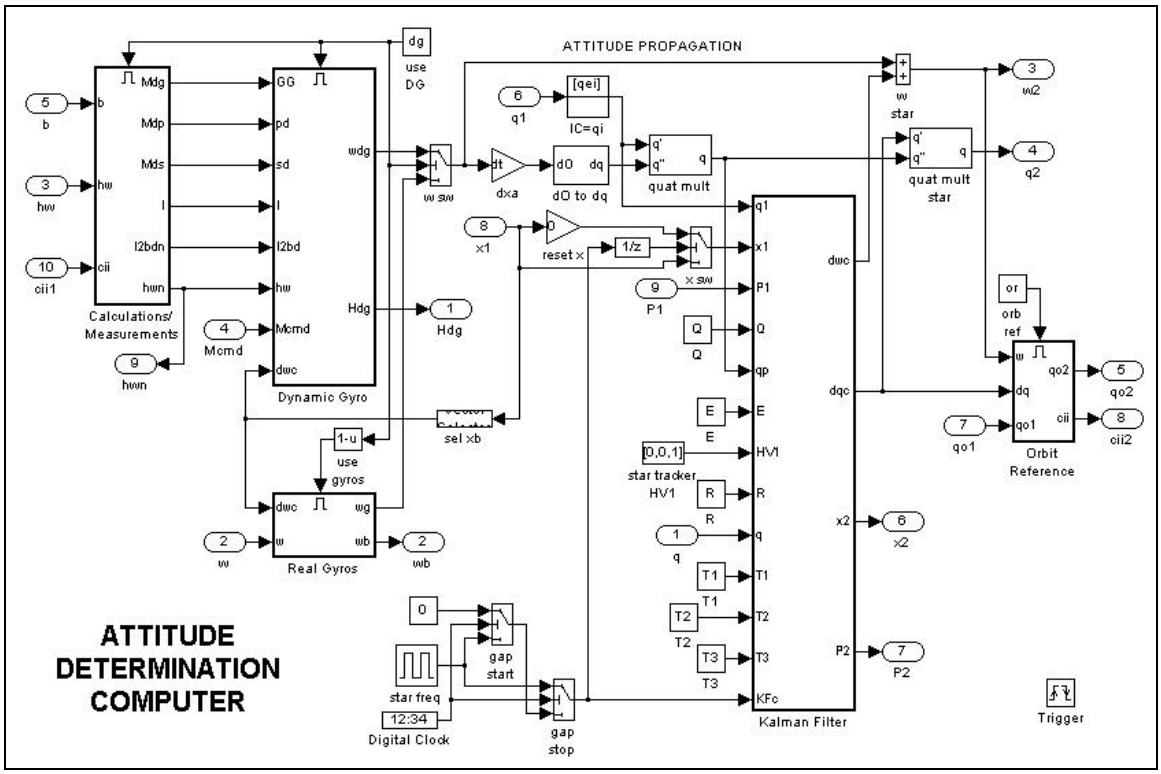

Figure 4. SIMULINK Attitude Determination Subsystem

Random noise and drift rates are added to the actual angular velocity vector for the simulated rate input of the mechanical gyro option. Bias corrections from the Kalman estimator are applied to the angular rate before it is used in the attitude propagator. When the dynamic gyro option is simulated the angular rate is analytically determined from measured and known spacecraft parameters fed into a discrete dynamic model. Artificial errors and noise are applied to measured and derived parameters though internal sensor models. Momentum corrections to the dynamic gyro are derived from Kalman filter updates. The calculated rate is then supplied to the attitude propagator.

The error state Kalman filter algorithm depends on updates generated by star tracker measurements. A star tracker model is used to produce artificial noise corrupted horizontal and vertical measurements related to the star tracker orientation. The Kalman filter tracks rate errors for bias correction of gyro measurements or momentum corrections for the dynamic gyro. It also produces attitude corrections that are applied to the attitude propagator output.

The attitude Propagator uses discrete kinematics to convert angular rate to quaternion attitude. These estimated parameter are then used by the attitude control algorithm to complete the feedback loop.

III. DYNAMICS AND CONTROL

As three-axis stabilized spacecraft become more technologically advanced, their operations require more slewing maneuvers and their dynamic complexities increase. This often leads to multiple rigid or flexible components that have independent pointing and tracking requirements. Complex satellites often consist of a primary payload that demands strict pointing control while directional telemetry and command antennas or secondary payloads are controlled independently for other functions such as tracking a ground station throughout its maneuvers.

Here we consider the dynamics of a spacecraft that consists of a primary body with momentum exchange control devices and a coupled rigid secondary body or appendage. The secondary body rotates with one degree of freedom relative to the spacecraft about an axis through the centers of mass of both bodies. Under these conditions, the position of the spacecraft center of mass remains stationary during appendage relative motion.

A. BIFOCAL RELAY MIRROR SATELLITE DYNAMICS

The example spacecraft for which the equations of motion are derived is the Bifocal Relay Mirror satellite shown in Figure 5. This spacecraft is designed to receive laser energy from a ground station through a receive telescope and to redirect it through an optically coupled transmit telescope to a different point on the ground. The primary body is the transmit telescope and the rigidly attached spacecraft bus while the smaller receive telescope is treated as the secondary body or appendage. Weight and balance design ensures that the centers of mass of the two bodies lie close to the coupled axis of rotation so that the system center of mass is nearly constant during relative motion. Pointing control of the spacecraft is accomplished with reaction wheels while a drive motor is used to control the relative angle between the transmit and receive telescopes.

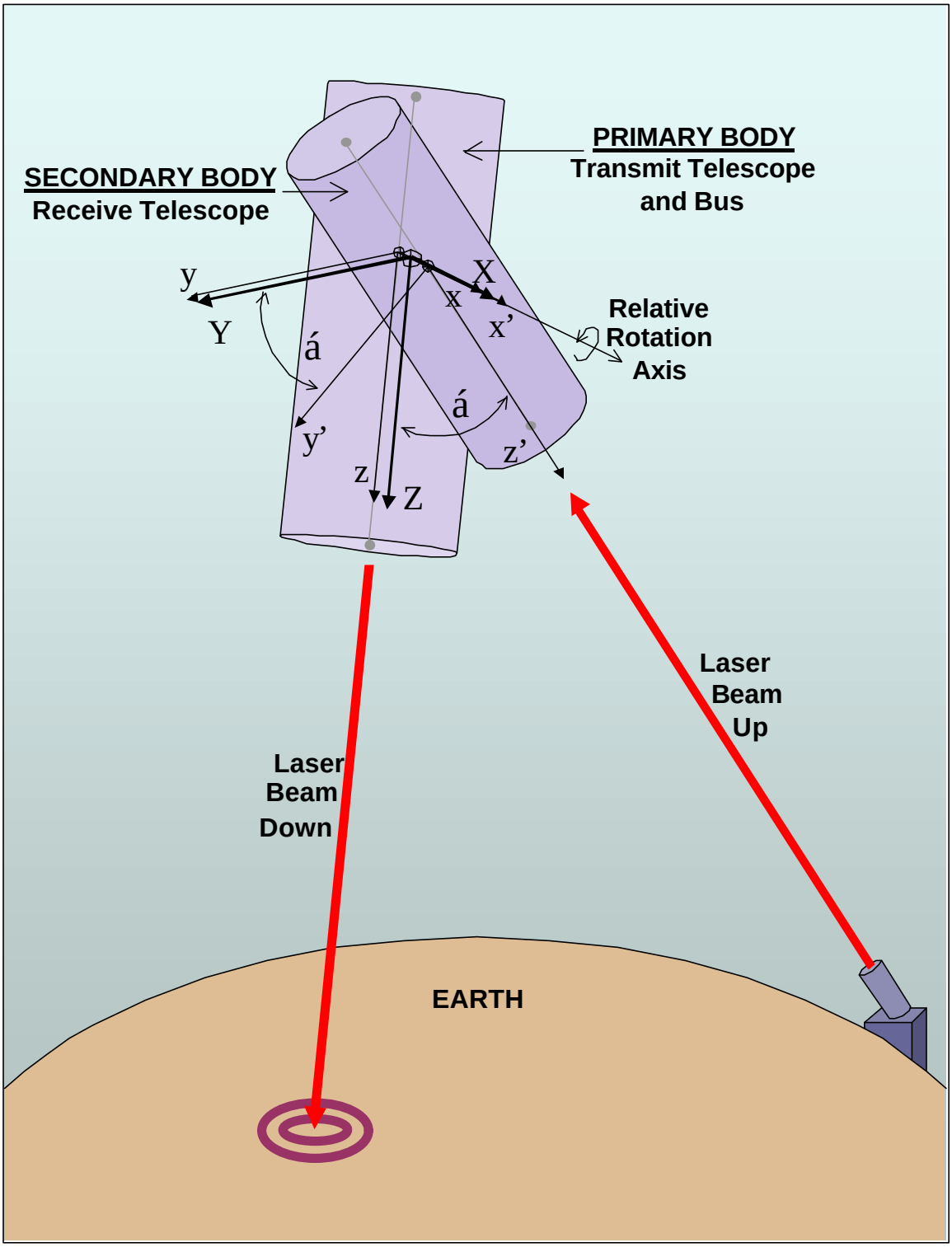

Figure 5. Bifocal Relay Mirror Satellite

There are three coordinate systems defined for the development of the dynamic equations. These coordinate frames are depicted in the system diagram shown in figure x. The xyz coordinate system is fixed to the primary body with the origin at its center of mass. The x-axis is oriented parallel to the axis of rotation between the primary and secondary bodies and the z axis is parallel to the optical axis of the telescope. The y axis is defined such that the xyz coordinate system is a right-handed mutually orthogonal frame. The x'y'z' coordinate system is similarly oriented to the secondary body with its origin at the center of mass. The x and x' axes remain parallel during appendage motion while the angular displacements of the y' and z' axes from the y and z axes respectively are defined by the relative rotation angle á. The equations of motion are derived for the spacecraft body coordinate system, XYZ, which is parallel to xyz frame. Its origin is at the total spacecraft center of mass. Unit vectors along the X, Y, and Z spacecraft body axes are given by $\vec{i}$, $\vec{j}$ and $\vec{k}$ respectively.

1. Rigid Body Equations of Motion

The angular equations of motion are derived from the application of Newton's second law to rotational dynamics. In the general case the equation of motion defined in an inertial frame for a rigid body about an arbitrary point P is given by

$$\vec{M}_P = \dot{\vec{H}}_P + \int_m \tilde{n}_c \ddot{\vec{r}}\, dm \qquad (3.1)$$

where $\vec{M}_P$ is the net external torque applied to the body about P, $\vec{H}_P$ is the angular momentum of the body about P, $\vec{r}_c$ is the position of the center of mass relative to P, $\tilde{n}_c$ is the vector from the center of mass to the position of dm in the body, and dm is an incremental unit of mass within the body

If point P is coincident with the body center of mass, then $\tilde{n}_c = \vec{0}$ and the equation simplifies to

$$\vec{M} = \dot{\vec{H}} \qquad (3.2)$$

Equation (3.2) applies in inertial reference frames. To extend it to body coordinates where it can be employed, we need to understand the concept of vector derivatives in a

rotating coordinate frame. If the body frame rotates relative to an inertial reference frame with angular velocity $\tilde{u}$ then the derivative of any vector $\vec{A}$ in inertial coordinates can be related to the derivative in the rotating body coordinates by

$$\dot{\vec{A}}\Big|_I = \dot{\vec{A}}\Big|_B + \tilde{u} \times \vec{A}\Big|_B \tag{3.3}$$

Applying this relation to the angular momentum, the equation of motion for a rigid body in rotating body coordinates becomes

$$\vec{M} = \dot{\vec{H}} + \tilde{u} \times \vec{H} \tag{3.4}$$

2. Multi-Body Equations of Motion

For the two body Bifocal Relay Mirror system with reaction wheels shown in figure 1, the total system angular momentum in body XYZ coordinates can be written

$$\vec{H} = \vec{H}_{S/C} + \vec{H}_{rel} + \vec{H}_w \tag{3.5}$$

where $\vec{H}$ is the total system angular momentum of the spacecraft, $\vec{H}_{S/C}$ is the angular momentum of the system due to the rotation of the body coordinate frame, neglecting the contribution due to relative motion of the receive telescope and reaction wheels, $\vec{H}_{rel}$ is the angular momentum due to the relative motion of the secondary body, and $\vec{H}_w$ is the angular momentum due to the relative motion of the reaction wheels

Since the Bifocal Relay Mirror spacecraft is approximated as a system of rigid bodies, we can substitute the total system angular momentum, $\vec{H}$, into Equation (3.4) to get the multi-body spacecraft equation of motion

$$\vec{M} = \dot{\vec{H}}_{S/C} + \dot{\vec{H}}_{rel} + \dot{\vec{H}}_w + \tilde{u} \times \left(\vec{H}_{S/C} + \vec{H}_{rel} + \vec{H}_w \right) \tag{3.6}$$

where $\vec{M}$ is the net external torque applied to the spacecraft about its center of mass including all control and disturbance torques.

3. Moments of Inertia

To determine these angular momentums we need to consider the moments of inertia of the spacecraft and it components. We define I_T to be the inertia matrix for the primary body (transmit telescope and bus) about its center of mass in the xyz coordinate frame.

$$I_T = \begin{bmatrix} I_{xx}^T & -I_{xy}^T & -I_{xz}^T \\ -I_{xy}^T & I_{yy}^T & -I_{yz}^T \\ -I_{xz}^T & -I_{zy}^T & I_{zz}^T \end{bmatrix} \tag{3.7}$$

The vector from the center of mass of the primary body to the spacecraft center of mass is given by

$$r_T = x_T i + y_T j + z_T k \tag{3.8}$$

The moment of inertia matrix for the receive telescope, I_R, about its center of mass given in the x'y'z' coordinate frame is given by

$$I_R = \begin{bmatrix} I_{x'x'}^R & -I_{x'y'}^R & -I_{x'z'}^R \\ -I_{x'y'}^R & I_{y'y'}^R & -I_{y'z'}^R \\ -I_{x'z'}^R & -I_{z'y'}^R & I_{z'z'}^R \end{bmatrix} \tag{3.9}$$

The vector from the center of mass of the receive telescope to the spacecraft center of mass is given by

$$r_R = x_R i + y_R j + z_R k \tag{3.10}$$

To align the receive telescope inertia matrix with the spacecraft body coordinate frame a transformation matrix is applied. This time varying matrix is the direction cosine matrix that defines a single rotation. The axis of rotation is parallel to the body X axis and is of magnitude á. The transformation matrix is given by

$$T_X = \begin{bmatrix} 1 & 0 & 0 \\ 0 & \cos(á) & \sin(á) \\ 0 & -\sin(á) & \cos(á) \end{bmatrix} \tag{3.11}$$

The SIMULINK subsystem used to generate this x-axis rotation matrix given an input angle is shown in Figure 6.

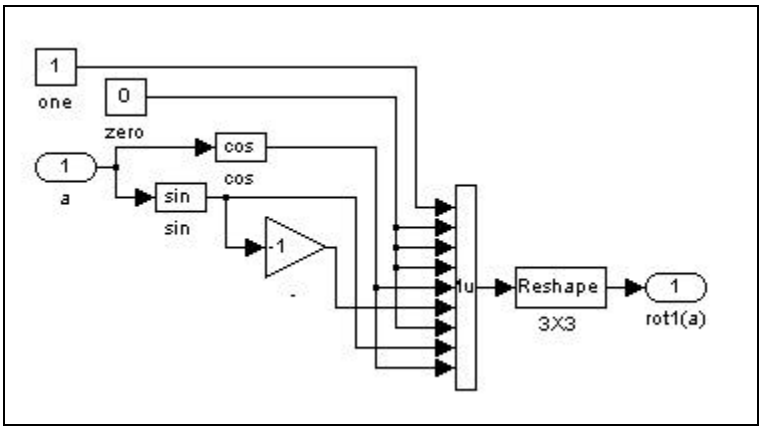

Figure 6. SIMULINK Subsystem Diagram: X-Axis Rotation Matrix

To obtain the total system inertia matrix about the spacecraft center of mass in the body coordinate frame XYZ the parallel axis theorem is applied to the inertia matricies of each body. Additionally the rotation matrix is applied to the receive telescope inertia matrix to align it with the body coordinates. If m_T and m_R are the masses of the transmit telescope and receive telescope respectively the total system inertia matrix is given by

$$I = I_T + m_T \begin{bmatrix} y_T^2 + z_T^2 & -x_T y_T & -x_T z_T \\ -x_T y_T & z_T^2 + x_T^2 & -y_T z_T \\ -x_T z_T & -y_T z_T & x_T^2 + y_T^2 \end{bmatrix} + T_X^T I_R T_X \cdots$$
$$+ m_R \begin{bmatrix} y_R^2 + z_R^2 & -x_R y_R & -x_R z_R \\ -x_R y_R & z_R^2 + x_R^2 & -y_R z_R \\ -x_R z_R & -y_R z_R & x_R^2 + y_R^2 \end{bmatrix} \qquad (3.12)$$

The calculation of the spacecraft system inertia matrix is implemented in the SIMULINK subsystem shown in Figure 7.

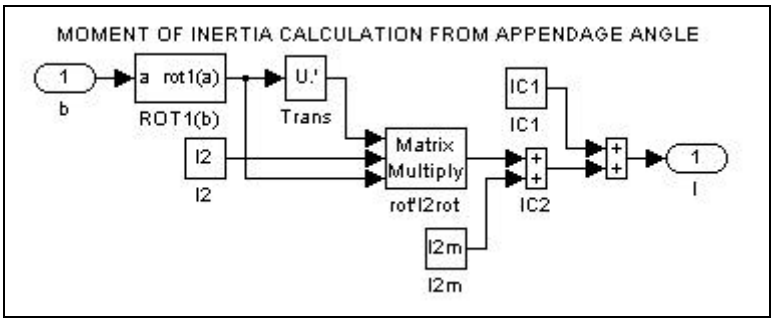

Figure 7. SIMULINK Subsystem Diagram: Spacecraft Moment of Inertia Matrix

a. Rate of Change of Spacecraft Inertia Matrix

All components of the system moment of inertia matrix are constant except $T_X^T I_R T_X$ which varies with the relative rotation angle θ. Therefore the rate of change of the system inertia matrix is given by

$$\dot{I} = \dot{T}_X^T I_R T_X + T_X^T I_R \dot{T}_X \tag{3.13}$$

where $\dot{T}_X = \begin{bmatrix} 0 & 0 & 0 \\ 0 & -\sin(\theta)\dot{\theta} & \cos(\theta)\dot{\theta} \\ 0 & -\cos(\theta)\dot{\theta} & -\sin(\theta)\dot{\theta} \end{bmatrix}$ and $\dot{T}_X^T = \begin{bmatrix} 0 & 0 & 0 \\ 0 & -\sin(\theta)\dot{\theta} & -\cos(\theta)\dot{\theta} \\ 0 & \cos(\theta)\dot{\theta} & -\sin(\theta)\dot{\theta} \end{bmatrix}$. It can be shown that $\dot{I}$ as a function of θ and $\dot{\theta}$ is given by

$$\dot{I}\dot{\theta} = I\begin{bmatrix} 0 & I_{x'y'}^R \sin(\theta) + I_{x'z'}^R \cos(\theta) & \cdots \\ I_{x'z'}^R \sin(\theta) - I_{x'y'}^R \cos(\theta) & 2I_{y'y'}^R \sin(\theta)\cos(\theta) + 2I_{y'z'}^R \cos^2(\theta) - 2I_{y'z'}^R \sin^2(\theta) - 2I_{z'z'}^R \sin(\theta)\cos(\theta) & \cdots \\ I_{y'y'}^R \sin^2(\theta) - I_{y'y'}^R \cos^2(\theta) + 4I_{y'z'}^R \sin(\theta)\cos(\theta) + I_{z'z'}^R \cos^2(\theta) - I_{z'z'}^R \sin^2(\theta) & I_{x'z'}^R \sin(\theta) - I_{x'y'}^R \cos(\theta) & \\ I_{y'y'}^R \sin^2(\theta) - I_{y'y'}^R \cos^2(\theta) + 4I_{y'z'}^R \sin(\theta)\cos(\theta) - I_{z'z'}^R \cos^2(\theta) + I_{z'z'}^R \sin^2(\theta) & 2I_{y'z'}^R \sin^2(\theta) - 2I_{z'z'}^R \sin(\theta)\cos(\theta) - 2I_{y'y'}^R \sin(\theta)\cos(\theta) + 2I_{y'z'}^R \cos^2(\theta) & \end{bmatrix} \tag{3.14}$$

The SIMULINK subsystem diagram that calculates the rate of change of the spacecraft inertia matrix based on appendage relative angular orientation and rate is shown in Figure 8.

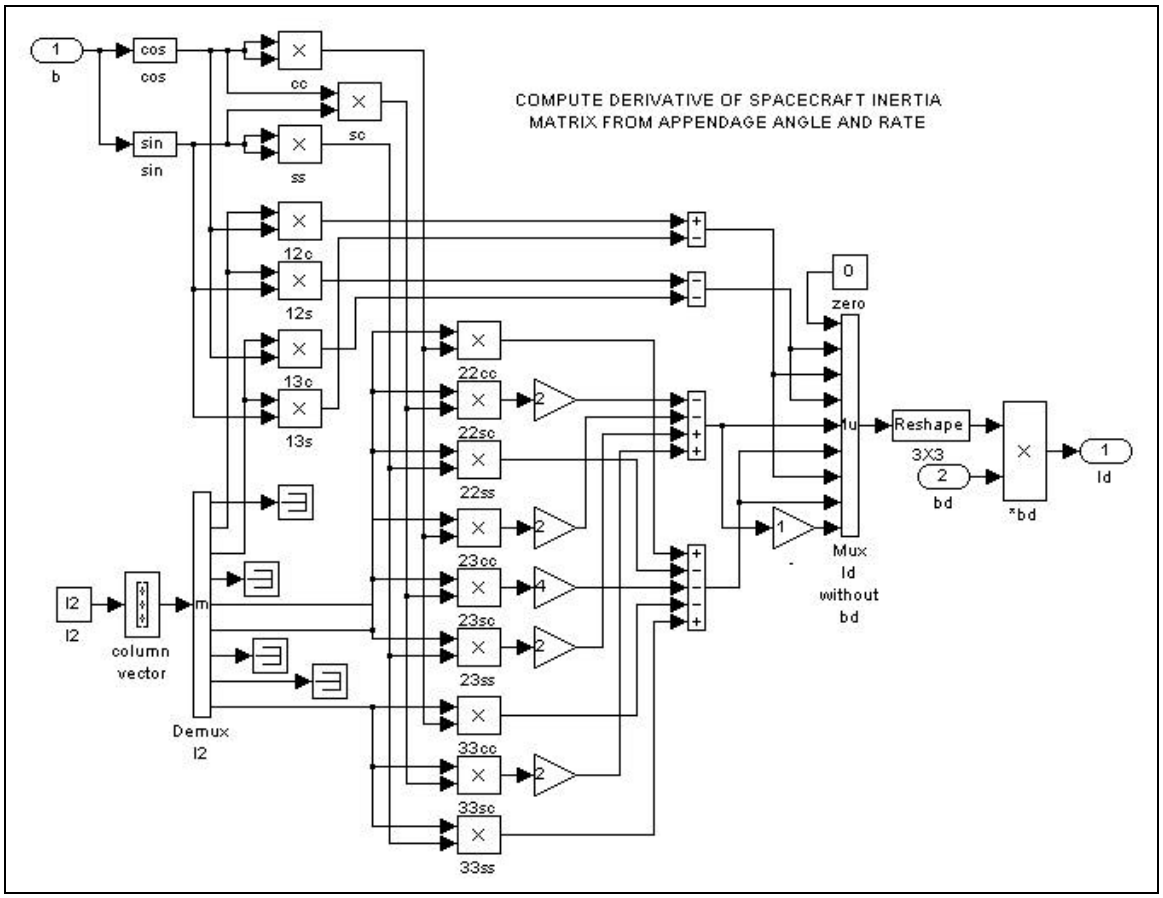

Figure 8. SIMULINK Subsystem Diagram: Rate of Change of Spacecraft Inertia Matrix

4. Angular Velocity

The spacecraft angular velocity is defined by the angular velocity of the primary body with respect to the inertial reference frame. This angular velocity vector is given by

$$\tilde{\omega}_T = \begin{bmatrix} \omega_x \\ \omega_y \\ \omega_z \end{bmatrix} \tag{3.15}$$

The relative angular velocity between the primary and secondary bodies due to the rotation about the body x axis is given by

$$\tilde{\omega}_{rel} = \begin{bmatrix} \dot{\alpha} \\ 0 \\ 0 \end{bmatrix} \tag{3.16}$$

The angular velocity of the receive telescope is equal to the spacecraft angular velocity plus the relative velocity

$$\tilde{\omega}_R = \tilde{\omega}_T + \tilde{\omega}_{rel} = \begin{bmatrix} \omega_x + \dot{\theta} \\ \omega_y \\ \omega_z \end{bmatrix} \tag{3.17}$$

5. Angular Momentum

The components of the total spacecraft angular momentums given in Equation (3.5) can now be defined. The system angular momentum neglecting the momentum due to the relative motion of the receive telescope and the reaction wheels is given by

$$\vec{H}_{S/C} = I\vec{\omega} \tag{3.18}$$

The angular momentum of the receive telescope relative to the spacecraft is given by

$$\vec{H}_{rel} = I_R\vec{\omega}_{rel} \tag{3.19}$$

Substituting Equations (3.18) and (3.19) into Equation (3.5) we get the total system angular momentum

$$\vec{H} = I\vec{\omega} + I_R\vec{\omega}_{rel} + \vec{H}_w \tag{3.20}$$

Substituting this relation into Equation (3.6), the spacecraft equation of motion can be rewritten as

$$\vec{M} = \dot{I}\vec{\omega} + I\dot{\vec{\omega}} + I_R\dot{\vec{\omega}}_{rel} + \dot{\vec{H}}_w + \vec{\omega} \times (I\vec{\omega} + I_R\vec{\omega}_{rel} + \vec{H}_w) \tag{3.21}$$

6. Solving for Spacecraft Angular Rate

To solve for the spacecraft angular rate, $\tilde{\omega}$, we can isolate $\dot{\tilde{\omega}}$ in Equation (3.21) and perform the integration using a computer solver. This however places an unnecessary burden on the processor to continuously calculate the time derivative of the spacecraft moment of inertia. A simpler method is accomplished by first solving for $\vec{H}_{S/C}$. The spacecraft equation of motion is rewritten as

$$\vec{M} = \dot{\vec{H}}_{S/C} + I_R \dot{\vec{\omega}}_{rel} + \dot{\vec{H}}_w + \vec{\omega} \times \vec{\omega} \tag{3.22}$$

which can be solved for $\dot{\vec{H}}_{S/C}$.

$$\dot{\vec{H}}_{S/C} = \vec{M} - I_R \dot{\vec{\omega}}_{rel} - \dot{\vec{H}}_w + \vec{H} \times \vec{\omega} \tag{3.23}$$

After the integration,

$$\vec{H}_{S/C} = \int_t \left(\vec{M} - I_R \dot{\vec{\omega}}_{rel} - \dot{\vec{H}}_w + \vec{H} \times \vec{\omega} \right) dt = \int_t \left(\vec{M} + \vec{H} \times \vec{\omega} \right) dt - I_R \vec{\omega}_{rel} - \vec{H}_w \tag{3.24}$$

the angular rate, $\vec{\omega}$, is obtained from

$$\vec{\omega} = I^{-1} \vec{H}_{S/C} \tag{3.25}$$

Figure 9 shows the SIMULINK diagram for implements the spacecraft dynamics for the Bifocal Relay Mirror attitude simulation. The integration is performed using the Dormand-Prince ode5 solver.

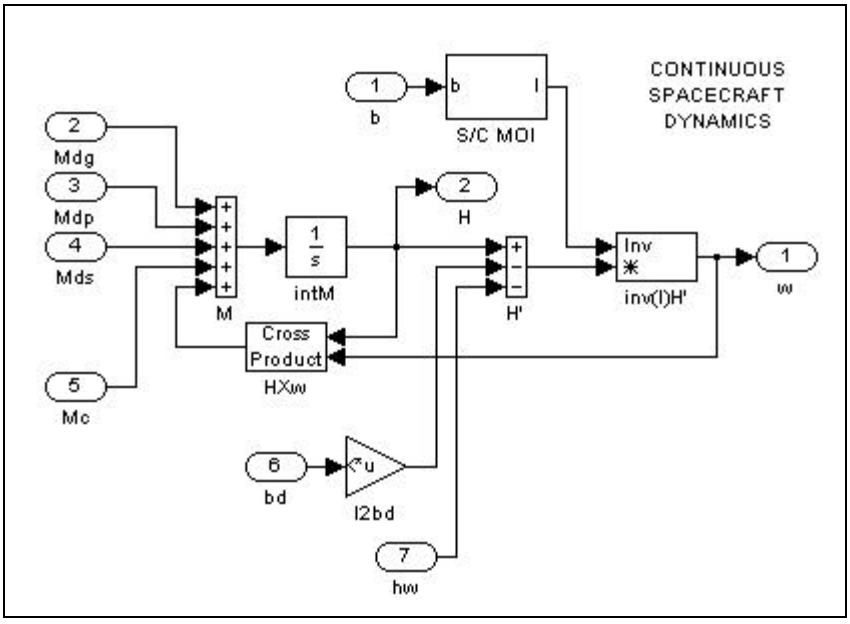

Figure 9. SIMULINK Subsystem Diagram: Spacecraft Dynamics

B. COMMAND

Maneuvering spacecraft often require feed forward command to maintain precise tracking requirements throughout their maneuvers. The Bifocal Relay Mirror satellite must maintain tightly controlled ground tracking by both the transmit and receive

telescopes in order to perform its mission. For this system the envisioned feed forward command will include control torques necessary to maintain a dynamic attitude profile, which includes the relative motion between the primary and secondary bodies, calculated in the absence of disturbances. The spacecraft control laws will be used to correct for errors in the calculated command profile and external disturbances based on errors in spacecraft attitude and angular rate from the attitude determination system.

The estimated spacecraft rotational profile is predetermined prior to the execution of a maneuver and tracking operation. The profile includes the spacecraft body attitude, angular rate and angular acceleration as well as the relative angle, rate and acceleration between the transmit and receive telescopes. The net external torque required to maintain this profile in the absence of disturbances is fed forward to the control devices. This torque can be calculated from the spacecraft equation of motion, Equation(3.21), neglecting the reaction wheel control devices

$$\vec{M}_c = \dot{\vec{I}}_c \vec{\omega}_c + \dot{\vec{\omega}}_c \left(\vec{I}_R + \vec{I}_{elc} \right) + \vec{\omega}_c \times \left(\vec{I}_c \left(\vec{I}_R + \vec{I}_{elc} \right) \vec{\omega}_c \right) \tag{3.26}$$

In this equation the subscript c is used to represent feed forward command. The equivalent SIMULINK subsystem used in the simulation to generate the feed forward command torque is shown in Figure 10.

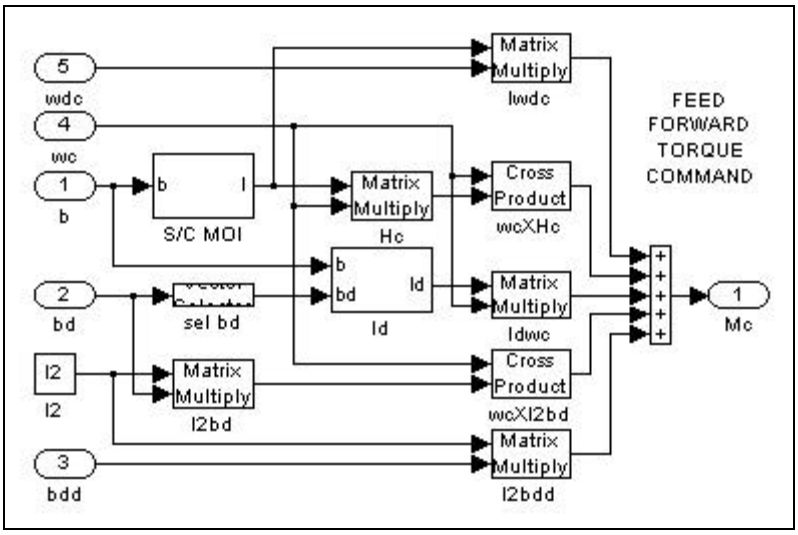

Figure 10. SIMULINK Subsystem Diagram: Feed Forward Torque Command

C. CONTROL

Primary attitude control of the Bifocal Relay Mirror satellite is accomplished with reaction wheels. Four reaction wheels are arranged in a pyramid constellation to achieve redundancy in the event of a single wheel failure. Under normal operations three wheels are operating while the forth is off line. Control torques commands are calculated in body coordinates and then distributed to the three operating wheels.

Torque commands are generated from the feed forward command profile plus the attitude control laws with compensation for the gyroscopic torques generated from the spinning reaction wheels. The simple partial plus derivative type controller is chosen for this satellite. The control laws are based on attitude quaternion and angular rate error as calculated from the outputs of the attitude determination system where the quaternion error is calculated by Equation (4.16) [Ref. 9]. The three body axis wheel control laws are given by

$$\begin{aligned} \dot{H}_{w1} &= K_{q1} q_{E1} \hat{u}_1 + K_{\omega 1} \omega_{E1} \hat{u}_1 \\ \dot{H}_{w2} &= K_{q2} q_{E2} \hat{u}_2 + K_{\omega 2} \omega_{E2} \hat{u}_2 \\ \dot{H}_{w3} &= K_{q3} q_{E3} \hat{u}_3 + K_{\omega 3} \omega_{E3} \hat{u}_3 \end{aligned} \qquad (3.27)$$

More exotic control schemes exist but the optimal state estimates provided by the attitude determination system are simply employed by these control laws.

The control law gains are chosen to minimize steady state errors attitude errors while ensuring that oscillations induced by the attitude control system do not interfere with on-orbit structural modes and payload components. To determine the optimal control gains, attitude control simulations are conducted with a representative maneuvering profiles and external disturbances. The state inputs used by the controller during gain adjustment simulations are perfect attitude and rate knowledge. As explained in Chapter I, the optimal controller can be determined independently from the attitude determination system since its outputs are based on optimal state estimation.

The reaction wheel control subsystem used in the SIMULINK attitude simulation model is shown in Figure 11. Saturation and rate limiting is applied to simulate nonlinear effects in real reaction wheel control systems. The net control torque is determined and

then distributed to the individual reaction wheels based on their orientation within the constellation.

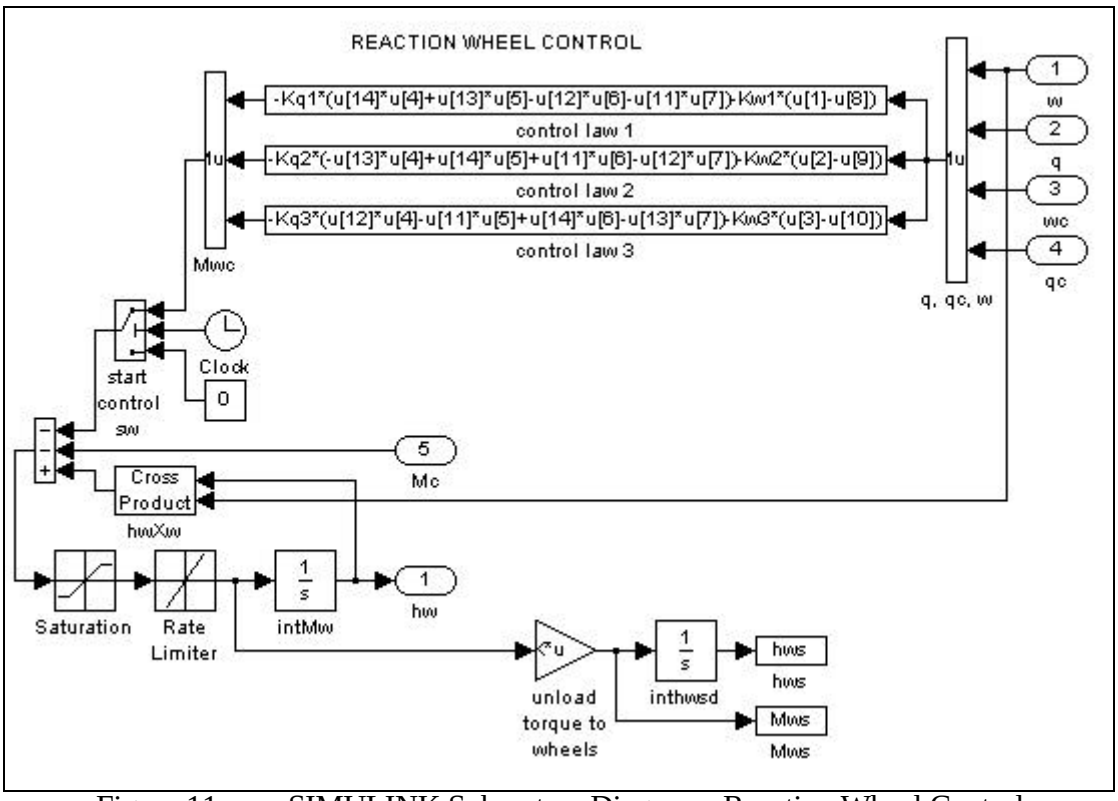

Figure 11. SIMULINK Subsystem Diagram: Reaction Wheel Control

D. DISTURBANCE TORQUES

Representative disturbance torques are simulated in order to observe spacecraft attitude performance in a realistic space environment.

1. Gravity Gradient Torque

At low altitudes the torque induced by gravity gradient on spacecraft without matched body moments of inertia can be significant. A model for the gravity gradient torque on a spacecraft in orbit is given by

$$\vec{M}_G = \frac{3\mu}{R_0^3}\vec{R}_0 \times I\vec{R}_0 \qquad (3.28)$$

where R_0 the distance from the spacecraft center of mass to the Earth's center, $\vec{R}_0$ is the unit vector in that direction given in body coordinates, and I is the total spacecraft

moment of inertia matrix. If the direction cosine matrix from the orbit to body frame, ${}^{B}C^{O}$, is known, $\vec{\mathrm{R}}_0$ is given by

$$\vec{\mathrm{R}}_0 = {}^{B}C^{O}\begin{bmatrix}0\\0\\1\end{bmatrix} = \begin{bmatrix}c_{13}\\c_{23}\\c_{33}\end{bmatrix} \tag{3.29}$$

In the attitude simulation model, the orbital reference frame direction cosine matrix components are propagated using the spacecraft angular rate relative to the rotating orbit frame from an initial orientation. The relative orbital rate is determined from the inertial rate minus the rate of rotation of the orbit frame. The SIMULINK subsystem for propagating the orbital reference is shown in Figure 12.

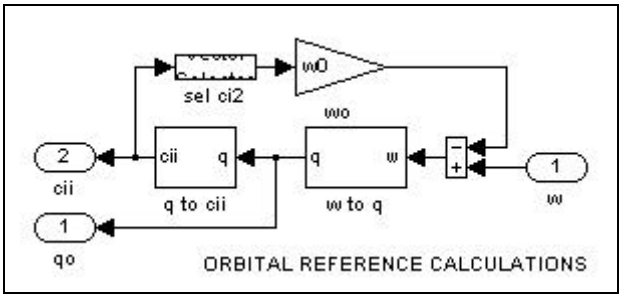

Figure 12. SIMULINK Subsystem Diagram: Orbital Reference Propagation

Using the orbital reference coordinates the gravity gradient torque can then be written

$$\vec{\mathrm{M}}_{\mathrm{G}} = \frac{3\grave{\imath}}{\mathrm{R}_0^3}\begin{bmatrix}c_{13}\\c_{23}\\c_{33}\end{bmatrix} \times \mathrm{I}\begin{bmatrix}c_{13}\\c_{23}\\c_{33}\end{bmatrix} \tag{3.30}$$

Figure 13 shows the SIMULINK subsystem that models the gravity gradient torque based on the orbital reference frame direction cosine matrix.

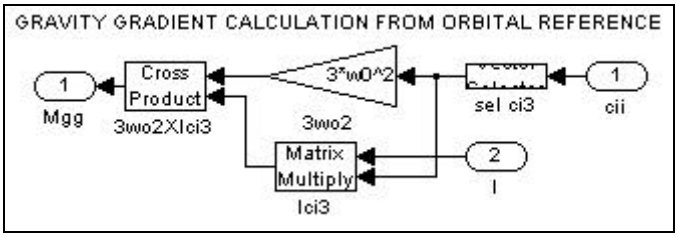

Figure 13. SIMULINK Subsystem Diagram: Gravity Gradient Torque Model

2. Other External Disturbance Torques

Other disturbance torques include those due to unbalanced solar pressure, magnetic interactions, and aerodynamic drag effects. These disturbances are not as easily modeled as gravity gradient but their characteristics and magnitudes are important considerations in the design of spacecraft attitude control systems. In the simulation model, secular and slowly varying periodic moments are introduced in each body axis to account for these unknown disturbances. Worst case magnitudes are chosen based on orbit profile and spacecraft characteristics to ensure robust control design.

E. MAGNETIC MOMENTS

The magnetic moment imparted on the spacecraft by the earth's magnetic field is dependent upon the magnetic field strength, $\vec{B}$, and the spacecraft's magnetic dipole vector, $\vec{m}$. The magnetic moment is given by

$$\vec{M}_m = \vec{m} \times \vec{B} \tag{3.31}$$

1. Magnetic Field Model

Highly accurate models of the earth's magnetic field have been developed but a simple dipole model is adequate for the purposes of this simulation. This approximation assumes a simple dipole magnetic field tilted 11 degrees from the earth's spin axis. The earth's magnetic field is a function of the earth's unit dipole vector, $\vec{M}$, the distance from the center of the earth to the center of mass of the spacecraft, R, and the unit vector in that direction, $\vec{R}$. The magnetic field is given by

$$\vec{B} = \frac{K}{R^3}\left[3\left(\vec{M} \cdot \vec{R}\right)\vec{R} - \vec{M}\right] \tag{3.32}$$

where K is the earth's magnetic field constant equal to 7.943 x 10^{15} Nm^2/a^2. Using classical orbital elements it can be shown that the components of the magnetic field vector in orbital coordinates are given by

$$\vec{B}_O = \frac{K}{R^3}\begin{bmatrix} \cos(n)\left(\cos(\varepsilon)\sin(i) - \sin(\varepsilon)\cos(i)\cos(u)\right) - \sin(n)\sin(\varepsilon)\sin(u) \\ -\cos(\varepsilon)\cos(i) - \sin(\varepsilon)\sin(i)\cos(u) \\ 2\sin(n)\left(\cos(\varepsilon)\sin(i) - \sin(\varepsilon)\cos(i)\cos(u)\right) + 2\cos(n)\sin(\varepsilon)\sin(u) \end{bmatrix} \tag{3.33}$$

where ν is the true anomaly of the spacecraft, ε is the magnetic dipole tilt angle, i is the orbit inclination, and u is the angle of the magnetic dipole normal to the line of ascending nodes. The SIMULINK subsystem that propagates the earth magnetic field vector with the orbital reference is shown in Figure 14.

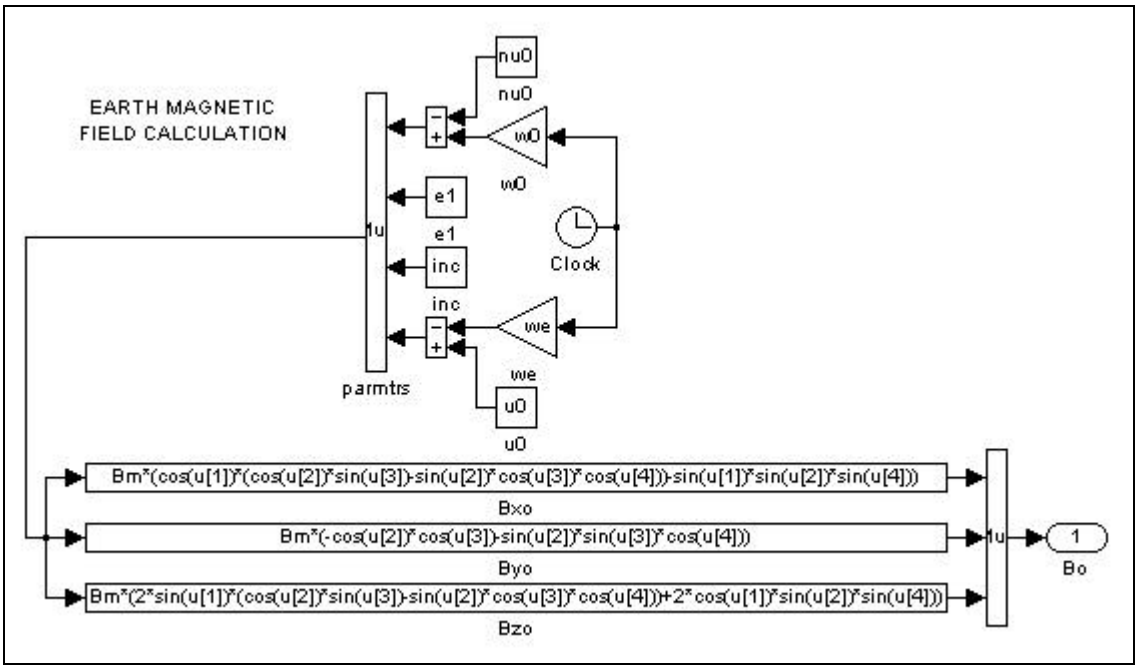

Figure 14. SIMULINK Subsystem Diagram: Earth Magnetic Field Vector in Orbital Coordinates

The magnetic field vector can be transformed to the spacecraft body coordinates with the direction cosine matrix.

$$\vec{B}_B = {}^{B}C^{O}\vec{B}_O \tag{3.34}$$

where ${}^{B}C^{O}$ is the transformation matrix from the orbit coordinate frame to the body frame. Figure 15 shows the subsystem that realizes this transformation using direction cosine matrix components.

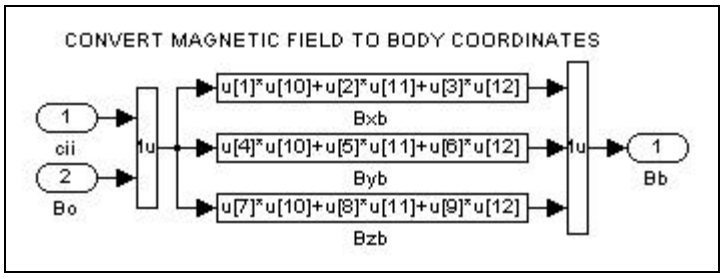

Figure 15. SIMULINK Subsystem Diagram: Magnetic Field Conversion to Body Coordinates

2. Magnetic Control Torque

Using magnetic torquers a spacecraft magnetic dipole can be generated to react with the earth's magnetic field to produce a control torque. In this simulation magnetic control can be used to help desaturate the reaction wheels. The control law for magnetic dumping of reaction wheel momentum is given by

$$\vec{M}_{cmd} = -k\left(\vec{B}_B \times \vec{H}_w\right) \tag{3.35}$$

where k is the magnetic torquer gain. Figure 16 shows the SIMULINK subsystem that simulates the magnetic dumping control torque. Saturation is added to simulate nonlinear effects in the torque rods.

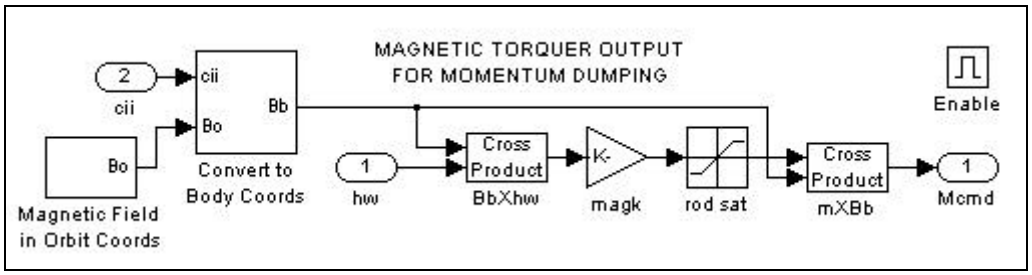

Figure 16. SIMULINK Subsystem Diagram: Magnetic Torquers for Momentum Dumping

Magnetic torquers can also be used for attitude control. The control laws for the torquers to produce a desired control moment, $\vec{M}_{CD}$, on the spacecraft is given by

$$\vec{M}_{cm} = \frac{\vec{B}_B \times \vec{M}_{CD}}{\left|\vec{B}_B\right|^2} \tag{3.36}$$

THIS PAGE INTENTIONALLY LEFT BLANK

IV. ATTITUDE REPRESENTATION AND KINEMATICS

There are many ways of describing the orientation of one coordinate system relative to another. The most common descriptors used in spacecraft attitude determination include Euler angles, direction cosine matricies and quaternions, also known as Euler parameters [Ref. 10]. Euler angles provide a convenient way to represent attitude and are usually the easiest to visualize. However, singularities arise when the relative orientation from the reference coordinate system becomes large. Therefore, highly maneuverable spacecraft require other means of attitude representation. Direction cosine matricies and quaternions overcome this problem. Direction cosine matricies provide the most convenient way of transforming vectors between coordinate systems but require significantly higher attitude processor throughputs than quaternions. As an example, propagating an attitude matrix with angular rate data requires the integration of nine elements while the quaternion has only four. For these reasons, the quaternion representation is chosen for this attitude simulation model.

A. QUATERNION DEFINITION AND CHARACTERISTICS

The four vector quaternion based representation $\vec{q} \in R^4$ can be written as

$$\vec{q} = \begin{bmatrix} q_1 \\ q_2 \\ q_3 \\ q_4 \end{bmatrix} \tag{4.1}$$

or equivalently,

$$\vec{q} = q_1 i + q_2 j + q_3 k + q_4 \tag{4.2}$$

where the quaternion has a three vector imaginary part

$$\vec{q}_I = \begin{bmatrix} q_1 \\ q_2 \\ q_3 \end{bmatrix} \text{ and a scalar real part } q_R = q_4 .$$

1. Meaning of Quaterions

Quaternions represent the angular orientation of a body relative to a reference coordinate frame by a single axis rotation of magnitude è about the eigenvector axis given by $\vec{e}$ corresponding to the +1 eigenvalue of the direction cosine or attitude matrix. The direction cosine matrix can be written in terms of these four parameters

$$A = \begin{bmatrix} 1 & 0 & 0 \\ 0 & 1 & 0 \\ 0 & 0 & 1 \end{bmatrix} \cos(\grave{e}) + \begin{bmatrix} 0 & -e_3 & e_2 \\ e_3 & 0 & -e_1 \\ -e_2 & e_1 & e \end{bmatrix} \sin(\grave{e}) + \vec{e}\vec{e}^{\,T}(1-\cos(\grave{e})) \quad (4.3) \qquad (4.4)$$

Similarly these parameters can be represented by the four quaternions

$$\vec{q}_I = \begin{bmatrix} q_1 \\ q_2 \\ q_3 \end{bmatrix} = e \begin{bmatrix} e_1 \\ e_2 \\ e_3 \end{bmatrix} \sin\left(\frac{\grave{e}}{2}\right) \qquad (4.5)$$

$$q_R = q_4 = \cos\left(\frac{\grave{e}}{2}\right)$$

which have the added property that

$$\|\vec{q}\| = q_1^2 + q_2^2 + q_3^2 + q_4^2 = 1 \qquad (4.6)$$

2. Attitude Matrix

The equivalent attitude or direction cosine matrix can be generated from quaternions using

$$A = \begin{bmatrix} q_1^2 - q_2^2 - q_3^2 + q_4^2 & 2(q_1q_2 + q_3q_4) & 2(q_1q_3 - q_2q_4) \\ 2(q_1q_2 - q_3q_4) & -q_1^2 + q_2^2 - q_3^2 + q_4^2 & 2(q_2q_3 + q_1q_4) \\ 2(q_1q_3 + q_2q_4) & 2(q_2q_3 - q_1q_4) & -q_1^2 - q_2^2 + q_3^2 + q_4^2 \end{bmatrix} \qquad (4.7)$$

The SIMULINK subsystem used in this simulation model to convert a quaternion to the equivalent attitude matrix is shown in Figure 17.

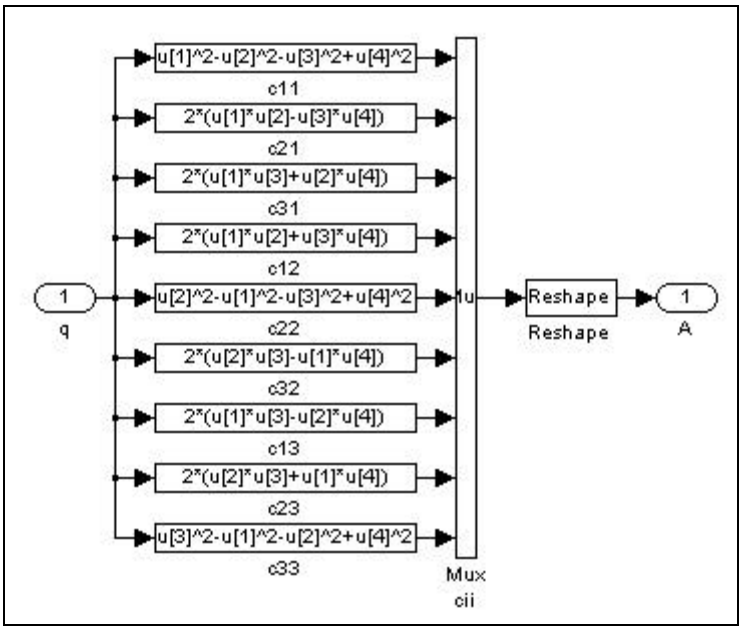

Figure 17. SIMULINK Subsystem Diagram: Attitude Matrix from Quaternions

3. Quaternion Multiplication

The multiplication of two quaternions to form a third defines an angular orientation resulting from two eigen-axis rotations. If $\vec{q}'$ represents the transformation from coordinate frame A to B and $\vec{q}''$ represents the transformation from frame B to C then the transformation from frame A to C is given by

$$\vec{q} = \vec{q}'\vec{q}'' \tag{4.8}$$

This multiplication can be implemented several ways. The two quaternions can be multiplied directly using the quaternion format given in Equation (4.2)

$$(q_1 i + q_2 j + q_3 k + q_4) = (q_1' i + q_2' j + q_3' k + q_4')(q_1'' i + q''_2 j + q''_3 k + q''_4) \tag{4.9}$$

using the equalities

$$\begin{aligned} i^2 = j^2 = k^2 = -1 \\ ij = -ji = k \\ jk = -kj = i \\ ki = -ik = j \end{aligned} \tag{4.10}$$

Quaternion multiplication can also be performed by treating the imaginary and real parts separately

$$\vec{q}_I = q'_R \vec{q}''_I + q''_R \vec{q}'_I + \vec{q}'_I \times \vec{q}''_I$$
$$q_R = q'_R q''_R - \vec{q}'_I \cdot \vec{q}''_I \tag{4.11}$$

In matrix form quaternion multiplication is given by

$$\begin{bmatrix} q_1 \\ q_2 \\ q_3 \\ q_4 \end{bmatrix} = \begin{bmatrix} q'_4 & -q'_3 & q'_2 & q'_1 \\ q'_3 & q'_4 & -q'_1 & q'_2 \\ -q'_2 & q'_1 & q'_4 & q'_3 \\ -q'_1 & -q'_2 & -q'_3 & q'_4 \end{bmatrix} \begin{bmatrix} q''_1 \\ q''_2 \\ q''_3 \\ q''_4 \end{bmatrix} \tag{4.12}$$

This multiplication method is used in the attitude simulation. The SIMULINK subsystem is shown in Figure 18.

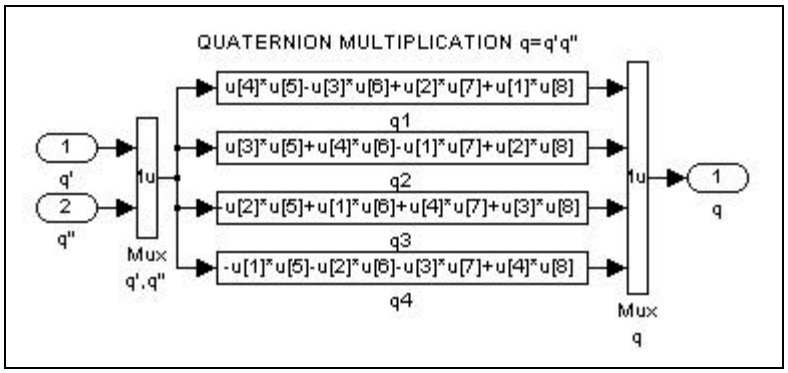

Figure 18. SIMULINK Subsystem Diagram: Quaternion Multiplication

4. Coordinate Rotations

Sequential axis rotations such as those that define the three Euler angle representation can be realized by the successive quaternion products. Additionally, if there are three small simultaneous rotations $\dot{\theta}_1$, $\dot{\theta}_2$, and $\dot{\theta}_3$ about the coordinate axes x, y, and z respectively the resulting quaternion is determined as follows:

Let $\Theta = (\dot{\theta}_1^2 + \dot{\theta}_2^2 + \dot{\theta}_3^2)^{1/2}$ and $\vec{q} = \frac{1}{\Theta}\begin{bmatrix} \dot{\theta}_1 \\ \dot{\theta}_2 \\ \dot{\theta}_3 \end{bmatrix}$, then

$$\vec{q}_I = \begin{bmatrix} q_1 \\ q_2 \\ q_3 \end{bmatrix} = \vec{q} \sin\left(\frac{\Theta}{2}\right) \text{ and } q_R = q_4 = \cos\left(\frac{\Theta}{2}\right) \tag{4.13}$$

5. Quaternion Inverse and Identity

The inverse of a quaternion is its complex conjugate and is analogous to the transpose of a direction cosine matrix. A quaternion is conjugated by reversing the sign on the vector part.

$$\text{If } \vec{q} = \begin{bmatrix} q_1 \\ q_2 \\ q_3 \\ q_4 \end{bmatrix} \text{ then } \vec{q}^{*} = \begin{bmatrix} -q_1 \\ -q_2 \\ -q_3 \\ q_4 \end{bmatrix}.$$

The identity quaternion is found by multiplying any quaternion by its conjugate as shown below.

$$\vec{q}\vec{q}^{*} = \vec{q}^{*}\vec{q} = \begin{bmatrix} 0 \\ 0 \\ 0 \\ 1 \end{bmatrix} \tag{4.14}$$

6. Quaternion Error

A difference quaternion can be defined between to orientations that are referenced to the same coordinate frame. If $\vec{q}'$ represents the transformation from coordinate frame A to B and $\vec{q}''$ represents the transformation from frame A to C then the transformation from frame B to C is given by

$$\vec{q} = \vec{q}'^{*}\vec{q}'' = \begin{bmatrix} q_4' & q_3' & -q_2' & -q_1' \\ -q_3' & q_4' & q_1' & -q_2' \\ q_2' & -q_1' & q_4' & -q_3' \\ q_1' & q_2' & q_3' & q_4' \end{bmatrix} \begin{bmatrix} q_1'' \\ q_2'' \\ q_3'' \\ q_4'' \end{bmatrix} \tag{4.15}$$

This can be used to calculate the error quaternion where the target orientation is given by $\vec{q}'$ and the actual spacecraft orientation is $\vec{q}''$.

$$\vec{q}_e = \vec{q}'^{*}\vec{q}'' \tag{4.16}$$

The SIMULINK subsystem diagram for determining the error quaternion is given in Figure 19.

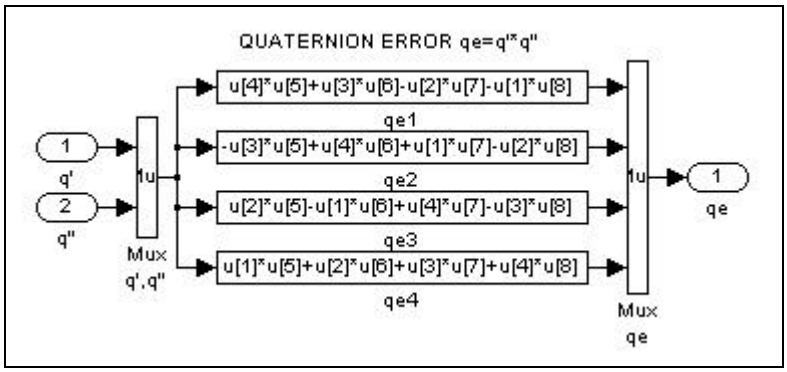

Figure 19. SIMULINK Subsystem Diagram: Error Quaternion

The angular difference in radians between the original quaternions is contained in the real part of the error quaternion.

$$\grave{e}_e = 2\cos^{-1}(q_{4e}) \tag{4.17}$$

7. Vector Transformations

Transforming vectors between coordinate systems requires two quaternion multiplications where the vector is treated as quaternion with a real part of zero. If $\bar{q}$ represents the orientation of coordinate frame B with respect to reference frame A then a vector given in coordinates of the reference frame, $\bar{v}_A$, can be transformed to the coordinates of frame B by

$$\bar{v}_B = \bar{q}^* \bar{v}_A \bar{q} \tag{4.18}$$

B. QUATERNION KINEMATICS

Actual spacecraft motion is simulated using the continuous quaternion differential equations. In the attitude determination computer simulation the attitude propagator uses the discrete kinematic equations.

1. Continuous Kinematics

The differential equation for the quaternions of a rotating coordinate system can be found by differentiating this equation with respect to a fixed reference frame A. If the rotational rates for coordinate frame B are given by

$$\tilde{\omega} = \begin{bmatrix} \omega_x \\ \omega_y \\ \omega_z \end{bmatrix}, \text{ then } \left.\frac{d\vec{v}_A}{dt}\right|_I = \left.\frac{d\vec{v}_B}{dt}\right|_B = 0 \text{ and } \left.\frac{d\vec{v}_B}{dt}\right|_I = \tilde{\omega} \times \vec{v}_B$$

The inertial derivative of equation (4.18) becomes

$$\tilde{\omega} \times \vec{v}_B = \frac{d\vec{q}^*}{dt} \vec{v}_A \vec{q} + \vec{q}^* \vec{v}_A \frac{d\vec{q}}{dt} \tag{4.19}$$

Using the properties of quaternions, substituting the original equation for $\vec{v}_B$ and noting that the vector $\vec{v}_A$ is arbitrary it can be shown that

$$\frac{d\vec{q}}{dt} = \frac{1}{2} \vec{q} \tilde{\omega} \tag{4.20}$$

or in matrix differential form

$$\frac{d\vec{q}}{dt} = \begin{bmatrix} \dot{q}_1 \\ \dot{q}_2 \\ \dot{q}_3 \\ \dot{q}_4 \end{bmatrix} = \frac{1}{2} \bar{S}(\tilde{\omega}) \begin{bmatrix} q_1 \\ q_2 \\ q_3 \\ q_4 \end{bmatrix} = \frac{1}{2} \begin{bmatrix} 0 & \omega_3 & -\omega_2 & \omega_1 \\ -\omega_3 & 0 & \omega_1 & \omega_2 \\ \omega_2 & -\omega_1 & 0 & \omega_3 \\ -\omega_1 & -\omega_2 & -\omega_3 & 0 \end{bmatrix} \begin{bmatrix} q_1 \\ q_2 \\ q_3 \\ q_4 \end{bmatrix} \tag{4.21}$$

where $\bar{S}(\tilde{\omega}) = \begin{bmatrix} -S(\tilde{\omega}) & \tilde{\omega} \\ -\tilde{\omega}^T & 0 \end{bmatrix}$ and $S(\tilde{\omega})$ is the skew symmetric matrix associated with the vector $\tilde{\omega}$. The kinematics subsystem diagram used in the SIMULINK model is shown in Figure 20. The integration is performed using the Dormand-Prince ode5 solver.

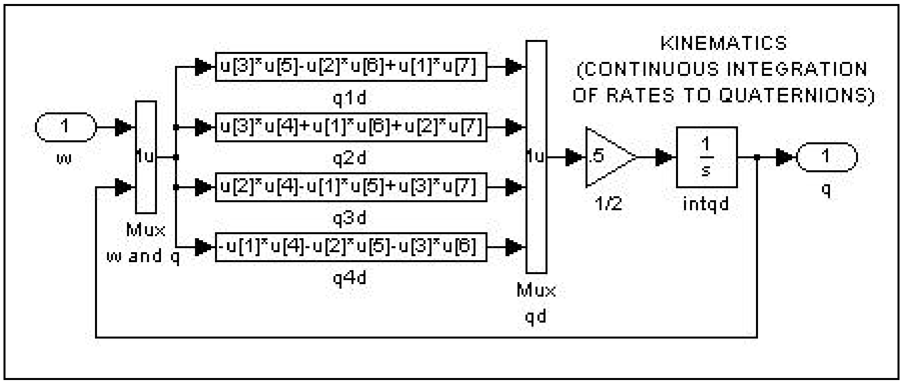

Figure 20. SIMULINK Subsystem Diagram: Continuous Kinematics

2. Discrete Kinematics

The solution to the continuous differential equation when $\vec{\omega}$ is held constant is

$$\bar{q} = e^{\left(\frac{1}{2}\bar{S}(\vec{\omega})t\right)}\bar{q}_0 = \left(\cos(\theta)\, I_{4x4} + \bar{S}\left(\frac{t\vec{\omega}}{2\theta}\right)\sin(\theta)\right)\bar{q}_0 \qquad (4.22)$$

where $\theta = \left\|\frac{\omega t}{2}\right\|$. This solution leads to the discrete implementation of the quaternion kinematic equations.

The attitude determination system uses angular rate information to kinematically propagate the spacecraft attitude quaternion in discrete time steps. The angular rate vector $\vec{\omega} \in R^3$ is integrated with time step Δt to produce the incremental angle vector $\Delta\vec{\theta} \in R^3$. For small time steps $\Delta\vec{\theta}$ approximates an eigen-axis rotation in the current body coordinate frame so it can be related to the change in the attitude quaternion by

$$\Delta\bar{q} \cong \sin\left(\frac{|\Delta\theta|}{2}\right)\left(\frac{\Delta\theta_1 i + \Delta\theta_2 j + \Delta\theta_3 k}{|\Delta\theta|}\right) + \cos\left(\frac{|\Delta\theta|}{2}\right) \qquad (4.23)$$

The SIMULINK subsystem used in the discrete attitude propagator to obtain the incremental quaternion step is shown in Figure 21.

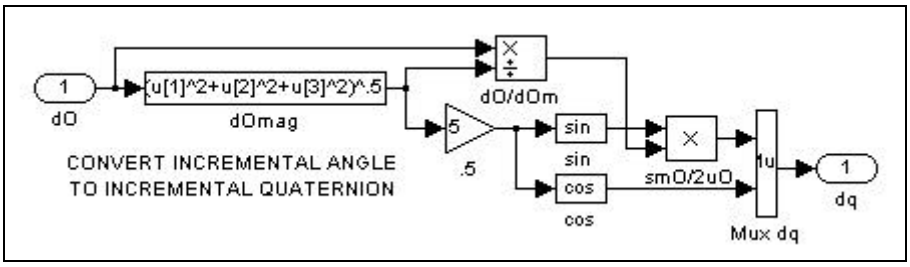

Figure 21. SIMULINK Subsystem Diagram: Discrete Attitude Propagator

The new attitude quaternion is simply determined by

$$\vec{q}_{new} = \vec{q}_{old} (\quad \ddot{A} \tag{4.24}$$

where the equation implies quaternion multiplication.

THIS PAGE INTENTIONALLY LEFT BLANK

V. KALMAN FILTER

The Kalman filter provides a non-deterministic means of estimating a system state vector using a state space mathematical plant model and sensor measurement data related to some subset of the state variables. It is a stochastic optimal estimator designed to minimize the weighted mean square error in the state estimate. The Kalman gain matrix determines the weighting based on the relative confidence between the past state estimate propagated to the current time and the current partial measurement of state variables. The error covariance matrix, the second statistical moment of the state vector, tracks the confidence in the state estimate while a measurement error covariance matrix relates the confidence in the measurement.

A. RECURSIVE DISCRETE KALMAN FILTER

The Kalman filter can be implemented recursively since all of the information from past state measurements is encapsulated in the previous state estimate and error covariance matrix with are both tracked. During state propagation the error covariance is updated to reflect additional error added by imperfections in the plant model. A recursive discrete Kalman filter is used in the proposed attitude determination scheme. Figue 22 illustrates the recursive nature of the Kalman filter.

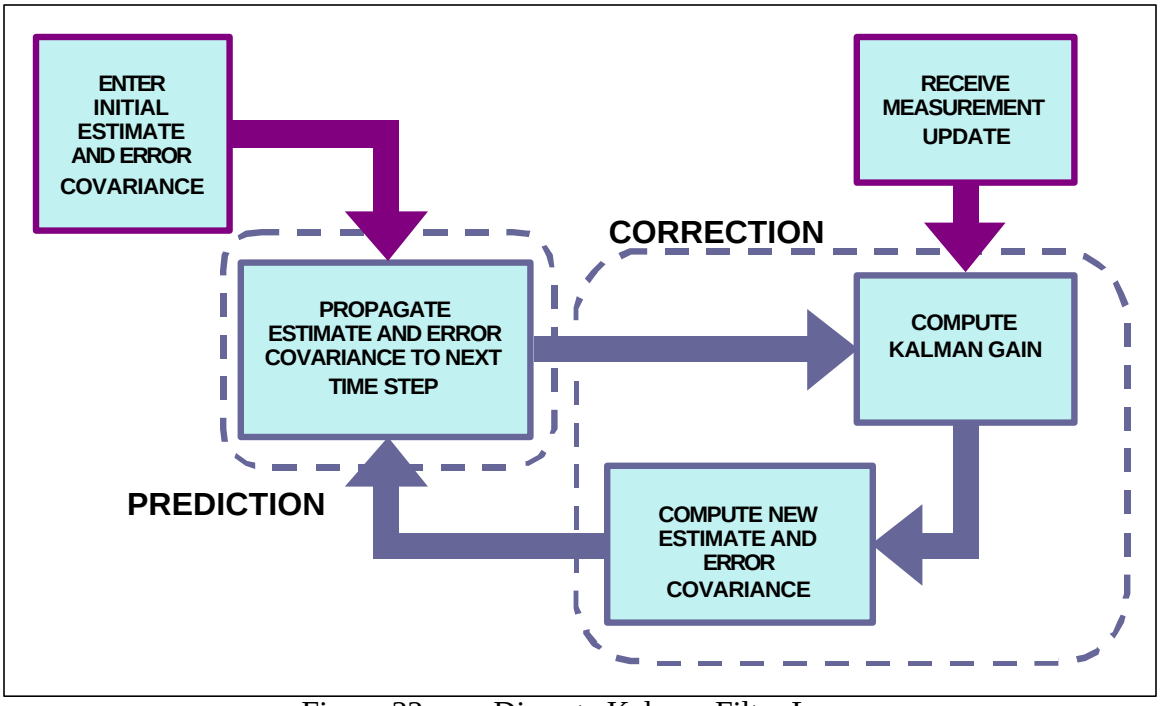

Figure 22. Discrete Kalman Filter Loop

The standard equations for a recursive discrete Kalman filter are summarized in Table 2 below. For full background development and equation derivations see Appendix A [Ref. 1].

System/plant Model		$\vec{x}_k = A\vec{x}_{k-1} + B\vec{u}_{k-1} + \vec{w}_{k-1}$ $\vec{w}_k \sim N(\vec{0}, Q_k)$
Measurement Model		$\vec{z}_k = H_k\vec{x}_k + \vec{v}_k$ $\vec{v}_k \sim N(\vec{0}, R_k)$
Initial Conditions		$\hat{\vec{x}}_0 = E[\vec{x}_0]$ $P_0 = E[(\vec{x}_0 - \hat{\vec{x}}_0)(\vec{x}_0 - \hat{\vec{x}}_0)^T]$
Assumptions (uncorrelated errors)		$E[\vec{w}_k \vec{v}_j] = 0$ for all j, k
Prediction	State Estimate Extrapolation Error Covariance Extrapolation	$\hat{\vec{x}}_k^- = A\hat{\vec{x}}_{k-1}^+ + B\vec{u}_{k-1}$ $P_k^- = AP_{k-1}^+A^T + Q_{k-1}$
Correction	Kalman Gain Matrix State Estimate Update Error Covariance Update	$K_k = P_k^-H_k^T(H_kP_k^-H_k^T + R_k)^{-1}$ $\hat{\vec{x}}_k^+ = \hat{\vec{x}}_k^- + K_k(\vec{z}_k - H_k\hat{\vec{x}}_k^-)$ $P_k^+ = (I - K_kH_k)P_k^-$

Table 2. Discrete Kalman Filter Equations

B. ERROR STATE EXTENDED KALMAN FILTER IMPLEMENTATION

A linear error state extended discrete Kalman filter is implemented in the simulated attitude determination model to estimate spacecraft attitude and angular rate. The nonlinear attitude propagation is performed discretely outside of the Kalman filter according to Equations (4.23) and (4.24) at the high bandwidth frequency of the attitude processor. The angular rate estimate used in the kinematic model is provided by the spacecraft gyros or pseudo gyro rate calculations. The Kalman filter is designed to provide bias corrections to the gyro outputs for attitude propagation [Ref.11]. If the pseudo gyro rate is used, the bias error is treated as a rate error from which a correction to the system angular momentum is determined. Measurement updates are provided by star trackers. The difference in the measured and predicted star vector is related to the attitude error and used to provide corrections to the state estimate.

1. State Variables

The Kalman filter used in this model estimates six state variables: a three vector of attitude errors, $\tilde{e} \in R^3$, and a three vector of gyro bias errors, $\tilde{b} \in R^3$. The total state vector is given by

$$\vec{x} = \begin{bmatrix} \tilde{e} \\ \tilde{b} \end{bmatrix} \in R^6 \tag{5.1}$$

The attitude error, $\tilde{e}$, represents the deviation in the spacecraft attitude relative to the inertial reference frame given by a vector of three simultaneous rotations. The bias error, $\tilde{b}$, represents the change in bias of the angular rate data in the spacecraft body coordinate frame.

2. Attitude Propagation Error Correction Methods

There are two ways to implement the Kalman filter corrections to the attitude propagator. In the first method, the attitude propagator is fed with raw gyro rate information and the Kalman filter maintains the total gyro bias tracking with the state bias error, $\tilde{b}$. In this method, the attitude quaternion must be corrected at each time step

by the filter. The attitude error vector, $\tilde{e}$, is converted to an incremental quaternion rotation, $\Delta\bar{q}$ and applied to the propagated attitude quaternion as shown in Chapter IV with Equations (4.23) and (4.24) or, using the small angle approximation $\Delta\bar{q}$ is given by

$$\Delta\bar{q}=\frac{\tilde{e}_1}{2}i+\frac{\tilde{e}_2}{2}j+\frac{\tilde{e}_3}{2}k+1 \tag{5.2}$$

Then by quaternion multiplication the propagated attitude quaternion is updated

$$\bar{q}_{new}=(\Delta\bar{q})\bar{q}_{old} \tag{5.3}$$

The alternative method of applying the filter correction to the propagator is to use the bias error state, $\tilde{b}$, to correct the unknown gyro bias, ω_b each time a measurement update is obtained

$$\omega_{bnew}=\omega_{bold}+\tilde{b} \tag{5.4}$$

For this method, the total unknown gyro bias is tracked separately from the filter and added to the gyro angular rate before it is fed to the attitude propagator.

$$\Delta\bar{\tilde{e}}=\left(\omega_g+\omega_b\right)\Delta t \tag{5.5}$$

The attitude error state correction is then only necessary at measurement updates. Using this method allows the Kalman filter error vector $\bar{x}$ to be reset after each bias measurement update. Since the filter approximates nonlinear errors with a linear model, keeping the errors as close to zero as possible improves the estimate. This Kalman filter correction method is used in the simulated attitude determination model.

3. Plant Model

A nominal plant model is chosen for this Kalman filter which assumes a constant rate bias between filter updates and uncoupled (linear) attitude errors between propagation steps. It is derived from the continuous equation of state

$$\frac{d\bar{x}}{dt}=\begin{bmatrix}d\tilde{e}/dt\\ d\tilde{b}/dt\end{bmatrix}=\begin{bmatrix}0_{3X3} & \hat{A}^T\\ 0_{3X3} & 0_{3X3}\end{bmatrix}\begin{bmatrix}\tilde{e}\\ \tilde{b}\end{bmatrix}=f(t)\bar{x} \tag{5.6}$$

where $\hat{A}$ is the estimate of the spacecraft attitude or direction cosine matrix. This linear

state equation includes coupled rotational effects through the time variant estimated attitude matrix which changes dynamically.

4. State Transition Matrix

For the discrete Kalman filter implementation of this model the state transition matrix, $\ddot{o}_k$, is calculated for each time step using the matrix exponential of f(t) from the continuous state equation

$$\ddot{o}_k = e^{f(t)\ddot{A}t} = \begin{bmatrix} I_{3X3} & \hat{A}_k^T\ddot{A}t \\ 0_{3X3} & I_{3X3} \end{bmatrix} \tag{5.7}$$

where $\hat{A}_k^T$ is the transpose of the estimated attitude matrix at the current discrete time, tk and $\ddot{A}t$ is the interval between steps. The SIMULINK subsystem used to calculate the state transition matrix is shown in Figure 23. The estimated attitude matrix is calculated from the propagated attitude quaternion using Equation (4.7).

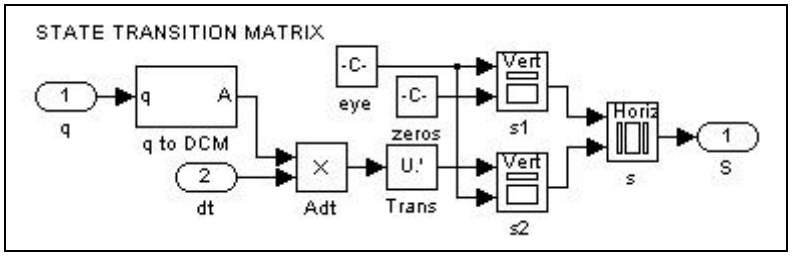

Figure 23. SIMULINK Subsystem Diagram: State Transition Matrix

5. Kalman Filter Prediction Equations

The state transition matrix allows the state estimate, $\hat{\bar{x}}$, and associated error covariance matrix, P, to be propagated forward in the discrete Kalman filter prediction step

$$\hat{\bar{x}}_{k+1}^{-} = {}_k\ddot{o}\,\hat{o}_k \tag{5.8}$$

$$P_{k+1}^{-} = {}_k\ddot{o}\,{}_kP_k^T\ddot{o} + \tag{5.9}$$

The subscript k+1 indicates next discrete time step, t_{k+1}, and the superscript – indicates predicted future value based only on information up to the current time step t_k. The covariance matrix relates the confidence in the associated state estimate. A larger P

indicates less confidence which means that the attitude determination system is assumed to have larger errors. Measurement updates taken when P is large will greater impact on the estimate than those taken when the confidence is high. The Kalman filter prediction step is implemented in the SIMULINK model as shown in Figure 24.

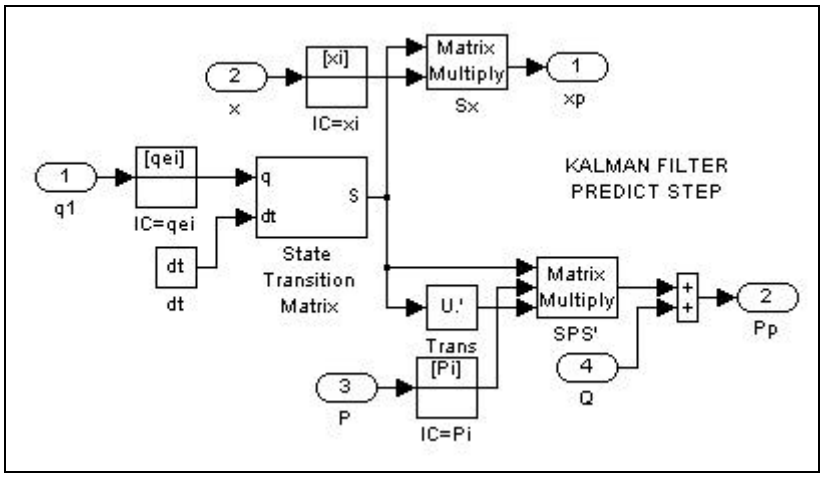

Figure 24. SIMULINK Subsystem Diagram: Kalman Filter Prediction Step

6. Plant Noise Covariance

The plant noise covariance, Q, is a positive definite matrix that characterizes the plant error accumulated through the time step, Δt, assuming that it can be modeled as Gaussian white noise meaning normally distributed with zero mean. Q is normally taken to be a diagonal matrix meaning that there is no known correlation between the errors of the six state variables. In terms of the variances of the state variables the plant noise covariance matrix is given by

$$Q=\begin{bmatrix} \sigma_{e1}^2 & 0 & 0 & 0 & 0 & 0 \\ 0 & \sigma_{e2}^2 & 0 & 0 & 0 & 0 \\ 0 & 0 & \sigma_{e3}^2 & 0 & 0 & 0 \\ 0 & 0 & 0 & \sigma_{b1}^2 & 0 & 0 \\ 0 & 0 & 0 & 0 & \sigma_{b2}^2 & 0 \\ 0 & 0 & 0 & 0 & 0 & \sigma_{b3}^2 \end{bmatrix} \qquad (5.10)$$

If the time step is varied or the plant error is known to be significantly changed due to operating mode, then Q should be modified to reflect that change. Decreasing Q effectively asserts that the plant generates less error and the predicted state estimate will

be weighted higher relative to the measurement updates. On the other hand, if it is increased less confidence is placed on the estimate predicted by the model and more significant corrections will be applied during measurement updates. In this simulation, Q is taken to be constant.

7. Kalman Filter Initialization

In order to initiate the Kalman filter algorithm, an initial state estimate, $\hat{x}_i$ and its associated covariance, P_i, must be chosen. Least squares batch processing can be performed on two or more star tracker measurements prior to initiating the filter or an educated guess can be used. Since the state represents errors from truth, the selected initial state estimate is

$$\hat{\bar{x}}_i = \begin{bmatrix} 0 \\ 0 \\ 0 \\ 0 \\ 0 \\ 0 \end{bmatrix} \text{ with associated covariance } P_i = n \begin{bmatrix} 100 & 0 & 0 & 0 & 0 & 0 \\ 0 & 100 & 0 & 0 & 0 & 0 \\ 0 & 0 & 100 & 0 & 0 & 0 \\ 0 & 0 & 0 & 1 & 0 & 0 \\ 0 & 0 & 0 & 0 & 1 & 0 \\ 0 & 0 & 0 & 0 & 0 & 1 \end{bmatrix}.$$ The

constant, n, is chosen to reflect confidence in the estimate at initialization. The attitude errors generated are normally about an order of magnitude up from the rate bias errors so the variances are weighted higher.

8. Sensor Measurement Update

The state estimate and the covariance matrix propagate forward without correction through each time step until a measurement update is produced. The state estimate is used to kinematically propagate the attitude quaternion while the covariance matrix builds up due to the added error through each step.

a. Measurement Vector

If an attitude measurement update is produced at the next time step, k+1, by one or more star trackers the Kalman filter correction step is applied. The star trackers produce horizontal and vertical outputs (H,V) corresponding to the position of the star on

the detector array. These outputs are internally compensated for with software and calibrated to form a measurement vector in tracker coordinates

$$\vec{s}_m = \begin{bmatrix} H \\ V \\ 1 \end{bmatrix} \text{ with the normalization } \vec{s}_m = \frac{\vec{s}_m}{\left\| \vec{s}_m \right\|} \tag{5.11}$$

which is the star tracker measurement vector. For simulation modeling purposes, noise is added to the H and V components to create an artificial star tracker measurement vector. The measurement vector is generated in the SIMULINK model as shown in Figure 25.

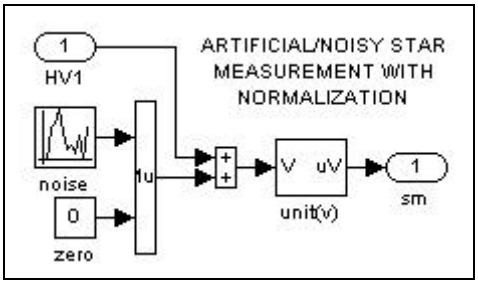

Figure 25. SIMULINK Subsystem Diagram: Star Tracker Measurement

At every integration cycle, Ät, the attitude estimate is available from the Kalman filter prediction step. If a star tracker observation has occurred during that time step, the measurement vector must be propagated ahead to correspond to the current discrete time of the attitude computer. Otherwise, the state vector and the state transition and covariance matricies must be interpolated to accomplish the filter update. Tracker processing latencies and transport delays must also be compensated for in the time difference. For simplicity in this model, it is assumed that the all observations occur at an exact discrete time step of the integration cycle. To produce star measurements for the model, an artificial star tracker reference is chosen with representative noise applied to the H and V outputs.

b. Predicted Measurement

The predicted vector in star tracker coordinates is needed to determine the measurement residual for the update. This is generated using the known position of the star in inertial space. The detected star goes through the identification process and gets

compensated for aberration to yield a unit vector, $\vec{s}_I$, in inertial coordinates. Using the estimate for the inertial to body attitude matrix generated from the filter state prediction, $\hat{A}_{k+1}^{-}$, and the calibrated body to star tracker transformation matrix, T, a predicted vector is generated in tracker coordinates.

$$\vec{s}_p = T\,\hat{A}_{k+1}^{-}\,\vec{s}_I \tag{5.12}$$

The inertial star vectors for the model are generated by applying the transpose of the body to star tracker and true attitude matricies to the same star tracker reference used to generate the measurement.

$$\vec{s}_I = A_{k+1}^{T}\,T^{T}\begin{bmatrix} H \\ V \\ 1 \end{bmatrix} \tag{5.13}$$

Figure 26 illustrates the SIMULINK subsystem used to produce a simulated inertial star reference vector.

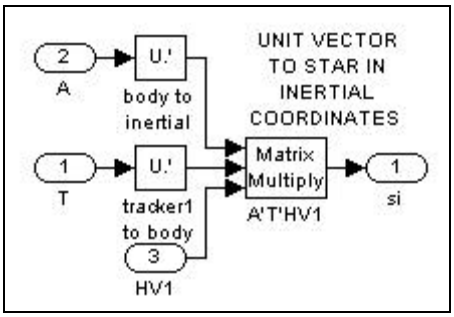

Figure 26. SIMULINK Subsystem Diagram: Inertial Star Vector

c. Measurement Residual

The measurement residual, z_{k+1}, is formed by subtracting the predicted from measured star vector and considering only the first two components.

$$\vec{z}_{k+1} = E(\vec{s}_m - \vec{s}_p) \tag{5.14}$$

where $E=\begin{bmatrix} 1 & 0 & 0 \\ 0 & 1 & 0 \end{bmatrix}$. The measurement residual is determined in the SIMULINK model as shown in Figure 27.

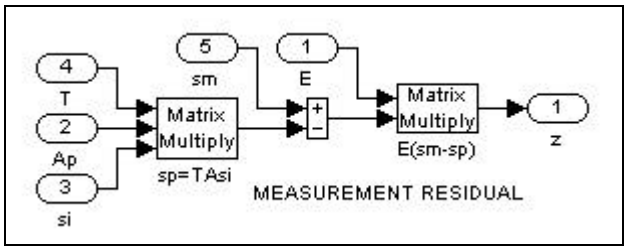

Figure 27. SIMULINK Subsystem Diagram: Measurement Residual

9. Observation Matrix

Since the measurement residual is simply the difference between unit vectors, it is easily related to the state attitude errors. The observation or feedback sensitivity matrix defined by the relationship to the state variables

$$H_{k+1}=\left[E\,T\,\hat{A}^{-}_{k+1}\,S\left(\bar{s}_I\right)\quad 0_{2x3}\right] \tag{5.15}$$

where $S(\bar{s}_I)$ indicates the skew symmetric matrix associated with the inertial star reference vector. Figure 28 shows the subsystem diagram used in the SIMULINK model to produce the observation matrix.

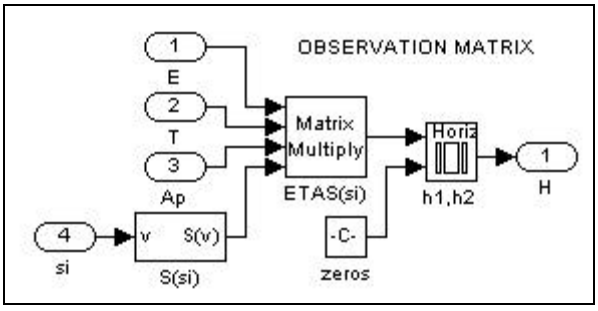

Figure 28. SIMULINK Subsystem Diagram: Observation Matrix

10. Kalman Gain

The Kalman gain can then be calculated for the correction step at k+1 from the standard discrete filter equation

$$K_{k+1}=P^{-}_{k+1}H^{T}_{k+1}(R_{k+1}+H_{k+1}P^{-}_{k+1}H^{T}_{k+1})^{-1} \tag{5.16}$$

where $R\in R^{2X2}$ is the measurement noise covariance matrix associated with the assumed Gaussian white noise in the H and V outputs of the star trackers. Since these errors are

usually similar and uncorrelated, the R matrix is normally taken to be a multiple of the identity.

$$R=\begin{bmatrix} \sigma_H^2 & 0 \\ 0 & \sigma_V^2 \end{bmatrix}$$

Noisier or less accurate star trackers will generally have a larger R matrix which decreases the Kalman gain and thus provides less of a correction to the state and covariance matricies. In reality, the measurement error may not be constant for each correction step even when the same star tracker is used. Higher intensity stars, although easier to detect and identify, produce slightly larger noise. Also stars detected toward the field of view limits of the tracker usually have larger errors due to distortions than those detected near the star tracker optical axis.

The Kalman gain SIMULINK subsystem is shown in Figure 29.

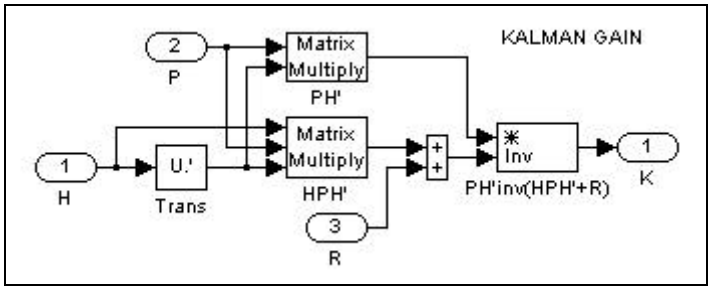

Figure 29. SIMULINK Subsystem Diagram: Kalman Gain

11. Kalman Filter Correction Equations

With the Kalman gain, the state and covariance matricies can be corrected with the measurement update

$$\Delta\hat{\bar{x}} = -K_{k+1}\bar{z}_{k+1} \tag{5.17}$$

$$\hat{\bar{x}}_{k+1} = \hat{\bar{x}}_{k+1} + \Delta\hat{\bar{x}} \tag{5.18}$$

and

$$P_{k+1} = (I_{6X6} - K_{k+1}H_{k+1})P^{-}_{k+1} \tag{5.19}$$

The covariance matrix update is accomplished in the simulation model as shown in Figure 30.

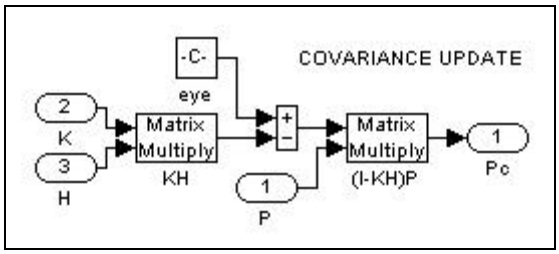

Figure 30. SIMULINK Subsystem Diagram: Covariance Updeate

In general, the estimated state drifts away from the true state as it is propagated forward with the non-ideal plant model and is corrected back toward truth as measurement updates occur. Corrections to the attitude components associated with the body axes closely aligned with the star tracker optical axis will be corrected much less than those that are aligned perpendicular. The spacecraft attitude error continues to grow during periods where there are no cataloged stars in the sensor field of view or when the tracker information is unavailable. Additionally, when only one tracker provides updates for extended periods the angular orientation about that star tracker's axis in body coordinates goes unchecked.

C. CONTROLLER DESIGN IMPLICATIONS

Since the Kalman filter is an optimal least squares estimator, the development of an optimal controller can be accomplished independently. Therefore, the attitude determination output should not affect the controller design. In this model, quaternion and rate error control laws are used as well as feed forward torque to generate reaction wheel commands. The optimal gains for the controller as determined by simulation with ideal deterministic attitude knowledge remain optimal with the attitude determination based on Kalman filter state estimates.

VI. DYNAMIC RATE CALCULATION

The continuous dynamic equations of motion for the Bifocal Relay Mirror spacecraft are derived in Chapter III. These equations produce the spacecraft angular rate from external control and disturbance moments applied to the body. A similar discrete model can be applied in the spacecraft attitude processor software to produce a real time calculated estimate of the angular rate, referred to as the dynamic gyro. This process is borrowed from The Aerospace Corporation's "Pseudo Gyro" concept [Ref. 8]. At high bandwidth processor execution the discretization of the dynamics introduces little error. The angular rate generated by this method can be used as a substitution for conventional gyroscope outputs. Attitude determination based on the dynamic gyro can be implemented as a back up failure mode or a primary operating mode to increase the expected lifetime of the satellite gyroscopes.

A. DISCRETE EQUATIONS OF MOTION

The discretized equations of motion are derived from

$$\Delta\vec{H} = \sum \vec{M}\,\Delta t \tag{6.1}$$

where $\sum \vec{M}$ is the sum of external moments applied to the spacecraft including controls, modeled disturbances and gyroscopic stiffness. This allows the total system angular momentum to be tracked with

$$\vec{H}_{k+1} = \vec{H}_k + \Delta\vec{H} \tag{6.2}$$

Then subtracting the relative momentum of the reaction wheels and secondary body produces

$$\vec{H}_{S-} = \vec{H} - \vec{H}_w - \vec{H}_{rel} \tag{6.3}$$

The calculated spacecraft angular rate is then given by

$$\tilde{u} = I^{-1}\vec{H}_{S-} \tag{6.4}$$

B. MOMENTUM CORRECTION FROM KALMAN FILTER UPDATES

The accuracy of the dynamic angular rate calculation ultimately depends on the tracking of the system angular momentum. If uncorrected, the numerous error sources in the model will cause the angular rate error to grow over time. The error state Kalman filter designed for gyro-based attitude determination systems can be used to provide the necessary model corrections. The gyro bias error states, $\tilde{b}$, are interpreted as spacecraft body rate errors. Using the calculated spacecraft inertia matrix, I, a correction to the system moment of inertia can be generated by

$$\Delta\vec{H}_{corr} = I\tilde{b} \tag{6.5}$$

The Kalman filter momentum correction is applied as if the error in the dynamic gyro is attributable to the total spacecraft body. The relative momentum terms from the secondary body and the reaction wheels are treated as if they are without error.

The SIMULINK dynamic gyro subsystem used in the attitude simulation model is illustrated in Figure 31.

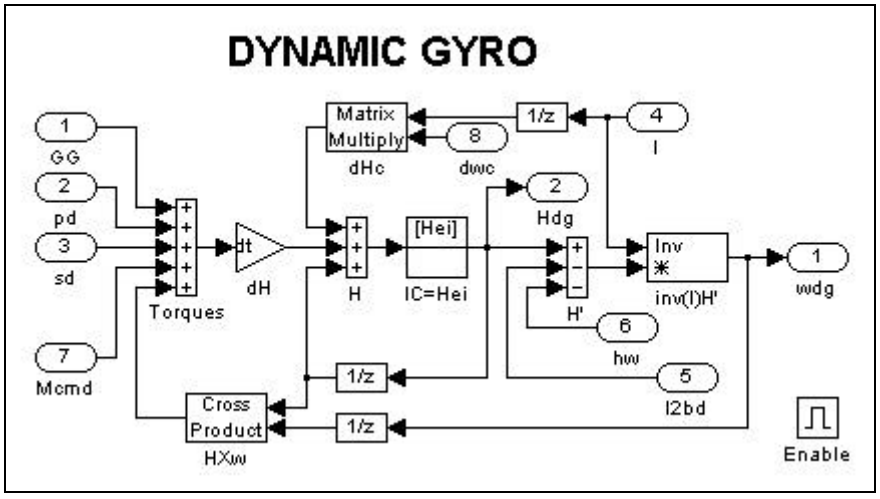

Figure 31. SIMULINK Subsystem Diagram: Dynamic Gyro

C. INPUTS AND ERROR SOURCES

After initial calibration, kinematic plant error in gyro-based attitude determination systems is almost entirely attributable to a single set of imperfect gyroscope rate sensors. As long as gyro data does not become erratic a Kalman estimator based on a slowly

changing rate bias plant model produces an effective attitude determination system even with relatively noisy rate inputs.

The error in rate calculations from dynamic modeling, on the other hand, is due to numerous factors and is much harder to characterize. There are multiple internal sensors involved as well as dynamic modeling simplifications. Since the dynamic calculation is produced from total system momentum tracking any error in knowledge of external torques directly correlates to rate error. Errors in system or component moments of inertia have the same effect. Like gyro outputs, internal position and rate sensor data are corrupted by measurement and alignment errors. These data from all moving appendages and momentum exchange devices are critical to the accuracy of the rate calculation. Satellites not designed to use dynamic rate calculations for attitude determination are usually not equipped with appendage relative rate measurement sensors. These data must either be derived adding more error to the calculation or substituted with commanded rates. It is important that all known biases be removed from sensor data and calculated input errors since the Kalman filter estimator is based on the assumption of uncorrelated zero-mean Gaussian noise. Even if all input parameters were known exactly the discrete modeling of the spacecraft dynamics introduces some error.

1. External Control and Disturbance Torques

In the dynamic gyro, known externally applied moments are integrated in the system angular momentum calculations. These include control moments other than those imparted by momentum exchange devices as well as modeled disturbance torques. Since control torques are normally of significant magnitudes, it is essential that they be modeled correctly. Moments from magnetic torque rods depend on the imperfectly controlled magnetic dipole and the earth's magnetic field strength. The magnetic dipole is provided by torquer current measurement. The earth's magnetic field must either be modeled or measured with magnetometer but is not precisely known. Reaction jet moments are almost impossible to model accurately. This often result in degraded pointing and tracking during firings operations.

The effects of external disturbance moments depends on spacecraft configuration and orbital profile. Those disturbances that have significant effects on vehicle dynamics

should be modeled whenever possible to increase the accuracy of the attitude control system. These types of errors are non-zero mean in the short term and therefore can only be corrected for with sensor measurement updates. An extended option for The Aerospace Corporation's Pseudo Gyro includes a torque bias estimator to reduce the effects of unknown external disturbances.

For the Bifocal Relay Mirror satellite, the gravity gradient torque is the most significant disturbance and can be modeled as an input to increase the accuracy of the dynamic rate calculation. The model is well understood and is generated from the inertia matrix which is already required by the dynamic gyro and vehicle orientation with respect to the gravity vector which can be determined from the estimated attitude and ephemeris data. The gravity gradient model used by the dynamic gyro is equivalent to the subsystem shown in Figure 13.

2. Reaction Wheel Relative Momentum

Instead of integrating the torques produced by momentum exchange devices their relative momentum effects are used directly in the dynamic rate calculation. The relative momentum of each reaction wheel is given by its orientation within the spacecraft, the component inertia of its spinning disk and the wheel spin rate. The imperfect sensor measurements from the reaction wheel tachometers introduce errors in system momentum calculation. Relative orientation angles of reaction wheels are fixed and errors can be corrected through calibration. Orientations of control moment gyros, however, are variable. Since these devices usually carry much more momentum small gimbal resolver errors can have a significant impact on total system momentum calculations. In this simulation, time varying artificial alignment errors are applied to the reaction wheel momentum measurements to observe these effects. The error corrupted wheel momentum measurement subsystem implemented in the SIMULINK model is shown in Figure 32.

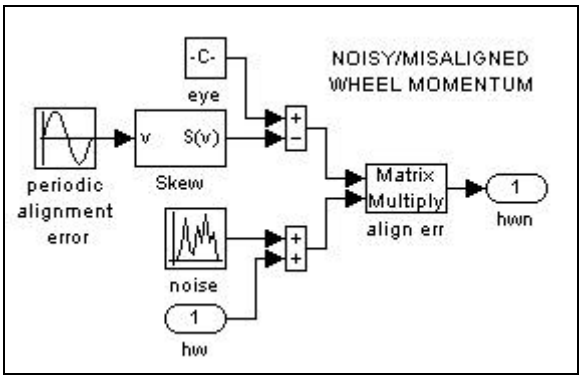

Figure 32. SIMULINK Subsystem Diagram: Error Corrupted Reaction Wheel Momentum Measurement

3. Moment of Inertia Calculations

The calculation of the total spacecraft inertia matrix is accomplished by Equation (3.12) using the SIMULINK subsystem illustrated in Figure 7. Fixed component moments of inertia and masses of the primary and secondary bodies are assumed to be known as well as the relative positions of their centers of mass from the system mass center. Imperfect knowledge of these parameters introduces errors in the angular rate calculation. Errors generated from rotating spacecraft components are not constant in the spacecraft body frame.

The inertia matrix also depends on internal sensor input from position encoders or potentiometers for relative angular orientation of appendages. The model of the potentiometer that measures the relative angle of the receive telescope includes quantization effects and additive noise. If appendage relative motion is slow or component moments of inertia are small, it may not be necessary to update the system inertia dyadic at the bandwidth of the attitude processor. A trigger is added to the SIMULINK subsystem that calculates the inertia matrix (Figure 7), so that the affects of update rate can be evaluated.

4. Appendage Relative Momentum

Knowledge of appendage relative momentums has direct bearing on the system momentum and therefore the dynamic rate calculation. The relative momentum of the Bifocal Relay Mirror satellite's secondary body is calculated from Equation (3.19). It

depends on the knowledge of the fixed secondary body inertia matrix and the relative angular rate. The attitude simulation model assumes that there is no directed measurement of the relative angular rate. The rate must therefore be derived from potentiometer measurements of the relative orientation about the axis of rotation. This sensor may have a minimum discernable incremental angle and noise corruption. Also, since the rate is derived from position measurements it exhibits increased noise and time lag. The simulation diagram that produces the error corrupted relative angle and rate for the spacecraft secondary body is shown in Figure 33.

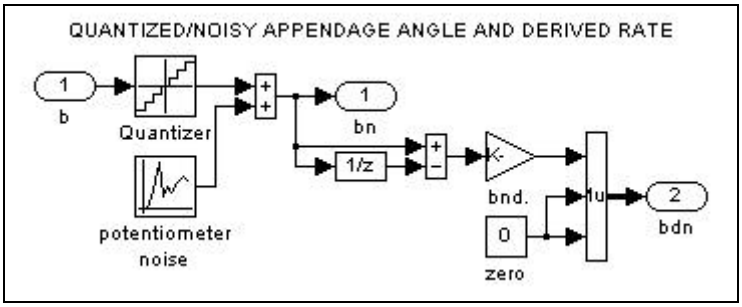

Figure 33. SIMULINK Subsystem Diagram: Appendage Relative Angle and Rate Measurement

Appendages of significant inertia or relative rates like the receive telescope of the Bifocal Relay Mirror satellite should be controlled with smooth gimbal drive motors in order to minimize nonlinear relative pointing errors. Ideally, all moveable appendages would have an associated rate sensor for each axis of rotation.

The other option for approximating appendage relative angular rates is to use the commanded drive input. In some systems, appendage controllers can provide a smooth relative rate through the drive motor, which significantly enhances angular momentum tracking. Drive actuators with considerably erratic friction effects will cause errors in the attitude control system during slew operations. Short term transients may introduce significant settling times for error corrections.

The subsystem of the attitude determination simulation that controls all of the internal sensor measurements and input parameter calculations for the dynamic gyro is shown in Figure 34.

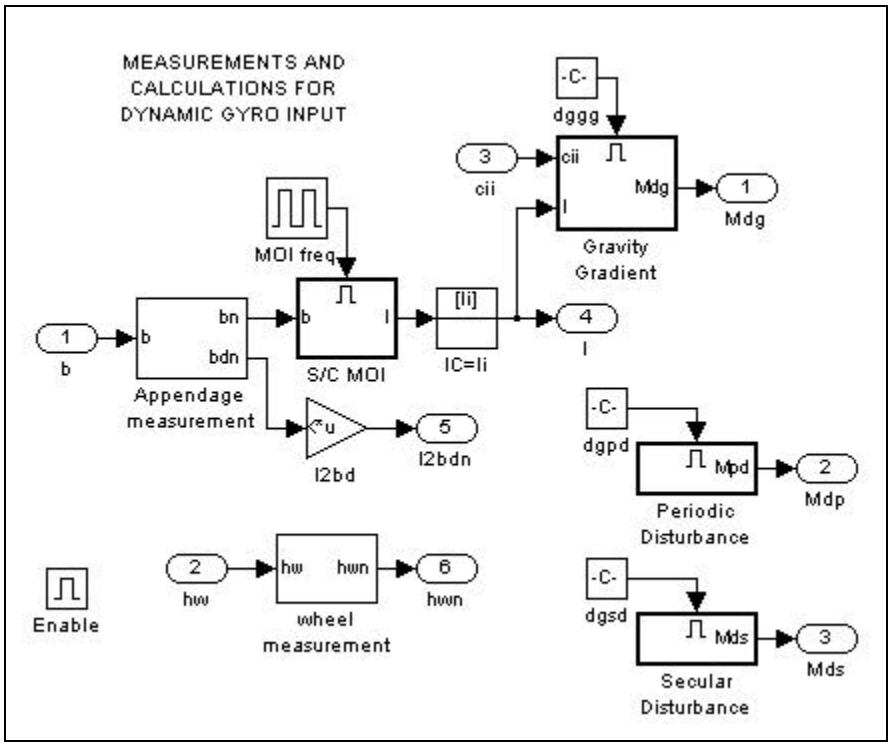

Figure 34. SIMULINK Subsystem Diagram: Dynamic Gyro Inputs

D. CALCULATED ANGULAR RATE ERROR CORRECTION

The error state extended Kalman filter is designed to track rate bias errors that are relatively constant in the spacecraft body frame. This is a good approximation for properly functioning gyro based systems. For the filter to remain effective when used with dynamic gyro, the bias in the output rate as seen in body coordinates due to the various error sources must be small and exhibit a bandwidth below the measurement update rate. Since it is the case that the common error sources are not zero-mean, their effects on the rate output must be relatively constant so that the momentum correction supplied by the Kalman filter applies over the update interval. Transient error spiking can require multiple star tracker measurement updates to correct. If the internal sensors provide inconsistent measurements, dynamic gyro angular rate will be degraded.

THIS PAGE INTENTIONALLY LEFT BLANK

VII. RESULTS

Simulation results demonstrate that multi-body spacecraft attitude control without the use of rate gyroscopes can be performed using the attitude and angular rate estimation scheme proposed in this thesis. The performance of dynamic gyro based attitude determination system is compared with a similar gyro based system using the Bifocal Relay Mirror attitude simulation. Simulation input parameters are varied to analyze the effects of major error sources on the dynamic gyro model. Also evaluated are the effects of star tracker accuracy and measurement update rates on the attitude determination system.

A. BASELINE SIMULATION

A full set of MATLAB plots are presented in this section for baseline analysis of the dynamic gyro based attitude determination and control scheme developed in this thesis. This set of results validates the potential effectiveness of the proposed attitude and angular rate estimating scheme used for multi-body spacecraft control. It also provides a common reference for analysis and comparison with subsequent simulation results. For other simulations, only selected plots that are required for analysis of results will be shown.

1. Simulation Input Parameters

Table 3 shows the inputs parameters that are held constant for each simulation run used to obtain results. These input parameters are set in the MATLAB script file that calls the SIMULINK attitude simulation. The MATLAB code file is included as Appendix B.

SIMULATION PARAMETERS (SIMULINK)	
Simulation Time Period	500 sec
Attitude Determination Bandwidth	20 Hz
SIMULINK Solver Method	ode5 (Dormand-Prince)
Solver Fixed Step Size	0.05 sec
ORBIT PARAMETERS (Circular Orbit)	
Altitude	715 km

COMMANDED MANEUVER PROFILE	
Inertial Attitude Quaternions	See Figure 35
Body Axes Angular Rates	See Figure 36
Secondary Body Relative Angle	See Figure 37
DISTURBANCE MOMENTS	
Gravity Gradient	Modeled
Secular (Magnitude)	1e-4 Nm
Periodic (Magnitude, Period)	4e-4 Nm, [400,500,600] sec
Disturbance Effect on System Angular Momentum	See Figure 38.
MOMENTS OF INERTIA MATRICIES	
Primary Body	[2997.28025,-3.9331,118.2824 -3.9331,3164.18285,1.1230 118.2824,1.1230,881.82105] kgm^2
Secondary Body	[1721.07340,-0.0116,-7.8530 -0.0116,1559.85414,-12.5463 -7.8530,-12.5463,182.89962] kgm^2
CENTER OF MASS OFFSET FROM SPACECRAFT C.M.	
Primary Body	[0.558354158, 3.91788e-4, 0.15226902] m
Secondary Body	[-1.302113918, -9.13673e-4, 0.355100092] m
WHEEL CONTROL LAWS	
Quaternion Error Gains (Kq)	[3000,7000,4500]
Angular Rate Error Gains (Kw)	[1000,2000,1000]
Control Law Delay for Initial Determination Errors	30 sec
GYROSCOPE CHARACTERISTICS	
Static Rate Biases	1e-4*[-1,1.5,1] rad/sec
Rate Noise Variance	1e-8
Acceleration Noise Variance (Rate Random Walk)	1e-12
3 Gyro Alignment	Aligned to Body Axes
ATTITUDE DETERMINATION INITIALIZATION ERRORS	
Quaternion Errors (q1,q2,q3)	[0.008,0.012,-0.008]
Angular Rate Errors	[-0.001,0.001,0.002] rad/sec
KALMAN FILTER INITIALIZATION	
State Estimate	[0,0,0,0,0,0]

State Error Covariance Matrix	5e2*[100,0,0,0,0,0 0,100,0,0,0,0 0,0,100,0,0,0 0,0,0,1,0,0,0 0,0,0,0,1,0,0 0,0,0,0,0,1,0 0,0,0,0,0,0,1]
STAR TRACKER ALIGNMENT TO BODY AXES	
Tracker 1 (x-rotation, y-rotation)	135 deg, 30 deg
Tracker 2 (x-rotation, y-rotation)	135 deg, -30 deg
Tracker 3 (x-rotation, y-rotation)	180 deg, 0 deg
REACTION WHEEL PARAMETERS (4 WHEEL PYRAMID CONSTELLATION)	
Number of Wheels Operating	3
Constellation Angle to xy-Plane	45 deg
Constellation Torque Saturation Limit	1 Nm
Constellation Torque Rate limits	10 Nm/sec

Table 3. Simulation Input Parameters

2. Command Attitude Profile

The 500 second maneuvering profile chosen for the Bifocal Relay Mirror attitude simulation analysis is illustrated in Figures 35, 36 and 37. This profile resembles the maneuver required to maintain transmit and receive telescope pointing control during an overhead operational pass to conduct laser relay operations. The majority of the maneuver is performed in the spacecraft pitch axis, q_2, as both telescopes orient to point at fixed ground sites. Less significant motion is required in the spacecraft roll and yaw axes in order to ensure that the relative axis of rotation of the receive telescope is correctly oriented during the tracking maneuver. Based on ground site separation distance and orbital altitude, the largest relative angle require between the telescopes is about 30 degrees during a near overhead pass between the uplink and downlink ground sites.

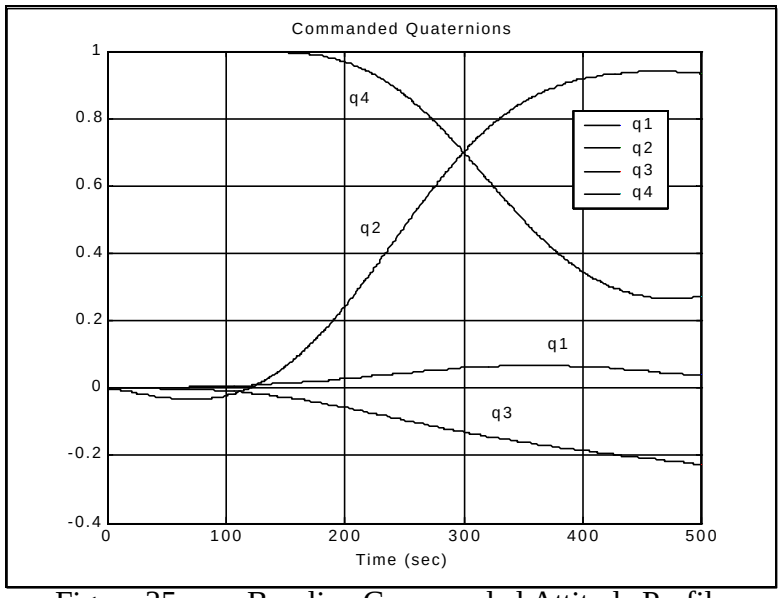

Figure 35. Baseline Commanded Attitude Profile

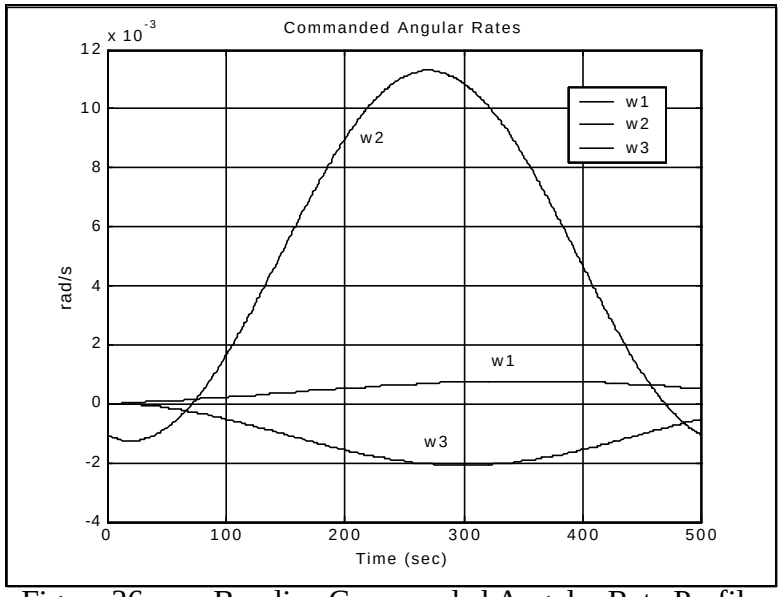

Figure 36. Baseline Commanded Angular Rate Profile

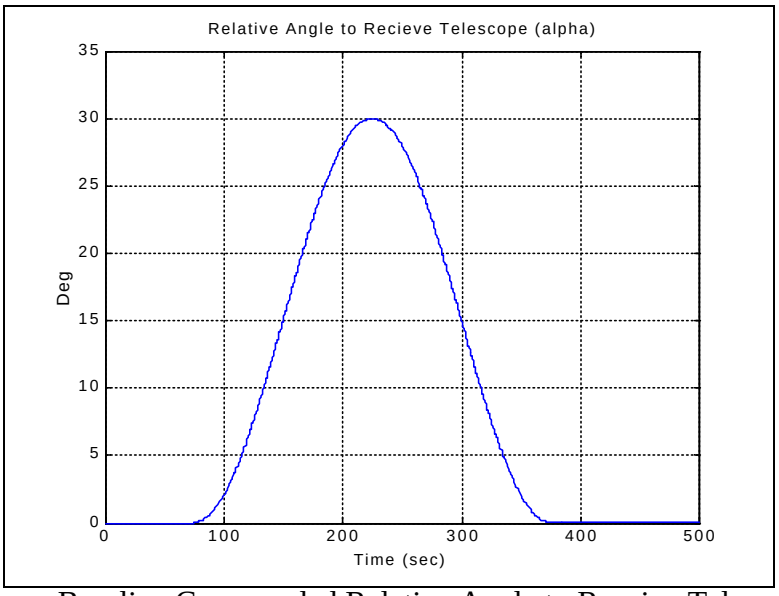

Figure 37. Baseline Commanded Relative Angle to Receive Telescope Profile

The magnitude of the total spacecraft angular momentum during the maneuvering profile is plotted in Figure 38. The spacecraft attitude is completely controlled by momentum exchange with the reaction wheels. Therefore, the changes to the angular momentum profile are attributable the external disturbance moments. The gravity gradient disturbance is modeled and the other disturbances are fixed so the angular momentum profile remains essentially common in all simulation runs.

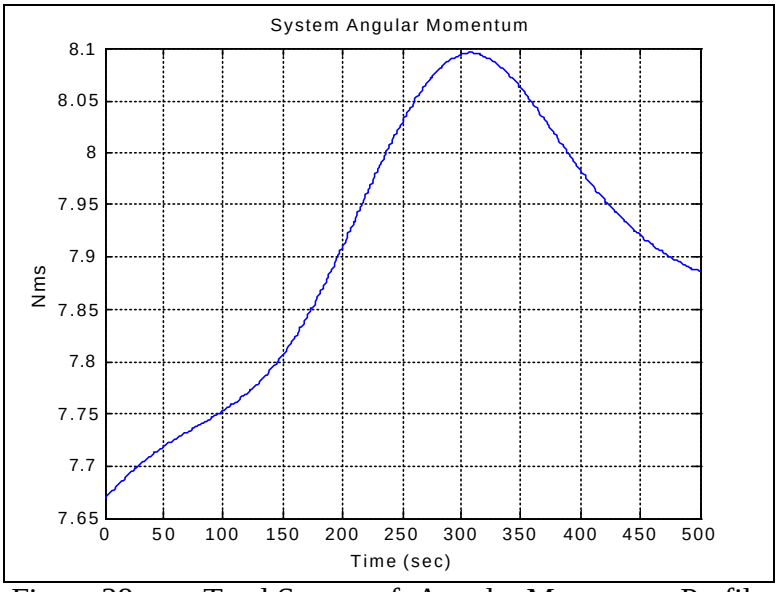

Figure 38. Total Spacecraft Angular Momentum Profile

3. Attitude Determination System Performance Results

In this baseline simulation, updates from randomly selected star trackers are provided to the dynamic gyro and the attitude propagator via the Kalman filter at two second intervals. The star tracker H and V measurements are corrupted with noise variance of $1x10^{-4}$. In order to observe the performance of the attitude determination system without updates, a 200 second star gap is simulated starting 100 seconds into the run. As a worst-case analysis, this star gap occurs during the peak maneuvering time of the satellite including the rotation of the secondary body. Attempt is made to tailor the plant and measurement error covariance matricies used in the Kalman filter. The attitude determination system is initiated with the errors given in Table 3.

The accuracy of the angular rate calculation is entirely dependent upon the ability of the dynamic gyro to track the total spacecraft angular momentum. The error in the magnitude of the total system momentum compared to the simulated actual momentum is shown in Figure 39. The steady state momentum error is held within 0.07 Nms with consistent star tracker data but builds to 0.35 Nms after 200 seconds without stars. No external disturbance torques are modeled as dynamic gyro inputs in this simulation run.

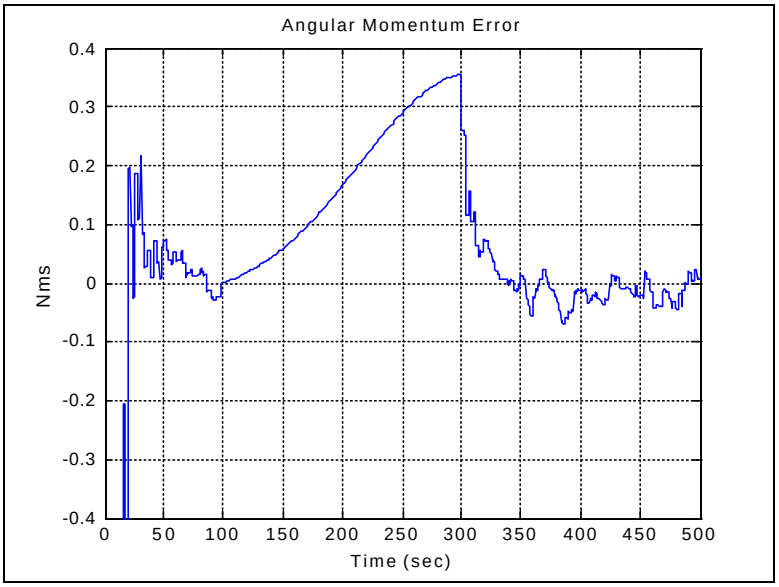

Figure 39. Baseline Dynamic Gyro Angular Momentum Error

After star tracker measurements are processed, the Kalman filter provides a momentum correction to the dynamic gyro determined from the spacecraft inertia and the

rate bias error state estimate. The attitude quaternion is also updated and the states are reset to zero. Figure 40 shows the magnitude of the error states determined by the Kalman filter. No updates are provided during the 200 second star gap.

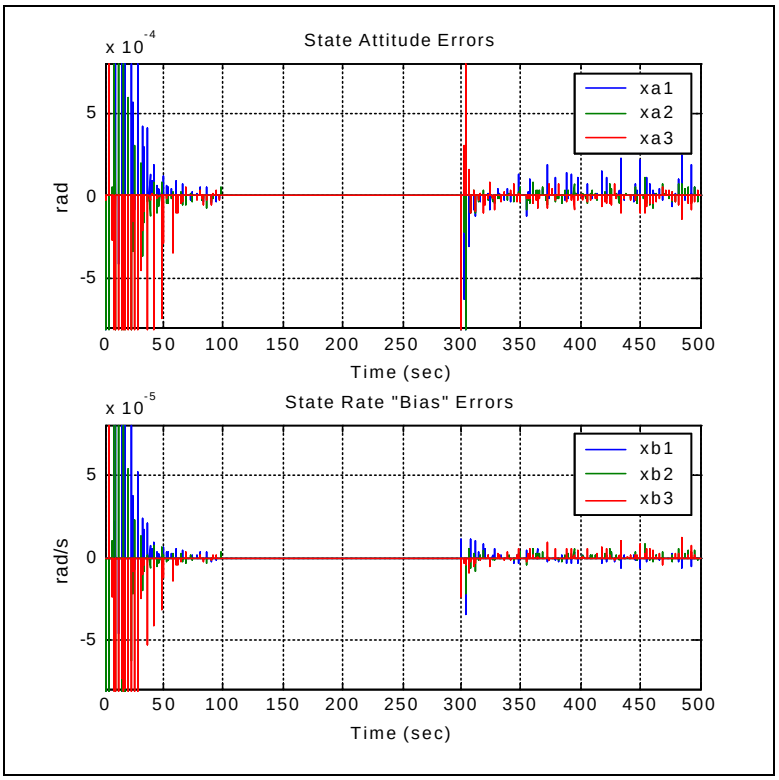

Figure 40. Baseline Kalman Filter Attitude and Rate Bias Errors

Quaternion errors in the attitude determination system are plotted in Figure 41. Steady state attitude errors are maintained within $3x10^{-4}$ during periods of continuous star coverage but are increased an order of magnitude by the end of the 200 second star gap. After the star gap, the attitude error build up is quickly removed through measurement corrections.

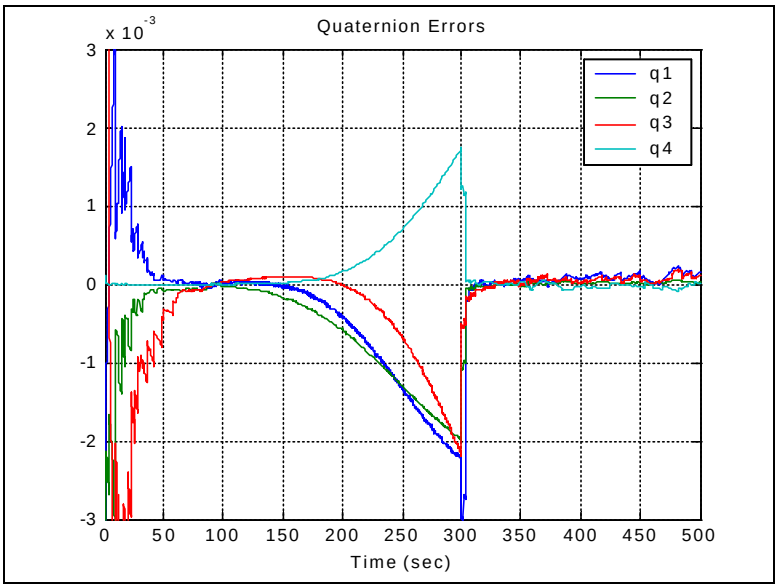

Figure 41. Baseline Estimated Attitude Quaternion Error

Figure 42 illustrates the nature of the angular rate estimation error produced by the dynamic gyro based determination system. The error generated in the roll axis, w_1, is the most significant because it is aligned with the axis of rotation of the secondary body. The relative rate is derived from imperfect potentiometer measurements. The rate errors increase during receive telescope motion due to the potentiometer quatization effect which produces the broken pattern of noise. The yaw axis is most coupled dynamically to roll axis and exhibits similar errors at less magnitude. The build up of the bias in the rate error is hard to perceive among the noise but the effects are evident in the quaternion error plot.

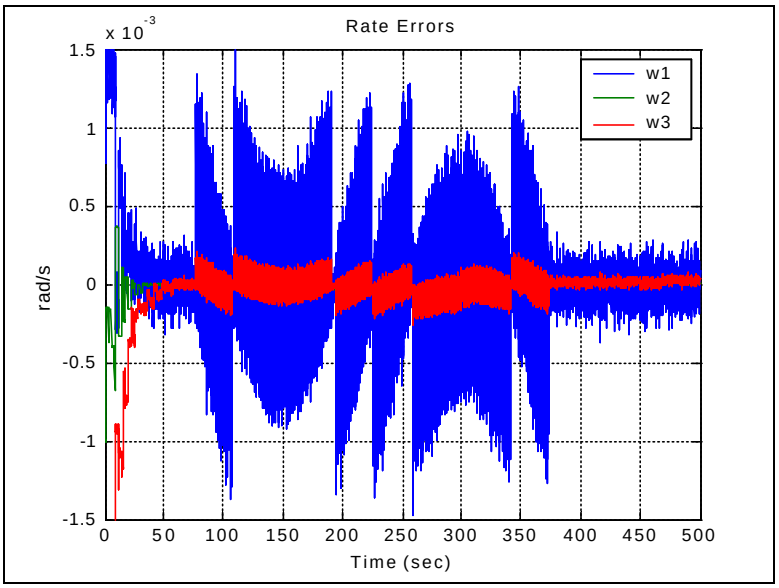

Figure 42. Baseline Estimated Angular Rate Error

4. Attitude Control System Performance Results

Attitude control is accomplished by three reaction wheels selected from a pyramid constellation of four. Nonlinear response of these control actuators is simulated by saturation and rate limiting the output torques as shown in Figure 11. Wheel torque commands are generated by combining feed forward and error based control laws. The control laws implementation is delayed at initiation to allow the attitude determination system to converge. High gain control laws dominate the wheel torque response. Figures 43 and 44 show the torque and momentum response of the three operating reaction wheels.

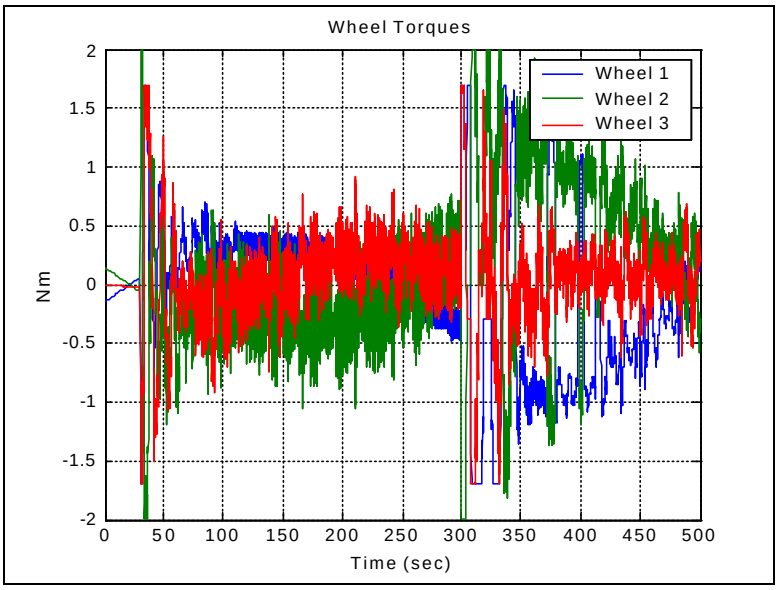

Figure 43. Reaction Wheel Control Torques

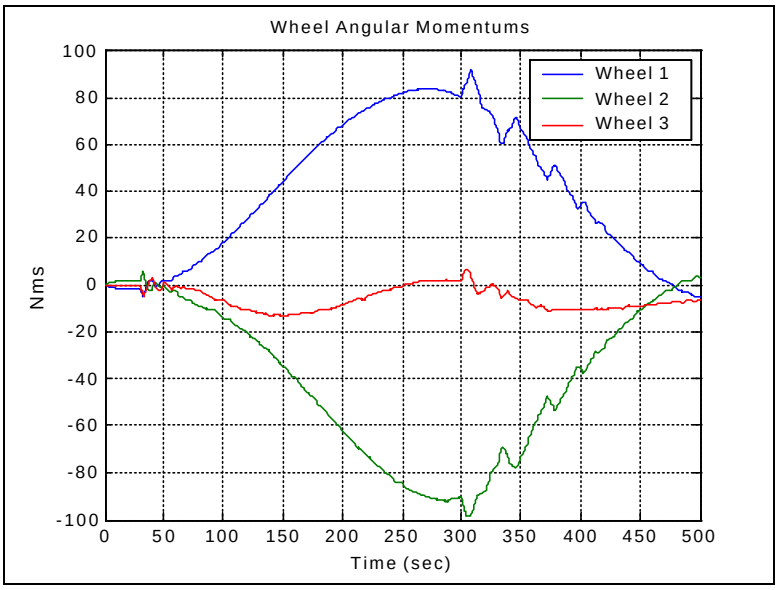

Figure 44. Reaction Wheel Angular Momentum

Attitude control performance is dominated by attitude determination errors. The control system is designed to limit steady state errors in the attitude quaternions to less than $2x10^{-7}$ with ideal attitude and angular rate knowledge. With the control laws applied, the attitude control response resembles the errors of the attitude determination system in steady state. Figure 45 shows the attitude quaternion error response for the baseline simulation run. Damped corrections back to steady state after the star gap are much slower than those realized by the attitude determination system.

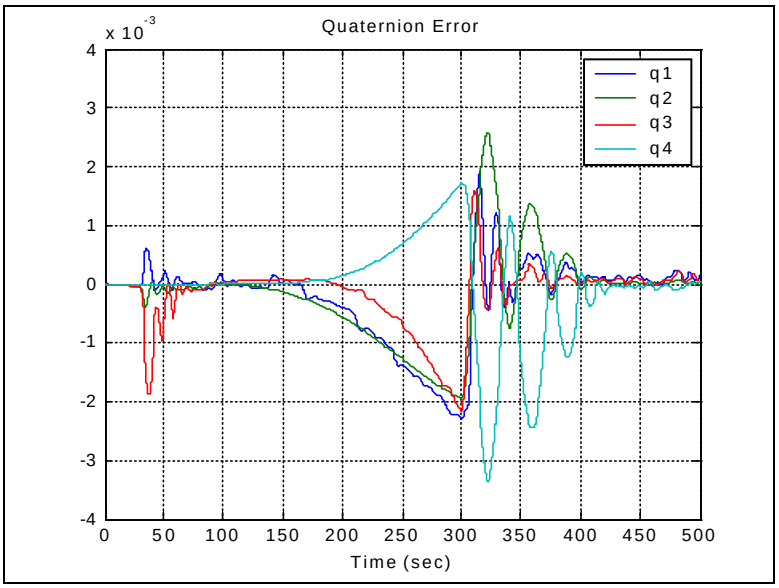

Figure 45. Baseline Control Attitude Quaternion Error

The error in the controlled spacecraft angular rate is shown in Figure 46. Since most of the attitude determination noise is removed by the controller, the uncorrected rate error bias due to the star gap is evident. Although the errors remain small during the star gap, the bias drives the attitude quaternion error build up.

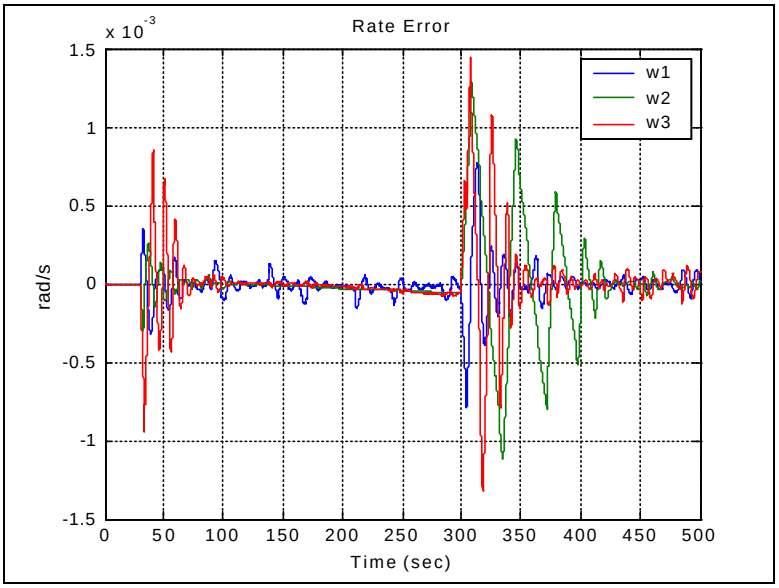

Figure 46. Baseline Control Angular Rate Error

B. DYNAMIC GYRO VS GYRO PERFORMANCE

Results presented in this section compare a gyro based attitude determination system with the dynamic gyro based system. Three orthogonally mounted gyroscopes

are modeled to provide simulated spacecraft body angular rate measurements to the attitude propagator when the gyro option is selected. The gyro model includes static bias, rate noise, and rate random walk supplied by integration of random noise. Gyroscope characteristics used for the simulation results are listed in Table 3. A bias error tracking system is also modeled in parallel with the gyro generated rates to accept bias corrections provided by the Kalman filter. Direct comparison of the dynamic gyro and gyro based attitude determination systems is accomplished using identical input parameters to obtain simulation results. The SIMULINK subsystem for gyro rate measurement and bias error tracking is illustrated in Figure 47.

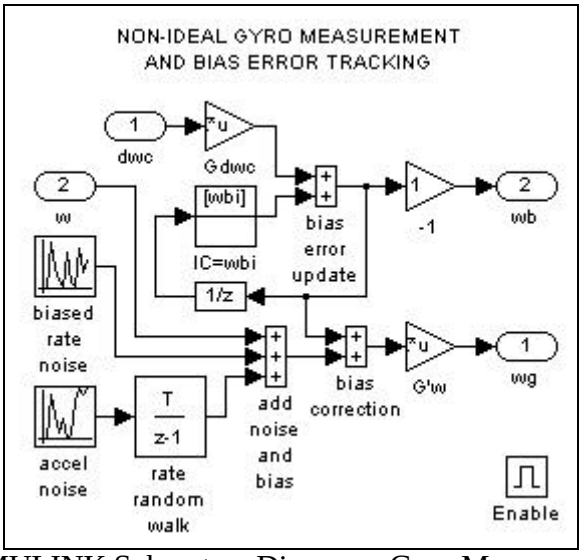

Figure 47. SIMULINK Subsystem Diagram: Gyro Measurement and Bias Error Tracker.

1. Continuous Star Tracker Coverage

With precise attitude updates from star trackers there is only little noticeable difference between the dynamic gyro and gyro based attitude determination systems. Figure 48 provides a side-by-side comparison of simulation results obtained with a continuous star update interval of 2 seconds.

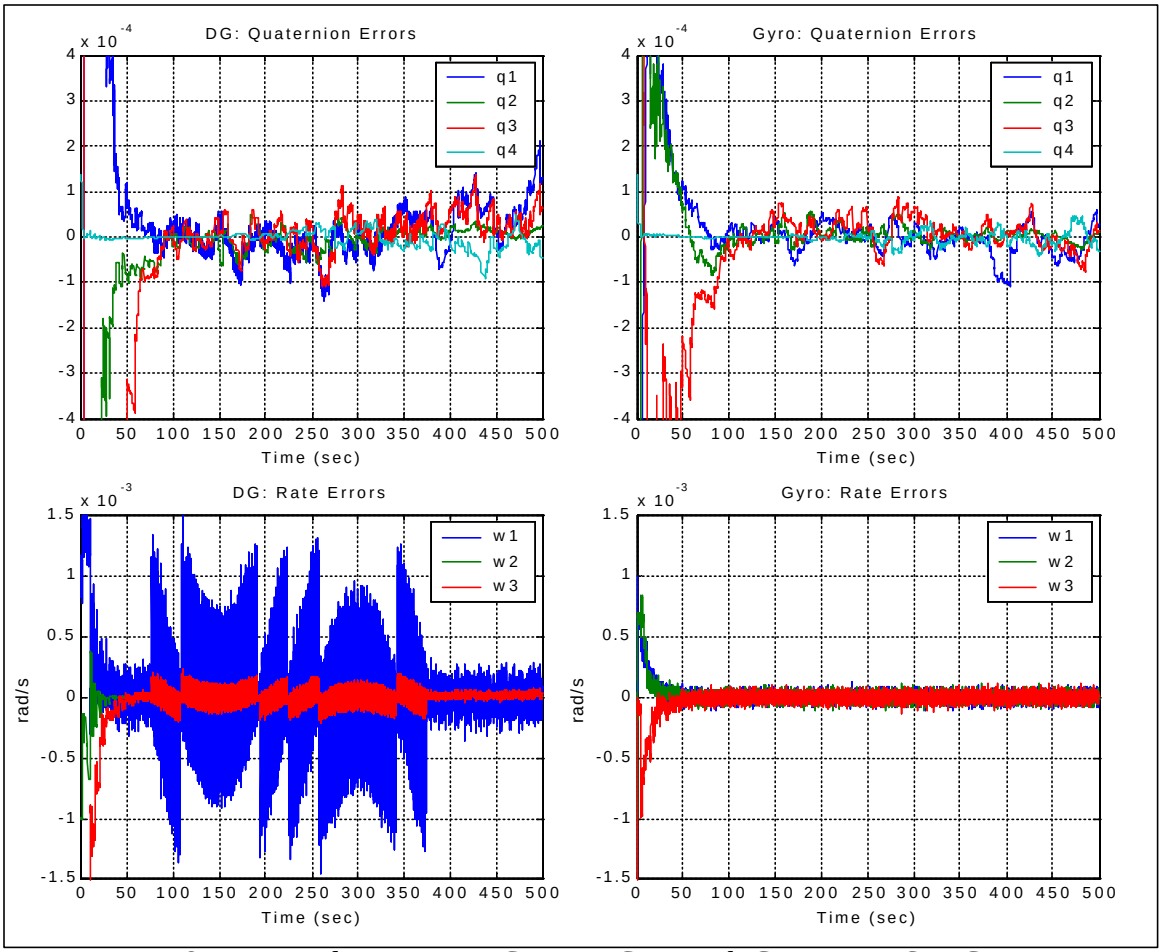

Figure 48. Results: Dynamic Gyro vs. Gyro with Continuous Star Coverage

Although the attitude quaternion errors show little difference between the two systems the rate errors from the gyros are noticeably more accurate and better resemble white noise. Since the characteristics of the rate errors are different between the two systems the plant error covariance matricies used in the Kalman filter are chosen differently. Table 4 shows the plant error covariance matricies used by the dynamic gyro and gyro based systems. These values were determined through tuning over several simulation runs.

Plant Error Covariance Matrix (Q)	
Dynamic Gyro	Gyro
$\begin{bmatrix} 50 & 0 & 0 & 0 & 0 & 0 \\ 0 & 50 & 0 & 0 & 0 & 0 \\ 0 & 0 & 50 & 0 & 0 & 0 \\ 0 & 0 & 0 & 0.5 & 0 & 0 \\ 0 & 0 & 0 & 0 & 0.5 & 0 \\ 0 & 0 & 0 & 0 & 0 & 0.5 \end{bmatrix}$	$\begin{bmatrix} 3 & 0 & 0 & 0 & 0 & 0 \\ 0 & 3 & 0 & 0 & 0 & 0 \\ 0 & 0 & 3 & 0 & 0 & 0 \\ 0 & 0 & 0 & 0.03 & 0 & 0 \\ 0 & 0 & 0 & 0 & 0.03 & 0 \\ 0 & 0 & 0 & 0 & 0 & 0.03 \end{bmatrix}$

Table 4. Plant Error Covariance Matricies

2. Gapped Star Tracker Coverage

Figure 49 shows the comparison of the dynamic gyro and gyro based attitude determination systems when a 200 second gap in star tracker coverage is encountered during maneuvering operations. Very little difference is evident in the rate error plots because the bias build up during the star gap is so small compared to the noise in the error. The effect of the bias, however, shows in the attitude quaternion error plots. At the end of the star gap the error in the dynamic gyro based system is about five times that of the gyro based system.

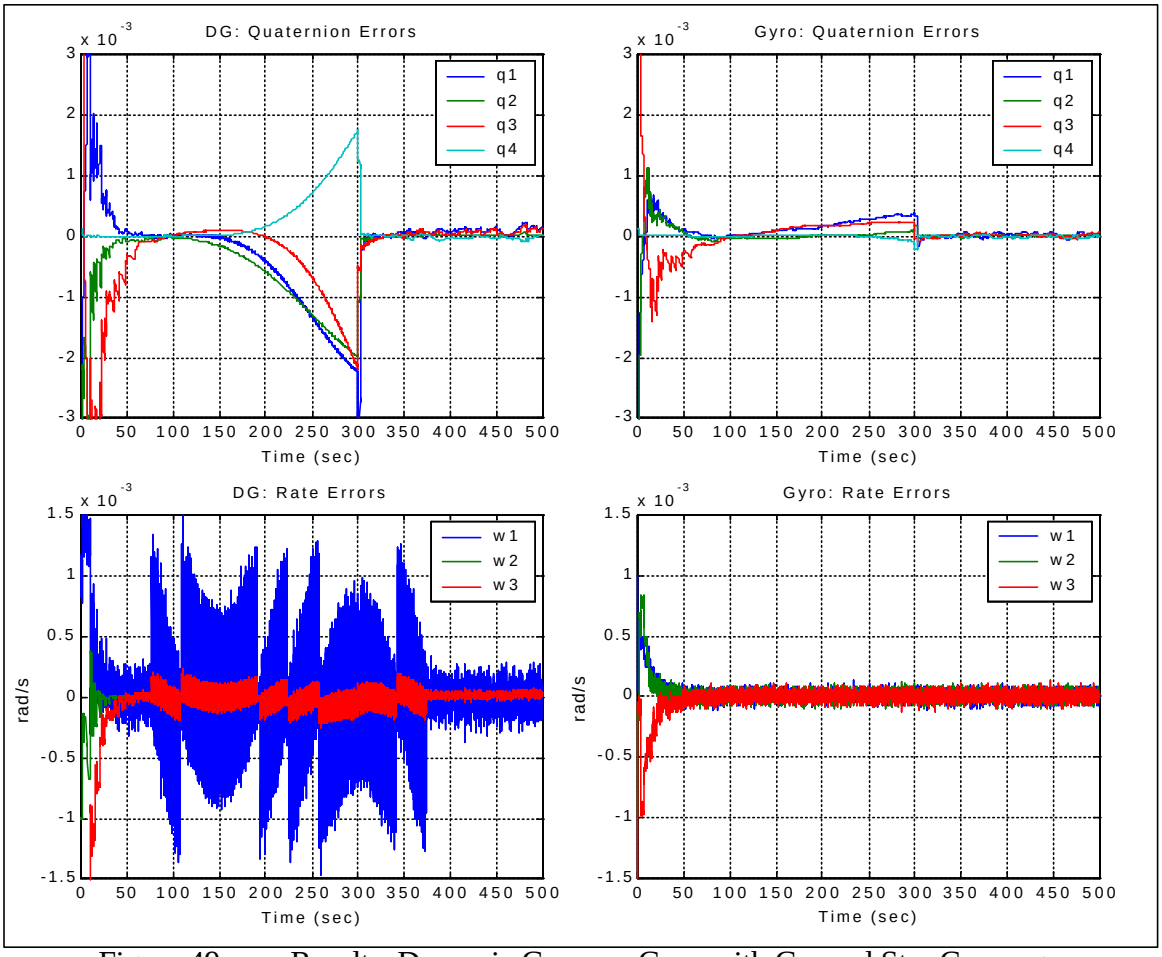

Figure 49. Results: Dynamic Gyro vs. Gyro with Gapped Star Coverage

C. DYNAMIC GYRO PLANT ERROR ANALYSIS

In this section the effects of major error sources on the performance of the dynamic gyro are analyzed. Figure 50 shows the attitude determination plots for the baseline simulation run. Dynamic gyro input parameters are varied and results are compared with these plots.

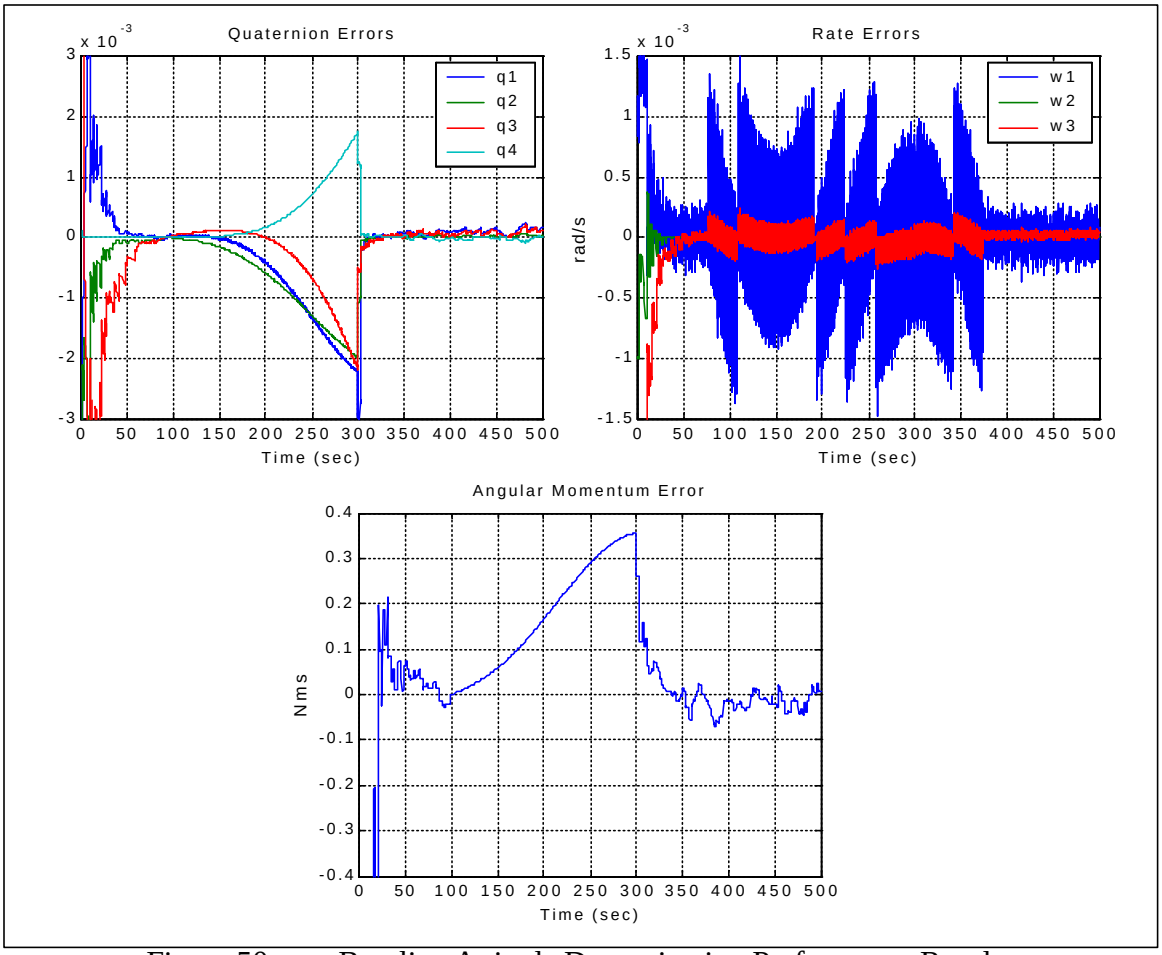

Figure 50. Baseline Attitude Determination Performance Results

1. Disturbance Torque Modeling

The accuracy of the dynamic gyro depends on knowledge of external disturbance moments and internal spacecraft momentum. For the baseline simulation run no external disturbances were modeled in the dynamic gyro. This leads to the relatively large drift in attitude quaternions when uncorrected during the star gaps. If the spacecraft's attitude with respect to the orbital reference frame can be determined the gravity gradient disturbance torque can be modeled. For the Bifocal Relay Mirror satellite this disturbance has the greatest effect. Figure 51 illustrates the increase in performance of the dynamic gyro based attitude determination system when the gravity gradient moment is modeled. At the end of the star gap the attitude errors are comparable to the gyro based system. The total system angular momentum error is much smaller during the star gap and improvement can even be seen during times of continuous star coverage.

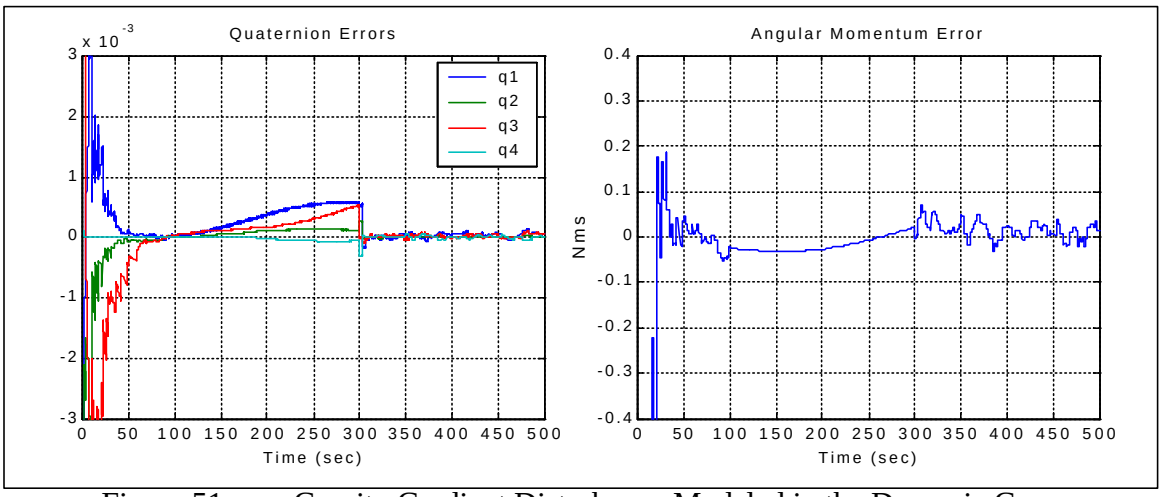

Figure 51. Gravity Gradient Disturbance Modeled in the Dynamic Gyro

2. Rotation Axis Alignment Error

Alignment errors of momentum exchange control devices and slewing appendages have direct effects on the dynamic gyro momentum error. Alignment errors of fixed reaction wheels are easily compensated for by calibration but control moment gyros have directionally variant momentum vectors with respect to the spacecraft body. The results plots shown in Figure 52 are produced when a periodic alignment error on the net momentum of the reaction wheels with a magnitude of approximately 0.5 degrees is added to the simulation. A significant increase in attitude error is developed during the star gap. The dynamic gyro does not track the system angular momentum as well even during continuous star coverage.

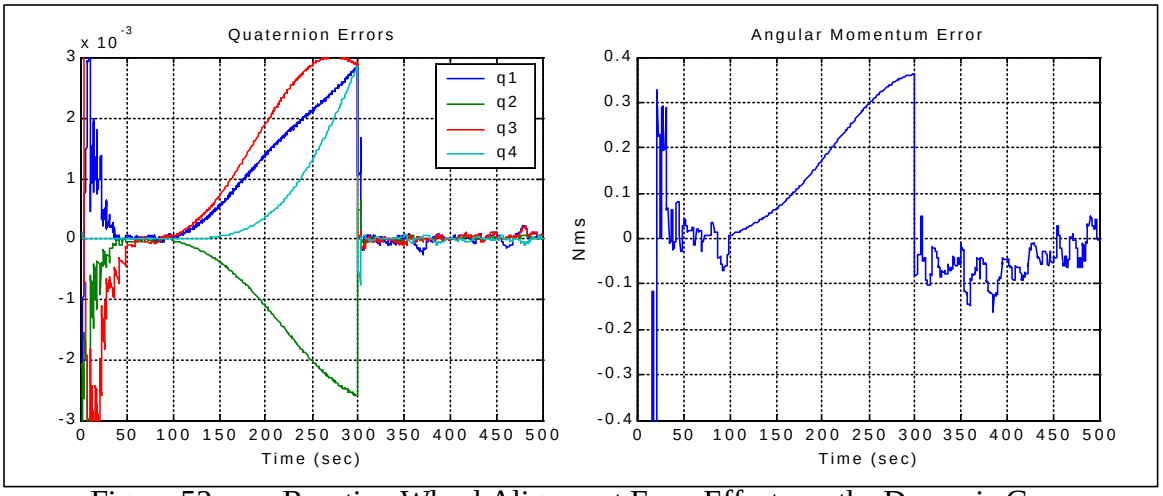

Figure 52. Reaction Wheel Alignment Error Effects on the Dynamic Gyro

3. Potentiometer Quantization

The patterns shown in angular rate error plots for the dynamic gyro do not appear as white noise during appendage motion because of quantization effects in the model of the potentiometer that measures the relative orientation. The simulated quantization level is 0.01 degrees in the baseline simulation. Since the effect alternates direction of error the attitude quaternion errors are not affected significantly. Figure 53 shows simulation performance results when the quantization level is decreased an order of magnitude. The angular rate error looks more like white noise and the bias build up during the star gap can be seen.

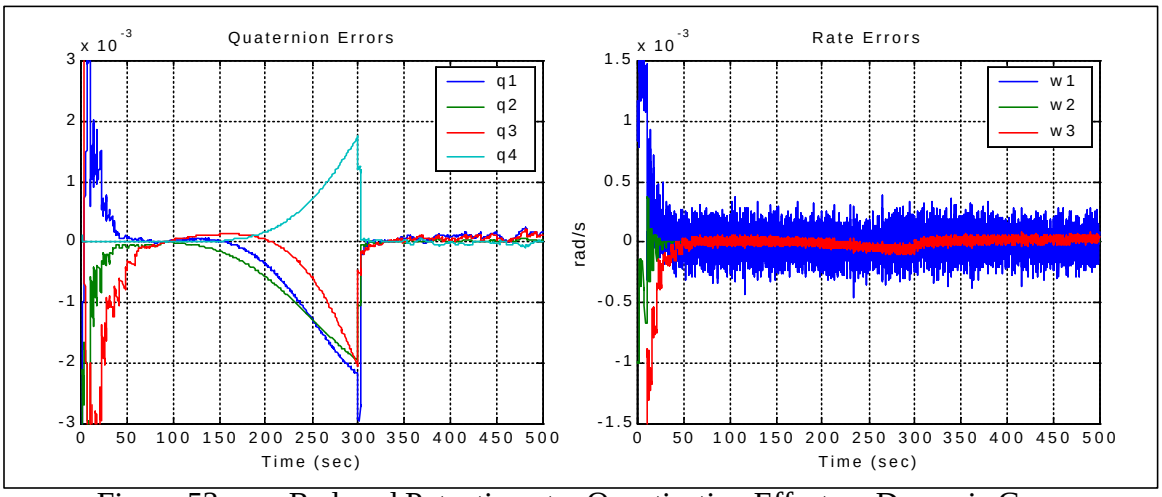

Figure 53. Reduced Potentiometer Quantization Effect on Dynamic Gyro Performance

4. Moment of Inertia Update Frequency

The inertia matrix for spacecraft with relatively small or slowly moving appendages does not change quickly. In these cases processing power may be saved by performing the system inertia calculation at a lower bandwidth than the dynamic gyro. In the Bifocal Relay Mirror satellite the secondary body is large so even small slew rates cause significant change in the system inertia matrix. Figure 54 shows the effects of decreasing the inertia calculation frequency from the 20 Hz rate of the dynamic gyro to once every 10 seconds. The quaternion error profile is significantly altered but the magnitude of the error is only slightly increased. The momentum error in the dynamic gyro takes longer to correct after the star gap since the Kalman filter attempts to correct for all errors as if they were due to spacecraft momentum.

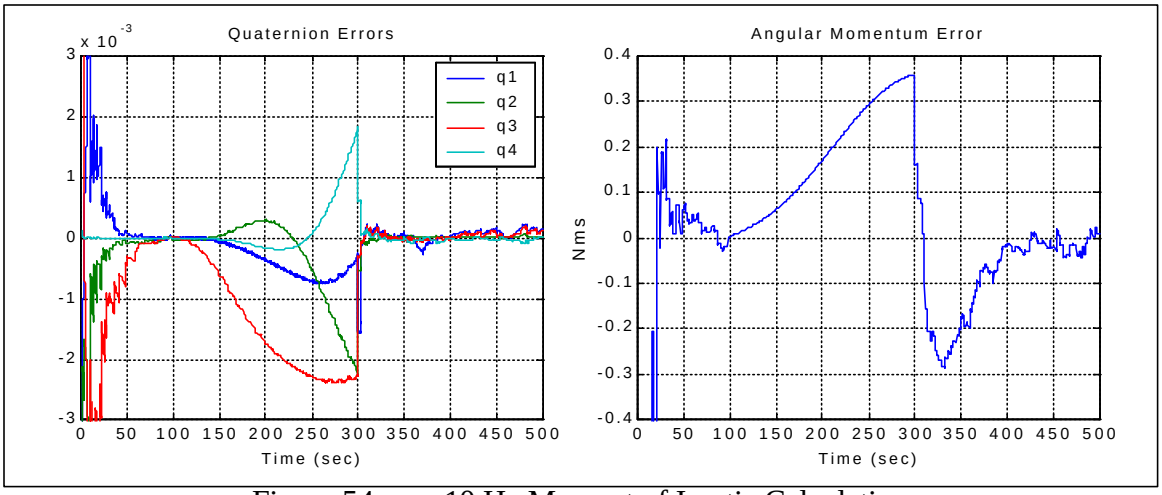

Figure 54. 10 Hz Moment of Inertia Calculation

D. STAR TRACKER MEASUREMENT ERROR ANALYSIS

The dynamic gyro based attitude determination system is highly reliant on Kalman filter updates based on star tracker measurements. The quality of the Kalman filter corrections depend on the accuracy of the trackers, the discrete measurement interval and number of trackers providing measurements.

1. Star Tracker Accuracy

The results shown in Figure 55 are from simulations using random selection at 2 second intervals. The plot on the left is generated using a 1 sigma variance of $1x10^{-4}$ in the horizontal and vertical measurements of the trackers. To generate the plot on the right the variance is reduced by four times. The direct effect on attitude determination performance is apparent.

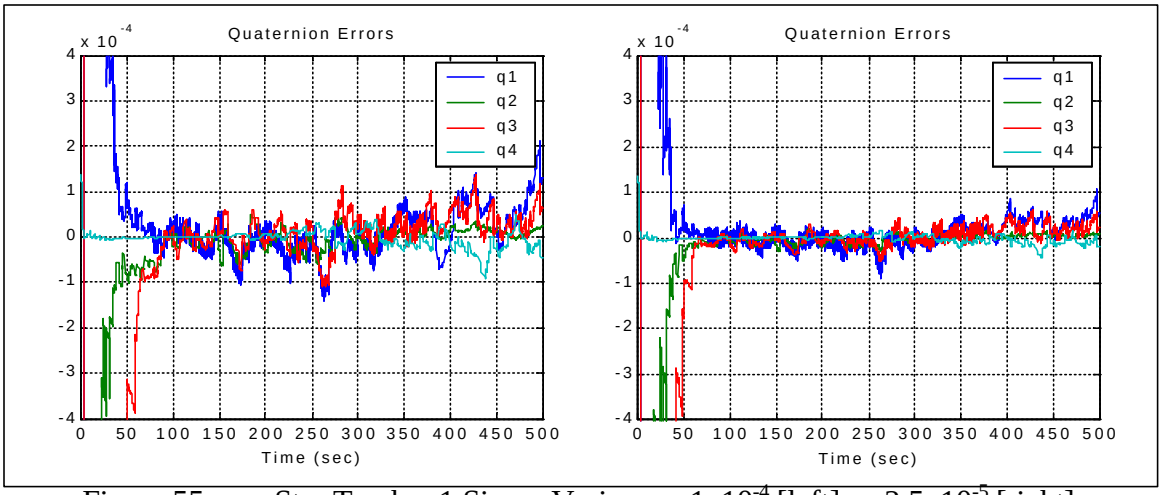

Figure 55. Star Tracker 1 Sigma Variance: $1x10^{-4}$ [left] vs $2.5x10^{-5}$ [right]

2. Update Interval

Figure 56 shows a comparison of attitude determination performance using 2 and 6 second star measurement intervals. Shorter update intervals result in quicker convergence and less steady state error.

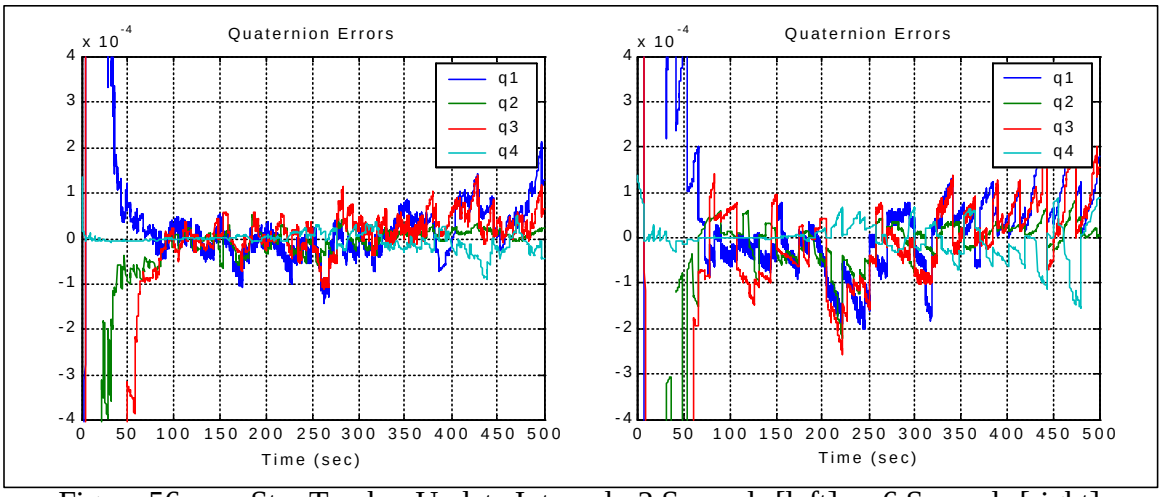

Figure 56. Star Tracker Update Interval: 2 Seconds [left] vs 6 Seconds [right]

3. Star Tracker Selection

Because the star tracker measurements provide useful information along only two axes at least two trackers must be active to maintain pointing control. Figure 57 shows the comparison of an attitude determination simulation with updates spread evenly between three trackers and one that uses two trackers with 95% of the updates coming from the same sensor. There is no apparent degradation when the updates are spread evenly between the two operational trackers.

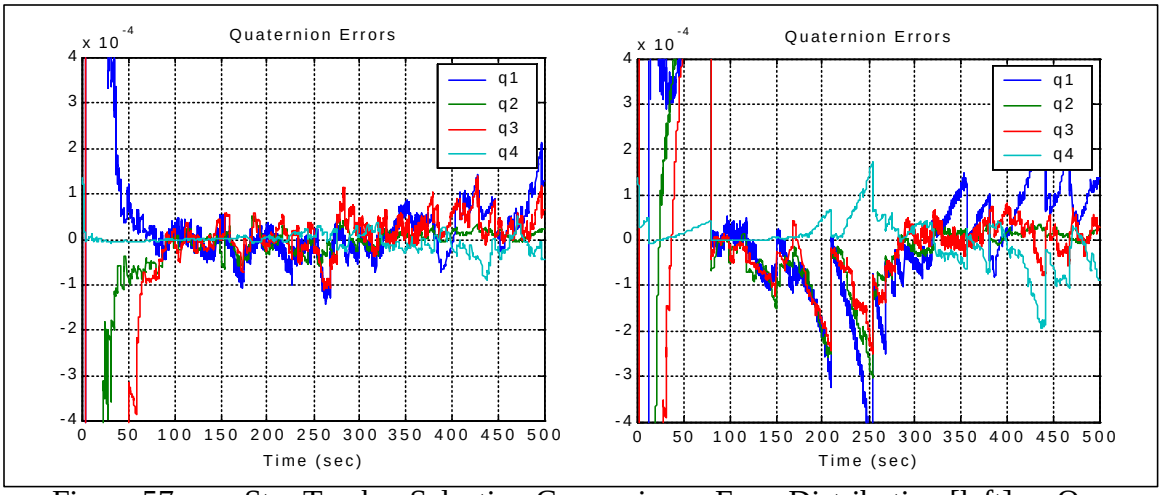

Figure 57. Star Tracker Selection Comparison: Even Distribution [left] vs One Tracker Favored [right]

THIS PAGE INTENTIONALLY LEFT BLANK

VIII. CONCLUSIONS

Dynamic modeling provides an imperfect but operative means of estimating multi-body spacecraft angular rates when mechanical gyro data are not available. An attitude and angular rate estimation scheme is developed in this thesis that integrates the dynamic gyro concept with an error state extended Kalman filter estimator that provides precise attitude updates from star tracker measurements. Results indicate that the determination system provides effective estimates for performing attitude control.

A. SUMMARY

The attitude determination system is incorporated into a multi-body spacecraft attitude simulation for evaluation and analysis. Simulation is an extremely valuable analysis tool for understanding the effects of error sources on system performance. It is also a suitable mechanism for comparison with gyro based determination systems since a mechanical gyro model can easily be inserted.

The effects of the primary error sources on the dynamic gyro performance are investigated through simulation. It is shown that the corrections provided by a star tracker based Kalman filter make the system robust to measurement and parameter knowledge error sources. Significant improvement in attitude determination performance is realized when disturbance torques are modeled. The other primary error sources include the alignment of momentum exchange control devices and relative angle and rate knowledge in large or quickly slewing appendages. Error effects are amplified during star gaps when no corrections to the dynamic model are available.

The software implemented dynamic gyro essentially emulates the functions of a set hardware gyroscopes. In a spacecraft where the mechanical gyros have failed or become too erratic to be corrected by the Kalman filter the dynamic gyro may be a viable replacement. Operated in tandem with mechanical gyros, either system can provide redundant inertial angular velocity for improved attitude control.

This attitude determination concept is ideally suited to a spacecraft designed specifically for its implementation with precise internal sensors and mechanisms to monitor spacecraft parameters and integrated external torque estimation modeling. In these systems the dynamic gyro can increase the lifetime and reliability of the spacecraft while reducing the power requirements.

B. RECOMMENDATIONS

A strong recommendation for future work is simulation model tailoring to real spacecraft hardware. The multi-body dynamics can be expanded to model an actual satellite's mass and inertia characteristics. Additionally, sensor parameters can be modeled to match existing sensor error specs. With these modifications the simulation model can be used conduct analysis and predict performance when the dynamic gyro software is implemented on board the spacecraft. Future work may include using the simulation to compare the predicted dynamic gyro based attitude determination performance to actual gyro based performance recorded with telemetry data.

There are several improvements that can be made to the attitude determination simulation model. It could easily be modified to provide the capability to mix gyroscope and dynamic gyro data for redundant information. A parity matrix developed from the pseudo-inverse concept can be generated to account for system observability in the over determined case. This would allow performance analysis with selected gyro failures and further aid in the evaluation of its utility as a back-up attitude determination scheme. Another simulation improvement would be the incorporation of higher order dynamic effects into the model including center of mass offsets and flexibility modes for the appendage couplings.

Finally, improvements to the attitude determination scheme can be developed including a torque error estimator as suggested by The Aerospace Corporation [Ref. 8]. The better the dynamics are modeled in the processing software the more effective the dynamic gyro becomes as a replacement for the hardware gyroscope.

APPENDIX A: KALMAN FILTER BACKGROUND

"The Kalman filter combines all available measurement data, plus prior knowledge about the system and measuring devices, to produce an estimate of the desired variables in such a manner that the error is minimized statistically" [Ref. 2]. An understanding of the Kalman filter requires some background in the theory of probability of random variables and processes [Ref. 1].

A. PROBABILITY

The probability of an event, e, represents a possible outcome of a random experiment and is written Pr(e). A random variable, X, can be thought of as a function of the outcomes of some random experiment. The manner of specifying the probability with which different values are taken by a random variable is the probability distribution function, F(x)

$$F(x)=Pr(X \leq x) \tag{A.1}$$

This is a function over the range of possible values that shows the probability with which the random variable takes on a value at or less than the value of the range. Its derivative is the probability density function, f(x),

$$f(x)=\frac{dF(x)}{dx} \tag{A.2}$$

This function identifies the likelihood of a random variable assuming a particular value in its range of possible values. Over the range of all possible values a characteristic of any probability distribution or density function is

$$F(\infty)=\int_{-\infty}^{\infty} f(u)du = 1 \tag{A.3}$$

A joint probability density function can be defined for multiple variables. For two random variables the joint density is given by

$$f_2(x,y) = \frac{\partial^2 F_2(x,y)}{\partial x \partial y} \tag{A.4}$$

B. EXPECTATION

The expectation of a random variable is defined as the sum of all values the random variable may take, each weighted by the probability with which the value is taken.

$$E[X]=\int_{-\infty}^{\infty} xf(x)dx \tag{A.5}$$

which is also called the mean value or first moment of X. This is a precisely defined number toward which the average of a number of observations of the random variable X tends. Since a function of a random variable is itself a random variable, the expectation of a function of X, E[g(X)], can be expressed as

$$E[g(X)]=\int_{-\infty}^{\infty} g(x)f(x)dx \tag{A.6}$$

An important statistical parameter descriptive of X is its mean squared value defined by

$$E[X^2]=\int_{-\infty}^{\infty} x^2f(x)dx \tag{A.7}$$

which is also called the second moment of X. The root-mean-squared (rms) value of X is $\sqrt{E[X^2]}$. The variance of a random variable is defined as the mean squared deviation of the variable from its mean denoted by $ó^2$.

$$ó^2=\int_{-\infty}^{\infty} (x-E[X])^2 f(x)dx = E[X^2]-E[X]^2 \tag{A.8}$$

For zero mean random variables the variance is simply $E[X^2]$. The square root of the variance, $ó$, is called the standard deviation of the random variable.

A very important concept is that of statistical correlation between random variables. A partial indication of the degree to which one variable is related to another is given by the cross covariance, which is the expectation of the product of the deviations of the two variables from their means,

$$E[(X-E[X])(Y-E[Y])]=\int_{-\infty}^{\infty}\int_{-\infty}^{\infty}(x-E[X])(y-E[Y])f_2(x,y)dydx=E[XY]-E[X]E[Y] \tag{A.9}$$

For a vector of random variables a symmetric covariance matrix can be defined where the diagonal elements are the individual variances of the vector components and the off diagonals are given by the cross covariances between the corresponding vector components. The cross covariance, normalized by the standard deviations of X and Y, is called the correlation coefficient.

$$\tilde{n}=\frac{E[XY]-E[X]E[Y]}{\acute{o}_X\acute{o}_Y} \tag{A.10}$$

This is a measure of the degree of linear dependence between variables X and Y. If they are completely independent $\tilde{n}$ is zero.

C. LEAST-SQUARES ESTIMATION CONCEPT

The optimality condition used in the Kalman filter is the minimization of weighted least-squares error. The least-squares minimization problem involves a set of measurements, $\vec{y}$, which are linearly related to the vector of state variables, $\vec{x}$, by the expression

$$\vec{y}=H\vec{x}+\vec{v} \tag{A.11}$$

where $\vec{v}$ is an unknown vector of actual measurement errors with zero mean. The error we seek to minimize is the measurement residual, $\vec{z}$, given by

$$\vec{z}=\vec{y}-H\hat{\vec{x}} \tag{A.12}$$

where $\hat{\vec{x}}$ is the estimate of the actual state vector. Since the sum of the squares of a vector are generated by the inner product, the cost function, J, is

$$J=\left(\vec{y}-H\hat{\vec{x}}\right)^T\left(\vec{y}-H\hat{\vec{x}}\right) \tag{A.13}$$

Minimization is obtained by differentiating and setting the result to zero

$$\frac{\partial J}{\partial \hat{\vec{x}}} = \vec{0} \tag{A.14}$$

and ensuring that the Hessian is positive semidefinite

$$\left| \frac{\partial^2 J}{\partial \hat{\vec{x}}^2} \right| \geq 0 \tag{A.15}$$

The resulting least-squares solution for the state estimate is

$$\hat{\vec{x}} = \left(H^T H \right)^{-1} H^T \vec{y} \tag{A.16}$$

A weighted least-squares solution can be used when not all components of the measurement residual are treated equally

$$\hat{\vec{x}} = \left(H^T W H \right)^{-1} H^T W \vec{y} \tag{A.17}$$

where W is a positive semidefinite matrix relating scale factors between components. Expanding this solution to multiple estimates over time assumes all measurements are used together in a batch processing scheme. Every time a new measurement becomes available it is appended to the measurement vector and the estimated state vector includes estimates corresponding to each of the accumulated measurements. The Kalman filter is based on recursive processing where each measurement is used sequentially to generate an optimal estimate of the current state without recomputing estimates of all previous states. For this technique all previous information is embodied in the prior estimate and state covariance matrix.

D. STATE ESTIMATE AND COVARIANCE

The Kalman filter estimation algorithm maintains the first two statistical moments of the estimated state. The estimated state, $\hat{\vec{x}}$, is a vector of random variables whose mean (first moment) is the actual state vector, $\vec{x}$. The error in the state estimate is defined as

$$\tilde{\vec{x}} \equiv \hat{\vec{x}} - \vec{x} \tag{A.18}$$

and is thus assumed to be zero mean. The covariance of the state estimate error, designated P, is given by

$$P=E[\tilde{\bar{x}}\tilde{\bar{x}}^T] \tag{A.19}$$

This covariance matrix associated with the state estimate error (second moment) provides a statistical measure of the uncertainty in $\hat{\bar{x}}$ and the correlation between the errors of its components. For a state vector of two variables the state estimate error is given by

$$\tilde{\bar{x}}=\begin{bmatrix}\tilde{x}_1\\ \tilde{x}_2\end{bmatrix} \tag{A.20}$$

and has the covariance matrix

$$P=E\left\{\begin{bmatrix}\tilde{x}_1^2 & \tilde{x}_1\tilde{x}_2\\ \tilde{x}_1\tilde{x}_2 & \tilde{x}_2^2\end{bmatrix}\right\}=\begin{bmatrix}E[\tilde{x}_1^2] & E[\tilde{x}_1\tilde{x}_2]\\ E[\tilde{x}_1\tilde{x}_2] & E[\tilde{x}_2^2]\end{bmatrix} \tag{A.21}$$

The diagonal elements of the state covariance matrix are the mean square errors in the knowledge of the state variables while the off diagonal elements are indicators of cross correlation between elements of the estimated error.

E. STOCHASTIC LINEAR DYNAMIC MODEL

The Kalman filter requires representation of system dynamics in a linearized state-space form, a linear measurement model, and assumed characteristics of process and measurement noise. For a continuous linear system the general state-space model and measurement equations are given by

$$\begin{aligned}\dot{\bar{x}}(t)&=F(t)\bar{x}+G(t)\bar{w}(t)\\ y(t)&=H(t)\bar{x}(t)+\bar{v}(t)\end{aligned} \tag{A.22}$$

where $\bar{w}(t)$ and $\bar{v}(t)$ are random vectors representing the unmodeled disturbance inputs and measurement errors. These vectors are treated as unbiased (zero mean) white noise. Note that if one of these vectors is known to have a nonzero bias the mean can be augmented onto the state vector creating a new state space model with unbiased random error. The covariance matricies associated with the process disturbance, $\bar{w}(t)$, and the measurement noise, $\bar{v}(t)$, are

$$Q = E[\vec{v}(t)\vec{v}(t)^T]$$
$$R = E[\vec{w}(t)\vec{w}(t)^T] \tag{A.23}$$

The equivalent discrete representation is

$$\vec{x}_{k+1} = \ddot{o}_k \vec{x}_k + \tilde{A}_k \vec{w}_k$$
$$\vec{y}_k = H_k \vec{x}_k + \vec{v}_k \tag{A.24}$$

Here the subscript k represents values at time t_k and subscript k+1 represents values at the next discrete time step t_{k+1}. Note that for time invariant systems the discrete state transition matrix, $\ddot{o}_k$, is related to the continuous formulation by

$$\ddot{o}_k = e^{F(t_{k+1} - t_k)} \tag{A.25}$$

which depends only on the systems dynamics matrix, F, and the discrete time interval. If the discrete interval is kept short enough the relation holds as an approximation. The state transition matrix allows the calculation of state vector at the next discrete time step in the absence of forcing functions. It obeys the differential equation

$$\frac{d\ddot{o}_k}{dt} = F(t)\ddot{o}_k \tag{A.26}$$

F. PROPAGATION OF ERRORS

The recursive Kalman filter requires the propagation estimate and error covariance based on system dynamics. In the discrete implementation the error in the current estimate given by

$$\tilde{\vec{x}}_k = \hat{\vec{x}}_k - \vec{x}_k \tag{A.27}$$

has the covariance matrix representing the uncertainty in the estimate

$$P_k = E[\tilde{\vec{x}}_k \tilde{\vec{x}}_k^T] \tag{A.28}$$

The best estimate of the future state, $\hat{\vec{x}}_{k+1}$, is given by

$$\hat{\vec{x}}_{k+1} = \ddot{o}_k \hat{\vec{o}}_k \tag{A.29}$$

The error in the new estimate

$$\tilde{\vec{x}}_{k+1} = \ddot{o}_k \tilde{\vec{x}}_k - \tilde{A}_k \vec{w}_k \tag{A.30}$$

has the expected value

$$E[\tilde{\bar{x}}_{k+1}] = \Phi_k E[\tilde{\bar{x}}_k] - \tilde{A}_k E[\bar{w}_k] = \bar{0} \quad \text{(A.31)}$$

since $\tilde{\bar{x}}_k$ and $\bar{w}_k$ are assumed to be unbiased. Thus the predicted estimate remains unbiased. Note that if a deterministic input is added to the dynamic system model then the identical quantity is added to both the actual and estimated state leaving the estimation error unchanged. It can be shown that the associated state error covariance matrix is given by

$$P_{k+1} = E[\tilde{\bar{x}}_{k+1}\tilde{\bar{x}}_{k+1}^T] = \Phi_k P_k \Phi_k^T + \tilde{A}_k Q_k \tilde{A}_k^T \quad \text{(A.32)}$$

where Q_k is the covariance of the random system disturbance. It is evident from this equation that the size of disturbance directly impacts the uncertainty in the state estimate. The system dynamic stability reflected in the state transition matrix also effects the uncertainty. The covariance of neutrally stable or unstable systems will grow unbounded over time in the absence of measurement corrections. The propagation of the state estimate and its error covariance matrix is the prediction step of the Kalman filter algorithm.

G. MEASUREMENT UPDATES

The correction step of the Kalman filter algorithm incorporates measurement updates to refine the state estimate and error covariance. This step is executed only when a measurement becomes available. When a measurement is taken we use the superscripts '-' and '+' to denote values at a particular time before and after incorporation of the measurement correction. Given a prior estimate of the system state at time t_k we seek to update our estimate based on the measurement $\bar{y}_k$ in a linear, recursive form

$$\hat{\bar{x}}_k^+ = K_k' \hat{\bar{x}}_k^- + K_k \bar{y}_k \quad \text{(A.33)}$$

where K_k' and K_k are matricies, as yet unspecified, that determine the relative weighting of the prior estimate and current measurement. The error in this estimate can be shown to be

$$\tilde{\bar{x}}_k^+ = \left(K_k' + K_k H_k - I\right)\bar{x}_k + K_k' \tilde{\bar{x}}_k^- + K_k \bar{v}_k \quad \text{(A.34)}$$

Since $\tilde{\bar{x}}_k^-$ and $\bar{v}_k$ are unbiased

$$E[\tilde{\vec{x}}_k^-]=\vec{0}$$
$$E[\vec{v}_k]=\vec{0} \tag{A.35}$$

this estimate can only remain unbiased for all given states if

$$K_k^{'} = I - K_k H_k \tag{A.36}$$

With this requirement the estimator takes the form

$$\hat{\vec{x}}_k^+ = \hat{\vec{x}}_k^- + K_k\left(\vec{y}_k - H_k\hat{\vec{x}}_k^-\right) \tag{A.37}$$

and has corresponding error

$$\tilde{\vec{x}}_k^+ = \left(I - K_k H_k\right)\tilde{\vec{x}}_k^- + K_k\vec{v}_k \tag{A.38}$$

The state error covariance must also be updated.

$$P_k^+ = E[\tilde{\vec{x}}_k^+\tilde{\vec{x}}_k^{+T}]$$
$$= E\{(I - K_k H_k)\tilde{\vec{x}}_k^-[\tilde{\vec{x}}_k^{-T}(I - K_k H_k)^T + \vec{v}_k^T K_k^T] + K_k\vec{v}_k[\tilde{\vec{x}}_k^{-T}(I - K_k H_k)^T + \vec{v}_k K_k^T]\} \tag{A.39}$$

Using the definitions

$$P_k^- = E[\tilde{\vec{x}}_k^-\tilde{\vec{x}}_k^{-T}] \tag{A.40}$$

and

$$R_k = E[\vec{v}_k\vec{v}_k^T] \tag{A.41}$$

and noting that the measurement errors are uncorrelated

$$E[\tilde{\vec{x}}_k^-\vec{v}_k^T] = E[\vec{v}_k\tilde{\vec{x}}_k^{-T}] = 0 \tag{A.42}$$

The covariance can be simplified to

$$P_k^+ = (I - K_k H_k)P_k^-(I - K_k H_k)^T + K_k R_k K_k^T \tag{A.43}$$

The criterion for choosing the optimal K_k is to minimize a weighted scalar sum of the diagonal elements of the error covariance matrix, P_k^+. Thus the cost function is

$$J_k = E[\tilde{\vec{x}}_k^{+T} S\tilde{\vec{x}}_k^+] \tag{A.44}$$

where S is any positive semidefinite matrix. Choosing S = I,

$$J_k = \text{trace}[P_k^+] \tag{A.45}$$

which is equivalent to minimizing the length of the estimation error vector. To find the value of K_k which yields a minimum, it is necessary to take the derivative of J_k with respect to K_k and set it equal to zero. The result is

$$-2(I - K_k H_k)P_k^- H_k^T + 2K_k R_k = 0 \tag{A.46}$$

Solving for K_k,

$$K_k = P_k^- H_k^T [H_k P_k^- H_k^T]^{-1} \tag{A.47}$$

which is referred to as the Kalman gain matrix. Since the Hessian of J_k is positive semidefinite so K_k does indeed produce a minimum. Substituting into the equation for the updated error covariance gives

$$P_k^+ = P_k^- - P_k^- H_k^T [H_k P_k^- H_k^T + R_k]^{-1} H_k P_k^- = \left(I - K_k H_k\right) P_k^- \tag{A.48}$$

THIS PAGE INTENTIONALLY LEFT BLANK

APPENDIX B: MATLAB CODE

A. INPUT PARAMETERS AND SIMULATION CALL

```
%Bifocal Relay Mirror Spacecraft Attitude Control System
%Input parameters and control options for attitude simulation model

clear
tic

stoptime=500; %Simulation stoptime
dt=.05; %fixed step size and computer time step

m1=2267.6059; %Mass of X-mit telescope (kg)
m2=972.3628; %Mass of RCV telescope (kg)

%Orbital parameters (circular)
Re=6378.1363; %Earth radius (km)
mu=3.986004415e5; %gravitational constant (km^3/s^2)
h=715; %orbit altitude (km)
r=Re+h; %orbit radius (km)
we=7.2921158533e-5; %Earth rotation rate (r/s)
w0=sqrt(mu/r^3); %orbital rate based on circular orbit/altitude (r/s)
nu0=0; %initial true anomaly (r)
u0=0; %initial angle of the magnetic dipole normal to the
   %line of ascending nodes (r)
e1=11*pi/180; %magnetic dipole tilt angle
inc=40*pi/180; %inclination
Km=7.943e15; %magnetic constant (Nm^2/a)
Bm=Km/(r*1000)^3; %magnetic field strength (N/am)

%Disturbance torques
Mds=1e-4*[1;1;1]; %secular disturbance torques (Nm)
Mdp=4e-4*[1,1,1]; %periodic disturbances torque magnitudes (Nm)
pdper=[400,500,600]; %periodic disturbance torque periods (s)
pdfreq=2*pi./pdper; %periodic disturbance torque frequencies (r/s)
pdphase=[pi/4,pi/2,pi]; %periodic disturbance torque phase (r)

%Magnetic dumping control
magoo=0; %magnetic dumping on/off control (0=off, 1=on)
magsat=180; %maximum torque rod output
magk=5e5; %magnetic torquer gain

%Appendage (RCV scope) motion relative to body x-axis (sinusoidal)
```

```
bper=300; %period of oscillation (s)
bstart=.25*bper; %start motion (s)
bmotion=1*bper; %length of motion (s)
bstop=bstart+bmotion; %stop motion (s)
bfreq=2*pi/bper; %frequency of motion (rad/s)
bamp=15*pi/180; %amplitude/half maximum angular offset (rad)
bi=0; %initial angular offset (rad)
bdi=0; %initial relative angular rate (rad/s)
bacc=bamp*bfreq^2; %maximum realtive angular acceleration (rad/s^2)
bnv=1e-5^2; %relative angular noise variance from potentiometer (rad)
bns=0; %initial seed of potentiometer noise
bq=.01*pi/180; %quantization of potentiometer readings (rad)

%Command profile inertial to body accelerations (sinusoidal)
wdcfreq=2*pi*[1/800;1/500;1/600]; %frequency of acceleration profile variation
wdc=[.05*wdcfreq(1)^2;.5*wdcfreq(2)^2;-.1*wdcfreq(3)^2];
   %amplitude of acceleration profile
wdcphase=[pi/8;-pi/12;0]; %phase of acceleration profile
cpoo=1; %turn commanded profile on/off (0=off, 1=on)

I1=[2997.28025,-3.9331,118.2824;
   -3.9331,3164.18285,1.1230;
   118.2824,1.1230,881.82105];
   %moment of inertia matrix of primary body (XMIT scope) about its cm
I2=[1721.07340,-.0116,-7.8530;
   -.0116,1559.85414,-12.5463;
   -7.8530,-12.5463,182.89962];
   %moment of inertia matrix of appendage (RCV scope) about its cm

dx1=.558354158; %Distance of X-mit telescope cm from S/C cm in x dir (m)
dy1=3.91788e-4; %Distance of X-mit telescope cm from S/C cm in y dir (m)
dz1=-.15226902; %Distance of X-mit telescope cm from S/C cm in z dir (m)
dx2=-1.302113918; %Distance of RCV telescope cm from S/C cm in x dir (m)
dy2=-9.13673e-4; %Distance of RCV telescope cm from S/C cm in y dir (m)
dz2=.355100092; %Distance of RCV telescope cm from S/C cm in z dir (m)

IC1=I1+m1*[dy1^2+dz1^2,dx1*dy1,dx1*dz1;
          dx1*dy1,dx1^2+dz1^2,dy1*dz1;
          dx1*dz1,dy1*dz1,dx1^2+dy1^2];
   %moment of inertia matrix of primary body (XMIT scope) about S/C cm
roti=[1,0,0;0,cos(bi),sin(bi);0,-sin(bi),cos(bi)];
   %rotation matrix corresponding to initial relative angular position
   %of appendage (RCV scope)
   %x-axis rotation of magnitude bi
Ic2i=roti'*I2*roti; %initial rotated moment of inertia matrix of appendage
   %(RCV scope)
```

```
I2m=m2*[dy2^2+dz2^2,dx2*dy2,dx2*dz2;
        dx2*dy2,dx2^2+dz2^2,dy2*dz2;
        dx2*dz2,dy2*dz2,dx2^2+dy2^2];
    %moment of inertia of appendage (RCV scope) about S/C C.M.
    %due to mass offset
IC2i=roti'*I2*roti+I2m; %initial moment of inertia matrix of appendage
    %(RCV scope) about S/C cm
Ii=IC1+IC2i; %initial S/C moment of inertia about S/C cm

%Wheel control law gains
%u=-Kqqe-Kwwe=-Kq(qc*q)-Kw(w-wc)
cldel=30; %delay control laws for attitude determination
Kq1=3000;
Kq2=7000;
Kq3=4500;
Kw1=1000;
Kw2=2000;
Kw3=1000;

%Initial body with respect to inertial quaternions
q1i=0;q2i=0;q3i=0;
qi=[q1i,q2i,q3i,sqrt(1-q1i^2-q2i^2-q3i^2)];

%Initial body with respect to orbit quaternions
q1oi=0;q2oi=0;q3oi=0;
qoi=[q1oi,q2oi,q3oi,sqrt(1-q1oi^2-q2oi^2-q3oi^2)];

%Initial body with respect to inertial direction cosine matrix
dcmi(1,1)=qi(1)^2-qi(2)^2-qi(3)^2+qi(4)^2;
dcmi(1,2)=2*(qi(1)*qi(2)+qi(3)*qi(4));
dcmi(1,3)=2*(qi(1)*qi(3)-qi(2)*qi(4));
dcmi(2,1)=2*(qi(1)*qi(2)-qi(3)*qi(4));
dcmi(2,2)=-qi(1)^2+qi(2)^2-qi(3)^2+qi(4)^2;
dcmi(2,3)=2*(qi(2)*qi(3)+qi(1)*qi(4));
dcmi(3,1)=2*(qi(1)*qi(3)+qi(2)*qi(4));
dcmi(3,2)=2*(qi(2)*qi(3)-qi(1)*qi(4));
dcmi(3,3)=-qi(1)^2-qi(2)^2+qi(3)^2+qi(4)^2;
Ci=[dcmi(1,1);dcmi(1,2);dcmi(1,3);
    dcmi(2,1);dcmi(2,2);dcmi(2,3);
    dcmi(3,1);dcmi(3,2);dcmi(3,3)];
    %Direction cosine component vector
Ai=[dcmi(1,1),dcmi(1,2),dcmi(1,3);
    dcmi(2,1),dcmi(2,2),dcmi(2,3);
    dcmi(3,1),dcmi(3,2),dcmi(3,3)];
    %Direction cosine/attitude matrix
```

```
%Initialize S/C momentum with wi at orbital rate
wi=[0;-w0;0]; %Initial angular rate of S/C primary body due to orbital rate
Hi=Ii*wi; %initial angular momentum of S/C due to orbital rate

%Gyro characteristics
grsb=1e-4*[-1,1.5,1]; %arbitrary gyro static bias
grv=1e-9*[1,1,1]; %variance of gyro rate noise
grn=[0,1,2]; %initial seed of gyro rate noise
gasb=[0,0,0]; %gyro acceleration static bias (zeros)
gav=1e-12*[1,1,1]; %variance of gyro acceleration noise
gan=[3,4,5]; %initial seed of gyro acceleration noise
grrwi=[0,0,0]; %initial rate random walk (zeros)
wbi=[0;0;0]; %initial gyro bias correction
gx=0*pi/180; %body to gyro(IRU) x-axis rotation
gy=0*pi/180; %body to gyro(IRU) y-axis rotation
G=[cos(gy),sin(gy)*sin(gx),-sin(gy)*cos(gx);
   0,cos(gx),sin(gx);
   sin(gy),-cos(gy)*sin(gx),cos(gy)*cos(gx)];
   %Gyro alignment matrix - body to IRU

%Dynamic Gyro input options
dg=1; %choose Dynamic Gyro or regular gyros (1=DG, 0=gyros)
dggg=0; %calculate gravity gradient torque for DG (1=yes(requires or=1), 0=no)
dgsd=0; %secular disturbance torque known for DG (1=yes, 0=no)
dgpd=0; %periodic disturbance torque known for DG (1=yes, 0=no)
moiu=1; %steps per periodic moment of inertia calculation (1=every step)
or=0; %perform orbital reference calculations

%Attitude determination initialization with error
qe1i=q1i+.008;qe2i=q2i+.012;qe3i=q3i-.008;
qei=[qe1i,qe2i,qe3i,sqrt(1-qe1i^2-qe2i^2-qe3i^2)];
dcmei(1,1)=qei(1)^2-qei(2)^2-qei(3)^2+qei(4)^2;
dcmei(1,2)=2*(qei(1)*qei(2)+qei(3)*qei(4));
dcmei(1,3)=2*(qei(1)*qei(3)-qei(2)*qei(4));
dcmei(2,1)=2*(qei(1)*qei(2)-qei(3)*qei(4));
dcmei(2,2)=-qei(1)^2+qei(2)^2-qei(3)^2+qei(4)^2;
dcmei(2,3)=2*(qei(2)*qei(3)+qei(1)*qei(4));
dcmei(3,1)=2*(qei(1)*qei(3)+qei(2)*qei(4));
dcmei(3,2)=2*(qei(2)*qei(3)-qei(1)*qei(4));
dcmei(3,3)=-qei(1)^2-qei(2)^2+qei(3)^2+qei(4)^2;
Cei=[dcmei(1,1);dcmei(1,2);
   dcmei(1,3);dcmei(2,1);dcmei(2,2);dcmei(2,3);
   dcmei(3,1);dcmei(3,2);dcmei(3,3)];
Aei=[dcmei(1,1),dcmei(1,2),dcmei(1,3);
   dcmei(2,1),dcmei(2,2),dcmei(2,3);
   dcmei(3,1),dcmei(3,2),dcmei(3,3)];
```

```
qe1oi=q1oi+.02;qe2oi=q2oi+.03;qe3oi=q3oi-.02;
qeoi=[qe1oi,qe2oi,qe3oi,sqrt(1-qe1oi^2-qe2oi^2-qe3oi^2)];
wei=wi+1e-3*[-1;1;2];
Hei=Ii*wei;

%Initialize Kalman filter
xi=0*[ones(3,1)*eps*1e10;ones(3,1)*eps*1e8]; %initial state vector
Pi=[100*eye(3),zeros(3);zeros(3),eye(3)]*500; %initial covariance matrix
if dg==1
   Qn=.5;
else          %plant noise covariance constant DG vs gyro
   Qn=.03;
end
Q=[100*eye(3),zeros(3);zeros(3),eye(3)]*Qn; %plant noise covariance
   %small Q = good plant, biq Q = bad plant
R=10000*eye(2); %measurement noise covariance (10000)
E=[1,0,0;0,1,0]; %choose horizontal and vertical components only

%Star tracker parameters
corr=2*1/dt; %computer steps between stars
gapstart=100; %start gap in star tracker data (s)
stargap=200; %length of star gap (s)
gapstop=gapstart+stargap; %end gap in star tracker data (s)
t1x=135*pi/180; %body to star tracker one x-axis rotation
t1y=30*pi/180; %body to star tracker one y-axis rotation
T1=[cos(t1y),sin(t1y)*sin(t1x),-sin(t1y)*cos(t1x);
   0,cos(t1x),sin(t1x);
   sin(t1y),-cos(t1y)*sin(t1x),cos(t1y)*cos(t1x)];
   %body to star tracker one rotation matrix
t2x=135*pi/180; %body to star tracker two x-axis rotation
t2y=-30*pi/180; %body to star tracker two y-axis rotation
T2=[cos(t2y),sin(t2y)*sin(t2x),-sin(t2y)*cos(t2x);
   0,cos(t2x),sin(t2x);
   sin(t2y),-cos(t2y)*sin(t2x),cos(t2y)*cos(t2x)];
   %body to star tracker two rotation matrix
t3x=180*pi/180; %body to star tracker two x-axis rotation
t3y=0*pi/180; %body to star tracker two y-axis rotation
T3=[cos(t3y),sin(t3y)*sin(t3x),-sin(t3y)*cos(t3x);
   0,cos(t3x),sin(t3x);
   sin(t3y),-cos(t3y)*sin(t3x),cos(t3y)*cos(t3x)];
   %body to star tracker two rotation matrix
mixT3=1; %choose whether or not to mix in star tracker 3 data (1=yes, 0=no)
T3th=.3; %choose threshold for random mix of star tracker 3 data
   %(0=50%, higher=less, lower=more)
T12b=0; %choose to bias random selection between tracker 1 and 2
   %(0=50/50, lower=favor1, higher=favor2)
```

```
stnb=[0,0]; %unknown star tracker bias error
stnv=1e-4^2*[1,1]; %variance of star tracker noise
stns=[0,1]; %initial seed of star tracker noise

%3 of 4 reaction wheels in pyramid constellation
rwsat=1*[1,1,1]; %constellation wheel torque saturation limits (Nm)
rwrl=10*[1,1,1]; %constellation wheel torque rate limiter (Nm/s)
hwi=-I2*[bdi;0;0]; %initialize wheels to cancel appendage momentum
rwa=45*pi/180; %angle of reaction wheels to x-y plane
RW=inv([-cos(rwa)*cos(pi/4),-cos(rwa)*cos(pi/4),cos(rwa)*cos(pi/4);
        -cos(rwa)*cos(pi/4),cos(rwa)*cos(pi/4),cos(rwa)*cos(pi/4);
        -sin(rwa),-sin(rwa),-sin(rwa)]); %body to wheel transform matrix
hwsi=RW*hwi; %distribute initial wheel momentum
rwnm=[0;0;0]; %mean of wheel noise
rwnv=1e-2^2*[1;1;1]; %variance of wheel noise
rwns=[7;8;9]; %initial seed of wheel noise
rwev=1e-8*[1,1,1]; %variance of wheel alignment walk error noise
rwes=[10,11,12]; %initial seed of gyro acceleration noise
rwam=1*5e-3*[1,2,-1]; %reaction wheel constellation alignment error magnitudes
rwaf=2*pi*[100,50,20]; %reaction wheel constellation alignment error frequencies
rwap=[pi/4,pi/3,pi/2]; %reaction wheel constellation alignment error phase

sim('acs_sim509') %Call to SIMULINK simulation

%Call ploting files for simulation results analysis
profileplots %command profile
ADplots509 %attitude determination performance
ACplots509 %attitude control performance

toc
```

B. SIMULATION RESULTS PLOTS

1. Commanded Profile Plots

```
%Laser Realy Spacecraft command profile plots

figure(1)
clf
plot(tout,qc)
title('Commanded Quaternions')
legend('q1','q2','q3','q4')
xlabel('Time (sec)')
grid on
```

```
figure(2)
clf
plot(tout,wc)
title('Commanded Angular Rates')
legend('w1','w2','w3')
xlabel('Time (sec)')
ylabel('rad/s')
grid on
figure(3)
clf
plot(tout,b*180/pi)
xlabel('Time (sec)')
ylabel('Deg')
title('Relative Angle to Recieve Telescope (alpha)')
grid on
figure(4)
clf
Hm=sqrt(H(:,1).^2+H(:,2).^2+H(:,3).^2);
plot(tout,Hm)
title('System Angular Momentum')
xlabel('Time (sec)')
ylabel('Nms')
grid on
```

2. Attitude Determination Performance Results

```
%Bifocal Realy Mirror satellite attitude determination plots
%analyze performance of dynamic gyro and Kalman filter

%DG momentum error or gyro bias
if dg==1
figure(5)
clf
Hm=sqrt(H(:,1).^2+H(:,2).^2+H(:,3).^2);
Hmdg=sqrt(Hdg(:,1).^2+Hdg(:,2).^2+Hdg(:,3).^2);
plot(tout,Hm-Hmdg)
title('Angular Momentum Error')
xlabel('Time (sec)')
ylabel('Nms')
axis([0,stoptime,-.4,.4])
grid on
else
figure(5)
clf
plot(tout,wb)
title('Gyro Biases')
```

```
legend('wb1','wb2','wb3')
xlabel('Time (sec)')
ylabel('rad/s')
grid on
end

%KF states
figure(6)
clf
subplot(211),plot(tout,x(:,1:3))
title('State Attitude Errors')
legend('xa1','xa2','xa3')
xlabel('Time (sec)')
ylabel('rad')
axis([0,stoptime,-.0008,.0008])
grid on
subplot(212),plot(tout,x(:,4:6))
title('State Rate "Bias" Errors')
legend('xb1','xb2','xb3')
xlabel('Time (sec)')
ylabel('rad/s')
axis([0,stoptime,-.00008,.00008])
grid on

%AD errors
figure(7)
clf
plot(tout,(q-qkf))
title('Quaternion Errors')
legend('q1','q2','q3','q4')
xlabel('Time (sec)')
axis([0,stoptime,-3e-3,3e-3])
grid on
figure(8)
clf
plot(tout,w-wkf)
title('Rate Errors')
legend('w1','w2','w3')
xlabel('Time (sec)')
ylabel('rad/s')
axis([0,stoptime,-1.5e-3,1.5e-3])
grid on
```

3. Attitude Control Performance Results

%Bifocal Realy Mirror satellite attitude control plots

```
%analyze commanded versus controled attitude

figure(9)
clf
plot(tout,Mws)
title('Wheel Torques')
xlabel('Time (sec)')
ylabel('Nm')
legend('Wheel 1','Wheel 2','Wheel 3')
grid on
figure(10)
clf
plot(tout,hws)
title('Wheel Angular Momentums')
xlabel('Time (sec)')
ylabel('Nms')
legend('Wheel 1','Wheel 2','Wheel 3')
grid on
figure(11)
clf
plot(tout,(q-qc))
title('Quaternion Error')
legend('q1','q2','q3','q4')
xlabel('Time (sec)')
axis([0,stoptime,-4e-3,4e-3])
grid on
figure(12)
clf
plot(tout,w-wc)
title('Rate Error')
legend('w1','w2','w3')
xlabel('Time (sec)')
ylabel('rad/s')
axis([0,stoptime,-1.5e-3,1.5e-3])
grid on
```

THIS PAGE INTENTIONALLY LEFT BLANK

LIST OF REFERENCES

1. Gelb, Arthur (ed.), *Applied Optimal Estimation*, The M.I.T. Press, Cambridge, MA, 1974

2. Maybeck, Peter S., *Stochastic Models, Estimation, and Control*, Academic Press, New York, NY, 1979.

3. Azor, Ruth, Bar-Itzhack, Itzhack Y., Harman, Richard R., "Satellite Angular Rate Estimation from Vector Measurements", *Journal of Guidance, Control, and Dynamics*, Vol. 21, No. 3, May-June, 1998.

4. Harman, Richard R., Bar-Itzhack, Itzhack Y., "Pseudolinear and State-Dependent Riccati Equation Filters for Angular Rate Estimation", *Journal of Guidance and Control*, Vol. 22, No. 5, 1999, pp. 723-725.

5. Azor, Ruth, Bar-Itzhack, Itzhack Y., Deutschmann, Julie K., Harman, Richard R., "Angular-Rate Estimation Using Star Tracker Measurements", NASA Technical Paper 1999.

6. Oshman, Yaakov, Makeley, F. Landis, "Sequential Attitude and Attitude-Rate Estimation Using Integrated_Rate Parameters", *Journal of Guidance, Control, and Dynamics*, Vol. 22, No. 3, May-June 1999.

7. Gai, E., Daly, K., Harrison, J., Lemos, L. K., "Star-Sensor-Based Attitude/Attitude Rate Estimator", *Journal of Guidance and Control*, Vol. 8, No. 5, Sept.-Oct. 1985, pp. 560-565.

8. Herman, Louis K., Manke, Girard M., Heatwole, Craig M., Hamada, Brian T., McCain, Ian M., Pseudo Gyro, U.S. Patent, Docket No.: D365.

9. Wie, Bong, *Space Vehicle Dynamics and Control*, American Institute of Aeronautics and Astronautics, inc., Temple, AZ, 1998.

10. Kolve, D. I., "Describing an Attitude", American Astronautical Society Paper, AAS 93-037, 6-10 February 1993.

11. Gray, C. W., "Generic Star Tracker/IRU Attitude Determination Filter", Proceedings of the American Astronautical Society's Guidance and Control Conference, February 1999.

12. Stengel, Robert F., *Stochastic Optimal Control: Theory and Application*, John Wiley-& Sons, inc., New York, NY, 1986.

13. Brown, Robert G., *Introduction to Random Signals and Applied Kalman Filtering* 3rd ed., John Wiley & Sons, Inc., New York, NY, 1997.

14. Markeley, F. L., Nelson, J. D., "Zero-Gyro Safemode Controller for the Hubble Space Telescope", *Journal of Guidance, Control, and Dynamics*, Vol. 17, No. 4, pp. 815-822, July-Aug. 1994.

15. Crassidis, John L., Markeley, F. Landis, "Predictive Filtering for Attitude Estimation Without Rate Sensors", *Journal of Guidance, Control, and Dynamics*, Vol. 20, No. 3, May-June 1997.

16. Voth, Chris, Herman, Louis K., Heatwole, Craig M., Manke, Girard M., "Attitude Determination for the STEX Spacecraft Using Virtual Gyros", Technical Paper, October 15, 1999.

17. Kim, H. Y., Juang, J. N., Junkins, J. L., "Recursive attitude prediction", American Astronautical Society Paper, AAS 00-272, 20-21 March 2000.

18. Gray, C. W., Herman, L. K., Kolve, D. I., Westerlund, G. W., "On-Orbit Attitude Reference Alignment and Calibration", American Astronautical Society Paper, AAS 00-272, 20-21 March 2000.

INITIAL DISTRIBUTION LIST

1. Defense Technical Information Center 2
   8725 John J. Kingman Road, Suite 0944
   Ft. Belvoir, VA 22060-6218

2. Dudley Knox Library 2
   Naval Postgraduate School
   411 Dyer Road
   Monterey, CA 93943-5101

3. Department Chairman, Code AA 1
   Department of Aeronautics and Astronautics
   Naval Postgraduate School
   699 Dyer Road
   Monterey, CA 93943-5000

4. Professor Brij N. Agrawal, Code AA/Ag 2
   Department of Aeronautics and Astronautics
   Naval Postgraduate School
   699 Dyer Road
   Monterey, CA 93943-5000

5. Professor Hal A. Titus, Code EC/Ts 1
   Department of Electrical and Computer Engineering
   Naval Postgraduate School
   Monterey, CA 93943-5121

6. Professor Barry Leonard, Code AA/Ln 1
   Department of Aeronautics and Astronautics
   Naval Postgraduate School
   699 Dyer Road
   Monterey, CA 93943-5000

7. SRDC Research Library, Code AA 1
   Department of Aeronautics and Astronautics
   Naval Postgraduate School
   699 Dyer Road
   Monterey, CA 93943-5000

8. Donald I. Kolve, Associate Technical Fellow 1
Information, Space & Defense Systems
The Boeing Company
P.O. Box 3999 MC 8F-05
Seattle, WA 98124-2499

9. F. Landis Markley, Aerospace Engineer.....1
Guidance, Navigation and Control Systems Engineering Branch
CODE 571 NASA Goddard Space Flight Center
Greenbelt, MD 20771

10. Girard M. Manke, Senior Engineering Specialist.....1
The Aerospace Corporation
2350 East El Segundo Blvd
El Segundo, CA 90245-4691

11. LT William J. Palermo, USN.....2
402 Kemp Lane
Chesapeake, VA 23325